CR-151134

[redacted]

DEC 1976
RECEIVED
NASA STI FACILITY
INPUT BRANCH

MOTOROLA INC.

Government Electronics Division

(NASA-CR-151134) SHUTTLE/TDRSS Ku-BAND DOWNLINK STUDY Final Report (Motorola, Inc.) 230 p HC A11/MF A01 CSCL 17B

N77-13126

Unclas

G3/16 56941

FINAL REPORT
SHUTTLE/TDRSS KU-BAND
DOWNLINK STUDY

30 November 1976

Presented to
NASA/JSC

Contract No. NAS 9-14843

Approved by P. Leahy, Section Manager

D. Wolfe, Program Manager

Prepared by R. Meyer, Systems Engineer

DEC 1976
RECEIVED
NASA STI FACILITY
INPUT BRANCH

MOTOROLA *Government Electronics Division*
8201 E McDOWELL RD, SCOTTSDALE, ARIZ, 85252

TABLE OF CONTENTS

Paragraph	Title	Page
1.0	PROJECT SUMMARY	1
2.0	TASK RESULTS	4
2.1	Task #1	4
2.1.1	Bit Detection Losses	6
2.1.2	Distortion Noise in the FM Mode	7
2.2	Task #2	11
2.3	Task #3	15
2.3.1	Costas Loop Description	15
2.3.2	High Data Rate Coding	26
2.4	Task #4	30
2.5	Task #5	40
2.5.1	PM Mode Investigation	40
2.5.2	FM Mode Investigation	46
APPENDIX A	LINK MARGIN	
APPENDIX B	BIT DETECTION PERFORMANCE DEGRADATION PARAMETERS	
APPENDIX C	FM SIMULATION	
APPENDIX D	TRANSMITTER SPECIFICATION	
APPENDIX E	SIGNAL PROCESSOR SPECIFICATION	
APPENDIX F	COSTAS LOOP TRACKING SIGNAL TO NOISE RATIO	
APPENDIX G	METHODS FOR HANDLING THE HIGH RATE RETURN LINK DATA	
APPENDIX H	INVESTIGATION OF A 3-CHANNEL PM MODE	
APPENDIX I	MOTOROLA SPONSORED IMAGE CODING DEVELOPMENT STUDIES	

LIST OF FIGURES

Figure	Title	Page
1-1	Signal to Noise Mode 2, 2 Mbps Channel	8
1-2	Signal Above the Distortion-Free Signal Required to Meet a Particular E_b/Noise Density.	9
3-1	Simplified Functional Block Diagram of Costas Loop . .	17
3-2	Plot of S-Curves for Regular and Costas Loops Showing Maximum Linearized Phase Errors.	20
3-3	Loop Bandwidth vs Phase Jitter	22
3-4	Phase Noise Spectral Density $S_{\emptyset}$ (f).	24
3-5	High Data Rate Coder	27
4-1	Functional Diagram: Modified QPSK/QPSK Mechanization	31
4-2	TWTA Phase Shift as a Function of Input Amplitude . .	34
4-3	Distorting Waveforms	36
5-1	Number of Bits Allowable to Attain 10^{-6} BER at a Given S/N.	47
5-2	System Comparison	50

LIST OF TABLES

Table	Title	Page
1-1.	Allocation of EIRP	5
1-2.	Bit Detection Losses	6
2-1.	Crystal Oscillator Characteristics	14
2-2.	Commercially Available TCXO Characteristics	14
3-1.	Parameter Summary	25
5-1.	Comparison of Various Image Coding Techniques	43
5-2.	System Comparison	49

1.0 PROJECT SUMMARY

The signal design study addressed the practical design aspects of the Shuttle Orbiter/TDRSS (Tracking and Data Relay Satellite System) Ku-Band return link. The goal of assessing the adequacy of the baseline signal design approach, developing performance specifications for the return link hardware, and performing detailed design and parameter optimization tasks was accomplished by completing five specific study tasks. In general, the results of these tasks show that the basic signal structure design is sound and that the goals can be met. Constraints placed on return link hardware by this structure allow reasonable specifications to be written so that no extreme technical risk areas in equipment design are foreseen. A third channel can be added to the PM mode without seriously degrading the other services. The feasibility of using only a PM mode was shown to exist, however, this will require use of some digital TV transmission techniques. Further consideration should be given to this area of investigation before any particular scheme could be recommended.

Specifically, each task and its results are summarized as follows:

Task #1 - Assessment of Baseline Signal Design for Orbiter/TDRSS Ku-Band Return Link.

A minimum EIRP requirement was established which met the design margins for all the return link services. This EIRP was shown to be consistent with reasonable hardware mechanizations by examining the entries in the link margin calculations. Additional analysis was performed to show that crosstalk between TV and subcarrier channels was small relative to the performance requirements and to calculate the mechanization losses expected in the unbalanced QPSK link.

Task #2 - Development of Performance Specifications for Orbiter/TDRSS Return Link.

Detailed specifications for a transmitter which consists of a power amplifier, an exciter, a QPSK modulator, and an FM modulator were written. Analysis of incidental FM and oscillator stability was performed as an aid to specifying those parameters.

The return link signal processor which conditions or encodes the return link data as required was specified.

Task #3 - Detailed Design and Parameter Optimization.

Parameters which determine the design for the QPSK carrier synchronization phase locked loop were evaluated using the acquisition and tracking constraints imposed by the return link.

A baseline design and an alternative design for encoding the high rate (50 Mbps) channel were performed and evaluated.

Task #4 - Investigation of Three-Channel PM (Phase Modulated) Mode.

Evaluation of QPSK/QPSK and Interplex techniques for multiplexing three data channels yielded the recommendation that the QPSK/QPSK method be used. Additional design work demonstrated a mechanization which is simple to implement and allows the subcarrier modulator to be the same as that required for the FM mode. As a result of studying this three channel configuration, additional analysis was done which indicated that the expected AM to PM conversion caused by the TWTA will not significantly degrade the link performance.

Task #5 - Mode Simplification.

Techniques for using only a PM mode or only an FM mode to provide all return link services were investigated. Although this analysis showed that a PM mode was feasible, the choice of a dual mode design was reinforced. As part of the study various digital TV techniques were examined and as a result an overview is presented. Included as appendices

to this task are several reports of Motorola's in-house efforts relating to bandwidth compression of TV signals.

In the following sections the results of each of these tasks is presented in detail. Any portion of the task which formed a stand-alone unit has been included among the appendices and is referenced in the task description.

2.0 TASK RESULTS

2.1 Task #1 - Assessment of Baseline Signal Design for Orbiter/TDRSS Ku-Band Return Link.

The objective of this task was to evaluate and assess the adequacy of the signal design approach chosen for the Orbiter/TDRSS Ku-Band return link. This approach is summarized as follows:

a. PM Mode:

(1) A two-channel quadriphase (QPSK) modulation scheme has been selected, in which the high-rate (up to 50 Mbps) digital channel phase-shift-keys, say, an in-phase version of the carrier, while either real-time or recorded operational or experiments data (up to 2 Mbps) independently phase-shift-keys a quadrature version of the carrier.

(2) The high-rate channel is coded (rate $\frac{1}{2}$, constraint length 7 convolutional coding) to allow a power gain to be achieved.

(3) The two modulated carriers are weighted before summation so that morepower is allocated to the high-rate channel. The power division which has been tentatively selected is 80% for the high-rate channel and 20% for the low-rate channel.

b. FM Mode:

(1) The TV (or wideband analog or digital data, up to 4.5 MHz) is summed with an 8.5-MHz modulated subcarrier. The resulting signal frequency modulates the carrier.

(2) The 8.5-MHz subcarrier is QPSK modulated by two independent digital channels which include real-time operational voice/telemetry (192 kbps) and either recorded operational data or real-time (or recorded) experiments data (up to 2 Mbps).

Critical functions associated with this design were identified and evaluated as to their impact on the return link performance. The means for evaluation was a link budget which was set up on the computer so that any changes in the parameters could be quickly evaluated. Each discretionary parameter was examined to determine minimum requirements as well as practicality and equipment design problems. The resulting parameters were then used as inputs to the link budget program to derive the resultant margins. The baseline input parameter list and resultant link margin analysis tables are given in Appendix A. These tables show that a minimum EIRP of 51.0 dBw is required to yield a minimum design margin of 3.0 dB in all links. This can be readily achieved with a realizeable antenna size and circuit loss. A typical allocation of EIRP is given in Table 1-1.

Table 1-1. Allocation of EIRP

Transmit Power (50 watts)	17.0		dBw
Circuit Losses			
Polarizer	0.2		
Mismatch Losses	0.2		
Comparator Losses	0.5		
Rotary Joint Losses	0.4		
Circulator Losses	0.3		
Switches	0.2		
Filter Losses	0.4		
Pointing Losses	0.4		
Waveguide Runs (6')	0.5		
Total Circuit Losses	3.0		dB
Antenna Gain (27.8" at 40% eff)		37.0	dB
Net EIRP		51.0	dBw

This EIRP yields a net 3 dB margin in the 50 MBPS Mode 1 channel with the coding gain of 4.5 dB and signal losses of 1.9 dB contributed by the bit detector and bandwidth losses. An antenna size of around 28" with a conservative 40% efficiency is required in conjunction with the estimated 3.0 dB circuit losses to yield the 51.0 dBw EIRP.

Two additional supporting analyses were done to verify some initial estimates of parameters which affect the margin calculation. First, the bit detection losses were examined and were found to be nominally 2.dB. Secondly, the effect of distortion noise in the FM mode was calculated and determined to be small with respect to thermal noise. The following paragraphs outline the results of these analyses and refer to the appendices for details.

2.1.1 Bit Detection Losses

A typical allocation of losses due to bit detection is listed in Table 1-2 together with the apportioned degradation.

Table 1-2. Bit Detection Losses

Modulator rise time = .05T	.2 dB
Bandwidth	.8 dB
One/Zero Assymetry = 45/55	.1 dB
Sync jitter = .015T	.2 dB
Static phase error	.05 dB
Matched filter implementation loss	.3 dB
Detector threshold	.1 dB
Decision bias	.1 dB
Reset integrator T and dump interval	.05 dB
Total Bit Detection Losses	1.9 dB

Included in Appendix B of this report are graphs which parametrically indicate the expected values for many of the items listed in this table.

2.1.2 Distortion Noise in the FM Mode

The Mode 2 operation minimum link margin is 4.6 dB with 51 dBw EIRP. This link is balanced yielding equal threshold and performance margins. The required predetection bandwidth to yield this balance was 36 MHz. The input output S/N ratios for this bandwidth is shown in Figures 1-1 and 1-2 for the TV link and data channel. These two figures indicate a threshold point of C/N = 10 dB as used in the link margin tables. At 4.6 dB above the threshold level the input - output is linear with full FM improvement.

An analysis of the distortion vs modulation levels for the data subcarrier and TV link was made using a FM simulation program. A description of this program and the results are in Appendix C. This analysis utilized the 36 MHz predetection bandwidth determined in the link analysis to balance the margins. The analysis determined the peak deviation vs output S/N+D for each channel as well as utilizing a fixed peak deviation with a variable deviation ratio between channels to find optimum deviation ratio. The signal to distortion ratio was fairly insensitive to the ratio of deviations between channels. This allowed the choice of deviation to be made on thermal noise considerations. The S/N+D curves indicates a broad region of constant level in the 15 to 30 MHz peak deviation ratio region. The chosen 17 MHz peak deviation is about at the minimum level. At this point, the distortion adds less than 1 dB of noise into each channel. The link margin table does not reflect this added dB of degradation in the TV link. However, the TV link performance is higher than the data channel by 2.5 dB so that the added dB loss still leaves this channel with adequate performance margin.

ORIGINAL PAGE IS
OF POOR QUALITY

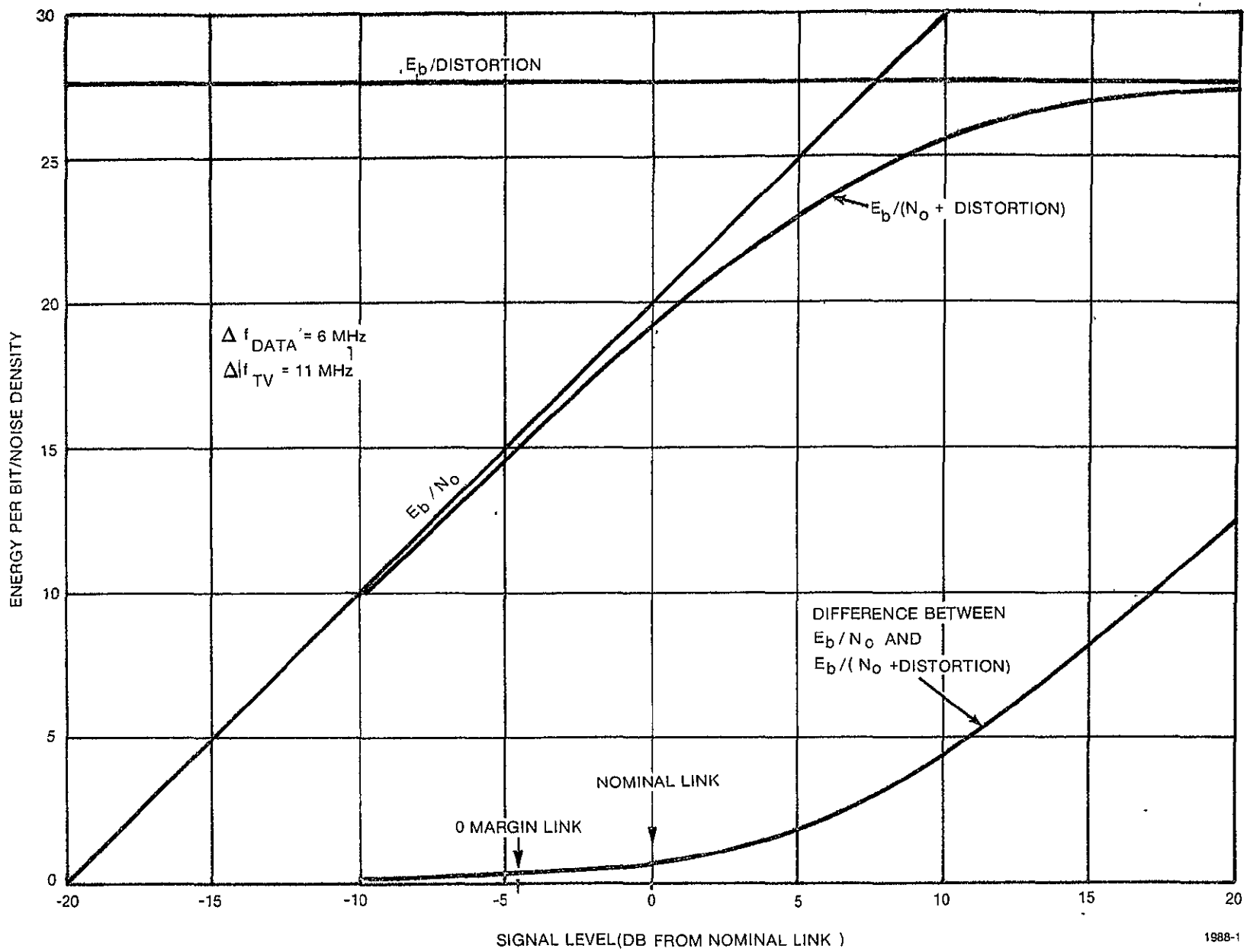

Figure 1-1. Signal to Noise Mode 2, 2 Mbps Channel

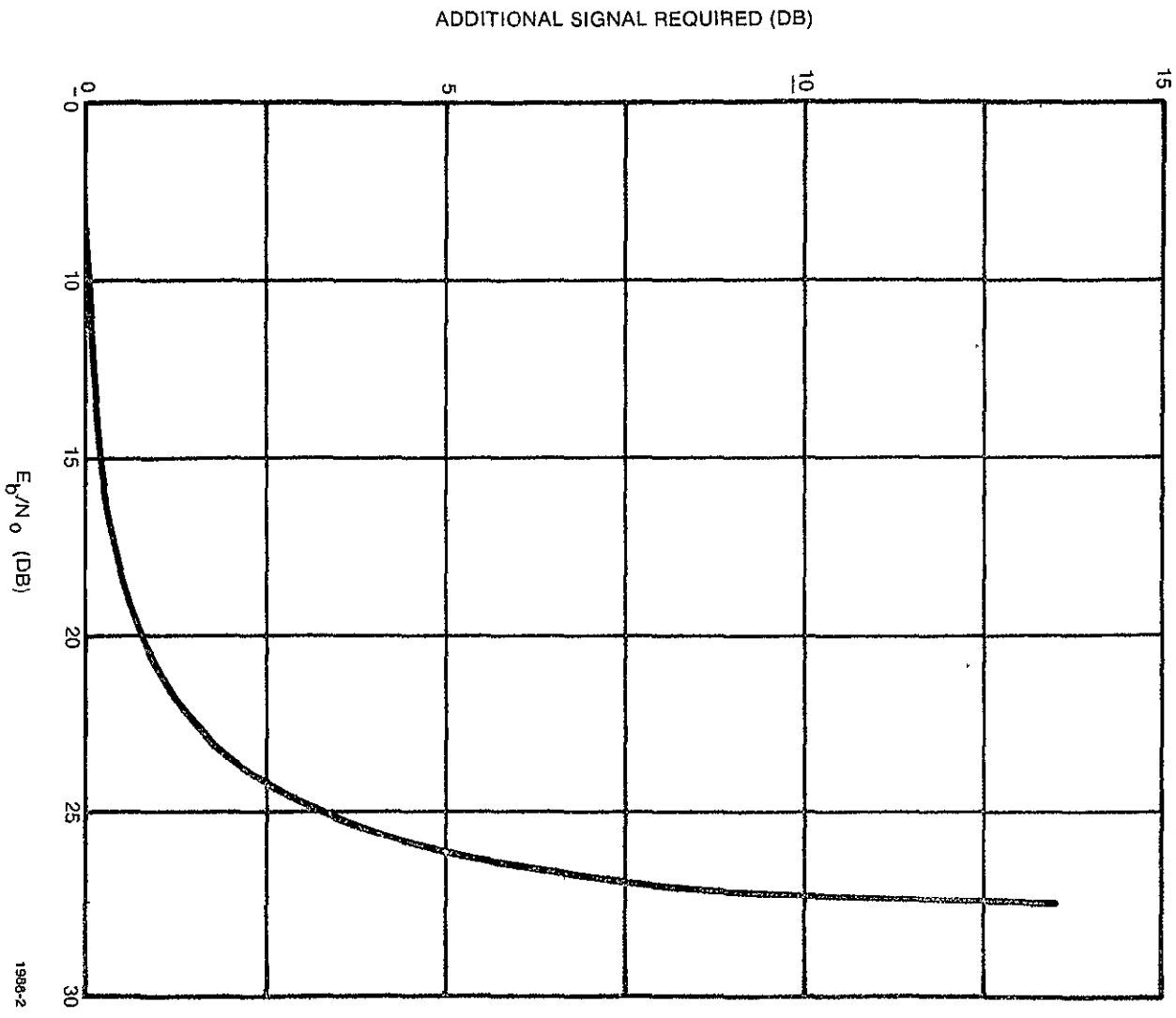

Figure 1-2. Signal Above the Distortion-Free Signal Required to Meet a Particular E_b/Noise Density.

Some additional evaluation of distortion in the Mode 2, 2 Mbps channel was done to determine the difference between E_b/N_o and $E_b/(N_o$ + Distortion) for this link. This is shown on Figures 1-1 and 1-2. The first chart indicates that the maximum achievable E_b/Noise density is limited by the distortion to 27.7 dB. Also shown is the E_b/thermal noise in direct relationship to the received signal level. Note that the nominal link signal level indicates 20.1 dB E_b/N_o as reported in the margin calculation. Combining these two yields the $E_b/(N_o$ + Distortion) durve. The effect of the distortion is indicated as the difference between the E_b/N_o and $E_b/(N_o$ + Distortion) curves. Figure 1-2 indicates the amount of additional signal level required to achieve the same E_b/noise density as would be available in the distortion-free situation. Source data for the distortion density was derived by simulation as described in Appendix C.

2.2 Task #2 - Development of Performance Specifications for Orbiter/ TDRSS Return Link.

Two sets of detailed specifications were developed. The first defines the requirements for transmitter hardware which consists of a power amplifier, an exciter, a QPSK modulator, and an FM modulator. The second details the signal processing equipment which accepts signals from the orbiter and payloads, conditions or encodes the data if necessary, then routes the signals to the appropriate modulator. These two specifications are included as Appendix D and Appendix E, respectively.

Effort on this task concentrated on specifying the hardware in such a way that the link performance requirements are assured and that these portions of the system can be tested as stand alone units.

Each of the parameters included in the specification were examined from the standpoint of assuring the desired link performance without requiring high risk hardware design. As a result the requirements for incidental FM and frequency stability were examined in more detail.

2.2.1 Incidental FM Analysis

The determination of the maximum IFM value of 5 kHz rms per MHz of bandwidth was done on the basis of a quality factor for the TV signal. The EIA recommendation for TV links via satellites is 53 dB peak to peak signal to rms noise for Grade 1 signals. This is calculated as:

$$\frac{S_{pp}}{N_{rms}} = \frac{C}{N} \; 3 \; \frac{f_p}{f_m}^{2} \; \frac{B_{IF}}{f_m} \; WP$$

where $\frac{C}{N}$ is the predetection signal to noise ratio in the IF bandwidth,

f_m is the baseband bandwidth,

B_{IF} is the IF bandwidth,

f_p is the peak deviation,

W is peak to peak to rms factor = 9 dB

P is the preemphasis factor = 3 dB

This equation can alternately be written

$$\frac{S_{pp}}{N_{rms}} = \frac{S_{rms}}{N_{rms}} \quad WP$$

Thus for the quality desired, $\frac{S_{rms}}{N_{rms}}$ = 41 dB. This ratio can also be treated as the ratio of a signal deviation and a noise deviation

$$\frac{S_{rms}}{N_{rms}} = 10 \log \frac{f_p^{\,2}/2}{f_{n\ rms}^{\,2}} = 41 \text{ dB}$$

It is assumed that this represents the thermal noise contribution and that any IFM should be minimal in comparison. Restricting the IFM contribution to 0.1 dB yields a required S_{rms} to N_{ifm} of 57 dB

$$10 \log \frac{f_p^{\,2}/2}{f_{ifm}^{\,2}} = 57$$

or f_{ifm} = 11 kHz rms

where f_{ifm} is the total allowable incidental rms deviation within the 4.5 MHz TV bandwidth. Assuming a uniform distribution of this noise over the 4.5 MHz, the density of the IFM can be calculated as:

$$f_{o\ ifm}^{\,2} = f_{ifm}^{\,2}/4.5 \text{ MHz}$$

or for a 1 MHz measurement bandwidth

$$f_{ifm}/\text{MHz} = 5.2 \text{ kHz rms/MHz}$$

Since this calculation was based on a TV requirement, the effect of this level IFM on the subcarrier channel must be examined. The signal to

noise ratio in a bit rate bandwidth of 2 MHz will be:

$$\frac{S}{N} = 10 \log \frac{(6x10^6)^2/2}{2(5x10^3)^2} = 55.6 \text{ dB}$$

where the 6 MHz is the subcarrier deviation. This large value assures that the IFM will not be a significant factor in data detection.

The result of these calculations was the specification that incidental FM will not exceed 5 kHz rms in any 1 MHz band from 500 kHz to 12.5 MHz.

2.2.2 Frequency Stability

Determination of the frequency stability requirements was based on practical hardware capabilities.

The reasonableness of these requirements is demonstrated first by the comparison of various crystal oscillator types given in Table 2-1 and second by the example characteristics of commercially available units designed for military and space system specifications given in Table 2-2.

The frequency characteristics contained in the preliminary transmitter specification are:

tolerance: $\pm 3 \times 10^{-5}$

stability: $\pm 1 \times 10^{-6}$/hour

aging: $+5 \times 10^{-6}$/year

Comparing the specified values with Tables 2-1 and 2-2 shows that the requirements can be met without using a temperature controlled oscillator and paying the concomitant power, size and weight penalties.

Table 2-1. Crystal Oscillator Characteristics (Adapted from "Crystal Controlled Oscillators," IEEE Transactions on Instrumentation and Measurement, Vol. IM-21, No. 3, August 1972).

Type	Frequency Stability (parts per million)	Input Power	Volume $(in.)^3$
Crystal Osc		10 to 50(mW)	.25 to 3
Temperature Range			
-55° to $+105^oC$	25		
-40° to $+90^oC$	15		
0° to $+50^oC$	4		
Temp. Compensated Crystal Osc		35 to 100(mW)	1 to 3
-55° to $+105^oC$	.5-10		
-40° to $+75^oC$	.3-10		
0° to $+50^oC$	.1-1		
Temp. Controlled Single Oven		1 to 10(watts)	7 to 35
-55° to $+75^oC$	$.1\text{-}5\times10^{-8}$		
-40° to $+70^oC$	$.1\text{-}5\times10^{-8}$		
0° to $+50^oC$	$.2\times10^{-9}$		
Dual Oven		5 to 15(watts)	36 to 360
-55° to $+60^oC$	$.2\text{-}2\times10^{-10}$		
0° to $+50^oC$	$.1\text{-}1\times10^{-10}$		

Table 2-2. Commercially Available TCXO Characteristics

Short term stability:	$\pm1 \times 10^{-9}$/sec
Long term stability:	$\pm3 \times 10^{-9}$/hour
Aging:	$\pm5 \times 10^{-7}$/year
Temperature Stability:	$\pm5 \times 10^{-7}$/for -20° to $+70^oC$
Variation with supply voltage:	2×10^{-8} per percent change
Input power:	150 mw
Size:	3 $(in.)^3$
Weight:	3 oz.

2.3 Task #3 - Detailed Design and Parameter Optimization.

The QPSK carrier synchronization phase locked loop was designed using acquisition and tracking constraints to determine the loop parameters. As a second part of this task, the high rate (up to 50 Mbps) coding strategy was examined with a resulting design for parallel coding as well as an alternate approach which would simplify synchronization of the signal received by the data processing equipment on the ground.

The examination of the Costas loop requirements for demodulating the return link signal established bounds on loop bandwidth as determined by the tracking, acquisition, and phase jitter requirements. Since these criteria do not result in a very tight constraint on the loop bandwidth, two additional factors considered were the minimum data rate and the noise contribution of the signal source. The results of the analysis indicate that a B_L of 100 kHz would be sufficient to meet the criteria established.

2.3.1 Costas Loop Description

The full suppression of the carrier by the modulation requires that some special steps be taken in the demodulation and carrier tracking methods to be considered. The absence of a steady carrier component means that a conventional phase-locked loop is not capable of tracking and providing an estimate of the incoming carrier to be used as a reference for data demodulation.

It has been shown (1) that a receiver which implements a Costas loop that tracks on the high rate signal of the unbalanced QPSK waveform can be used to recover and track the return link carrier. On this basis the design of the receiver loop can be accomplished using the procedures outlined for the Costas loop.

A simplified functional block diagram of the Costas' type loop is shown in Figure 3-1. The incoming signal is multiplied by in-phase and quadrature outputs of the VCO. The loop will lock in such a way as to force the VCO phase to be directly in-phase or out of phase with the data signal so that the upper arm of the loop acts as a coherent amplitude detector for the data. The loop error signal is developed by multiplying the in-phase output with the quadrature phase (lower arm of Figure 3-1) output. The error signal so developed is proportional to the signal power and the phase error between the VCO and the input. The expression that defines the dc portion of the error signal is:

$$\text{Error signal} = P_S \sin 2\epsilon$$

where ϵ is the loop phase error.

From this equation it may be noted that the loop S-curve is a function of twice the error phase. This implies that many of the conventional criteria applied to phase-locked-loop operation with regard to static and dynamic phase errors must be tempered by a factor of 2. As an example, the tendency of a phase-lock loop to skip cycles is related to the rms phase error, thus, where in a conventional phase lock loop 20 degree rms phase jitter might be acceptable for cycle skipping criteria, the Costas loop would respond as though the rms phase jitter was 40 degrees which produces a significantly different skipping rate.

COSTAS LOOP DESIGN

In a high gain carrier tracking loop, there are five basic parameters that must be determined to specify its mechanization and performance. These are frequency uncertainty, acquisition time, sweep rate, loop bandwidth, and threshold signal levels. For a Costas Loop, there is an additional parameter that influences the loop performance, namely, the bandwidth preceeding the IQ loop multiplier. These six parameters are

ORIGINAL PAGE IS
OF POOR QUALITY

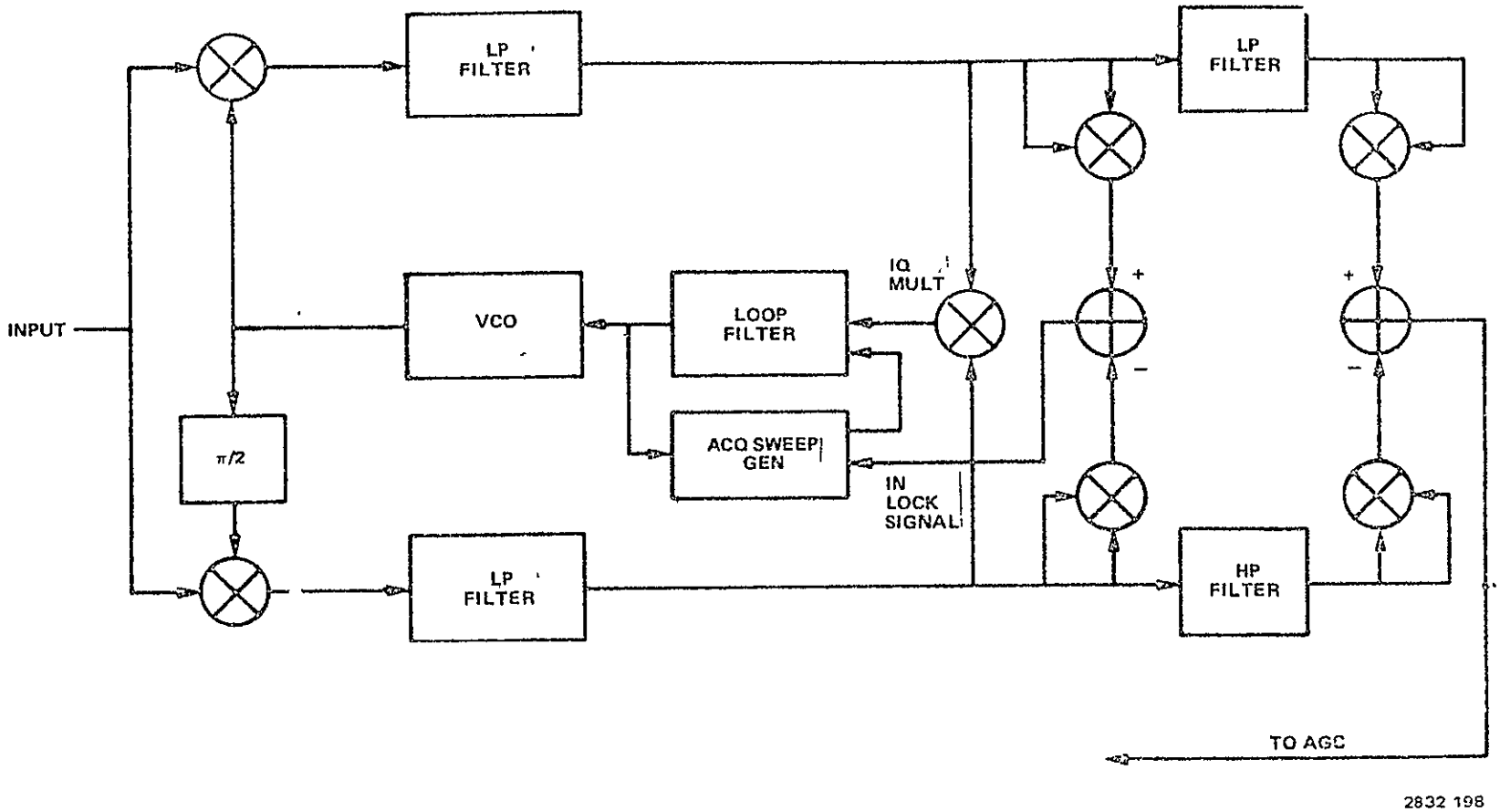

Figure 3-1. Simplified Functional Block Diagram of Costas Loop

interdependent so that the loop design procedure consists of choosing a couple of parameters, such as the acquisition time or frequency uncertainty, and then determining the rest of the parameters from this interrelationship. As an illustration of this procedure, a typical example will be used starting from an acquisition time and frequency uncertainty.

SWEEP RATE CALCULATION

If we use a sawtooth type of VCO frequency sweep for loop acquisition, we may calculate the sweep rate directly from the required acquisition time and frequency uncertainty. If we use a sawtooth sweep having a 10% of the cycle for flyback time, then the sweep rate is

$$R = \frac{F_u}{0.9T}$$

R = Sweep rate in Hz/Second

T = Acquisition time in Seconds

F_u = Frequency Uncertainty in Hz

For a frequency uncertainty of ± 1 MHz, then

$$R = \frac{2 \times 1 \times 10^6}{0.9T}$$

$$= 2.22 \times 10^6/T \text{ Hz/Sec}$$

Using a 4 second requirement for the acquisition time yields a sweep rate of 556 kHz/Second.

ACQUISITION BANDWIDTH

A phase lock loop tracking a frequency sweep will develop a phase error proportional to the sweep rate and inversely proportional to the bandwidth squared. Thus, the sweep rate will determine the minimum bandwidth that can be used during acquisition. This rate error plus the noise phase error must not exceed the maximum phase error that the loop can track if the loop is to acquire. A narrow bandwidth will result

in a large rate error from the sweep but will have a smaller noise phase error. The optimum design is to allocate half the allowable tracking phase error to the sweep and the other half to the phase noise in the loop. The linear loop rate error resulting from a frequency sweep is given by

$$\epsilon = \frac{101\ R}{B_L^{\ 2}} \text{ deg} \qquad (2)$$

where R = Frequency rate in Hz/Second

F_L = Single sided loop noise bandwidth (ζ = .707)

Figure 3-2 shows the "S" curves for a regular phase lock loop and a Costas loop. The maximum linearized phase error that a regular loop can track is 1.0 radian or 57.3 degrees, while the same error for a Costas Loop is only half that amount ($\frac{1}{2}$ radian or 28.6°) due to the 180° phase ambiguity of the loop. From past experience, for a 90% probability of acquisition, the total value of rms phase noise plus rate error must not exceed the maximum linearized phase error. If we allocate $\frac{1}{2}$ the maximum tracking phase error to the sweep rate error then for a Costas Loop from equation 2

$$B_L = \left(\frac{101\ R}{14}\right)^{\frac{1}{2}} \text{ Hz} \qquad (3)$$

where B_L = One sided noise bandwidth (ζ= .707)

R = Sweep rate in Hz/Second

Using the previously determined sweep rate of 50 kHz/Second then

$$B_L = \left(\frac{101 \times 556 \times 10^3}{14}\right)^{\frac{1}{2}}$$

= 2000 Hz.

ACQUISITION THRESHOLD

In order to determine the acquisition threshold, it is necessary to determine the signal level at which the phase noise in the loop is

ORIGINAL PAGE IS
OF POOR QUALITY

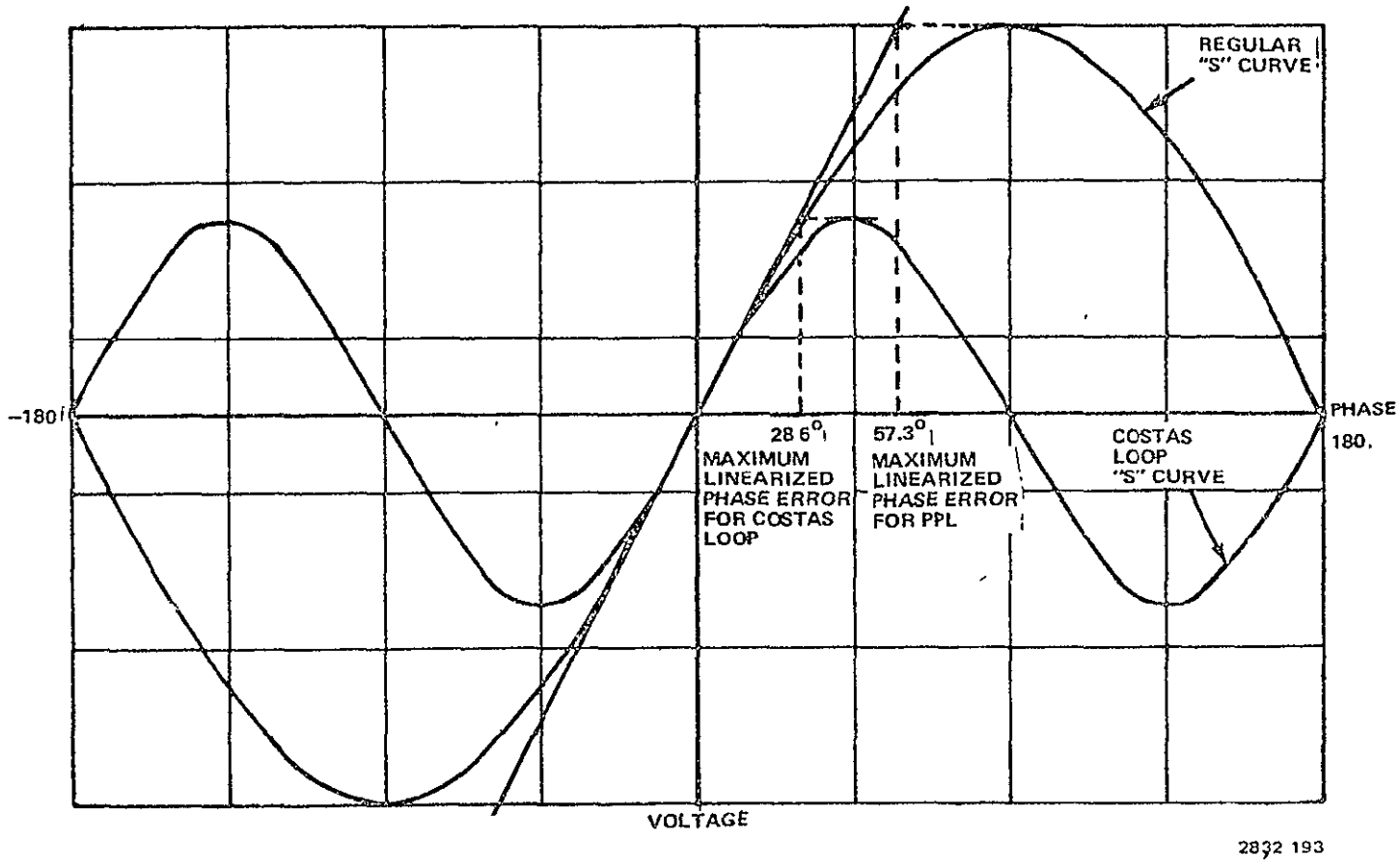

Figure 3-2. Plot of S-Curves for Regular and Costas Loops Showing Maximum Linearized Phase Errors

$\frac{1}{4}$ radian rms. The IQ multiplier in the loop degrades the signal to noise existing in the premultiplier bandwidth in a manner of a square law detector so that the phase noise including the effects of the multiplier is

$$\sigma^2 = \frac{\frac{2B_L}{B_{IF}}\left(1 + \frac{2P_T}{N_o B_{IF}}\right)}{(2\alpha-1)^2\left(\frac{2P_T}{N_o B_{IF}}\right)^2}$$

where P_T/N_oB_{IF} is signal/noise in premultiplier filters, and α is portion of the total power in the high rate channel. Basis for this formulation is shown by the analysis of Appendix F.

Figure 3-3 shows the jitter vs loop bandwidth for an input signal to noise density of 86.5 dB-Hz and 300 MHz predetection bandwidth. Note that the jitter is less than 0.1 radians for loop bandwidths less than 1 MHz. Thus, the acquisition threshold for 90% probability of acquisition with first passage of the sweep past the signal is -112.6 dBw for an 893°K receiver.

<u>OPERATING TRACKING THRESHOLD</u> (Data Detection Mode)

In order to minimize the signal loss to the bit detector, the maximum tracking rms noise is limited to 0.1 radian rms.

The phase error from the signal frequency rate of 35 kHz/Second can be calculated from equation (2) as

$$\epsilon = \frac{101 \times 35 \times 10^3}{B_L^{\,2}} \text{ deg}$$

If we set the maximum strong signal rate error equal to $\frac{1}{4}$ radian (14. deg) for signal loss reasons (assuming noise errors when this rate

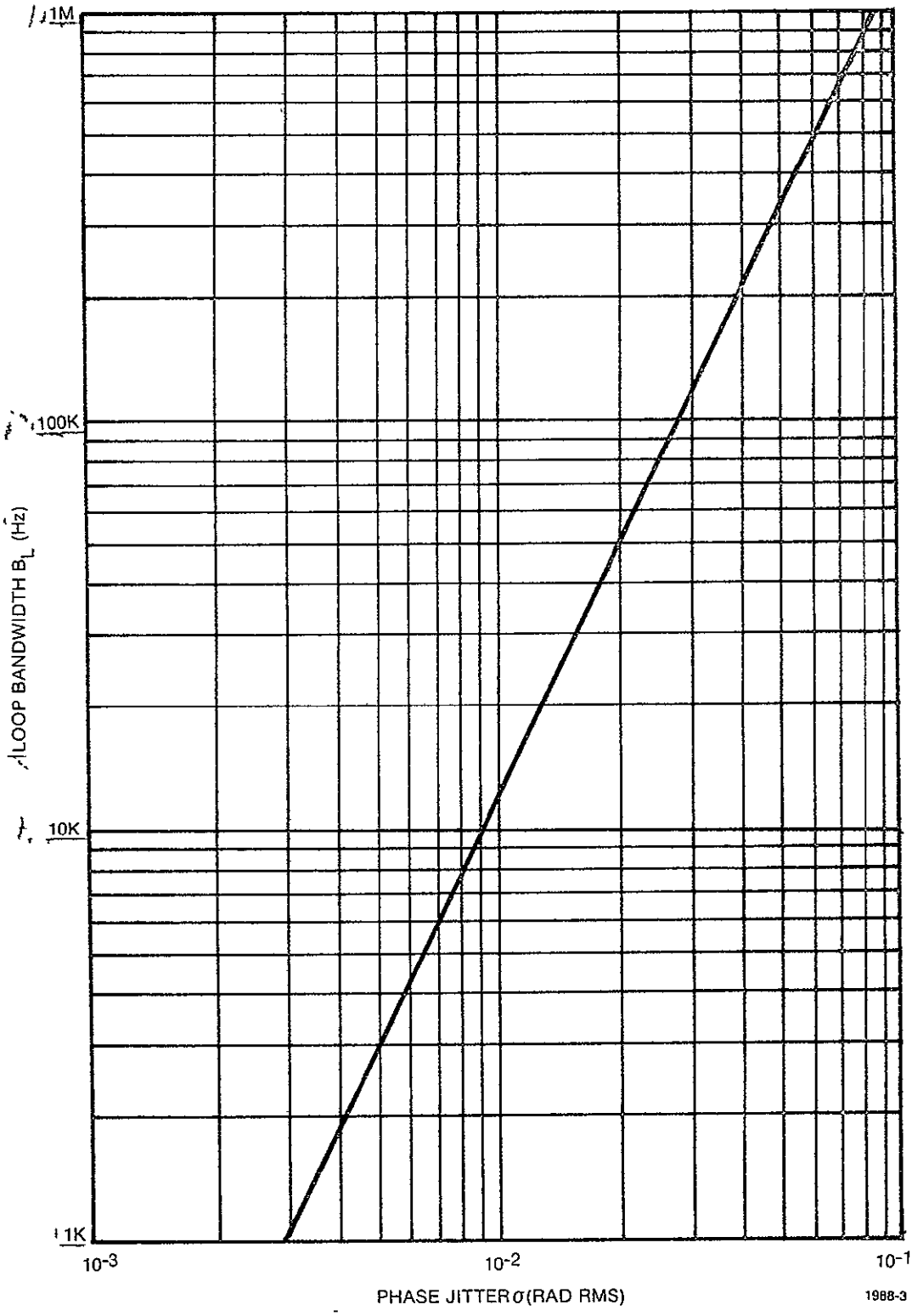

Figure 3-3. Loop Bandwidth vs Phase Jitter.

error occurs as negligible) then the minimum bandwidth for tracking will be given by:

$$B_L = \left(\frac{101 \times 35 \times 10^3}{14}\right)^{\frac{1}{2}} \text{ Hz}$$

$$= 500 \text{ Hz}$$

Note that a bandwidth this narrow cannot be used and still meet the acquisition requirement. Thus the minimum bandwidth of 2000 Hz will have a tracking error of

$$\epsilon = \frac{101 \times 35 \times 10^3}{(2000)^2} = .9^o$$

In order to establish an upper limit on the loop bandwidth, the data being demodulated must be considered. Because the data is being taken off at the error point of the loop its spectrum is modified by the 1-H(s) transfer characteristic. In order to reduce the effects of this filtering, the maximum loop bandwidth must not exceed 0.1 of the minimum symbol rate. In this case the symbol rate of concern is 8 Msps, the minimum expected on the high channel.

Using the acquisition requirement and the minimum data rate, the loop bandwidth has been loosely bounded between 2 kHz and 800 kHz. Another parameter to be considered in selecting this bandwidth is the noise contribution of the transmitter. A typical plot of the phase noise characteristics of a transmitter which will meet the requirements for Shuttle is shown in Figure 3-4. Superimposed on this plot is the expected thermal noise level for the "best case" circuit, i.e., no signal losses. Over most of the spectrum this noise predominates, however, at the low frequency end the oscillator noise exceeds the thermal. The effect of this can be reduced to tolerable levels by using a loop bandwidth of 100 kHz which will roll off the oscillator noise as shown on the graph. Using this loop the phase jitter in the data channel will

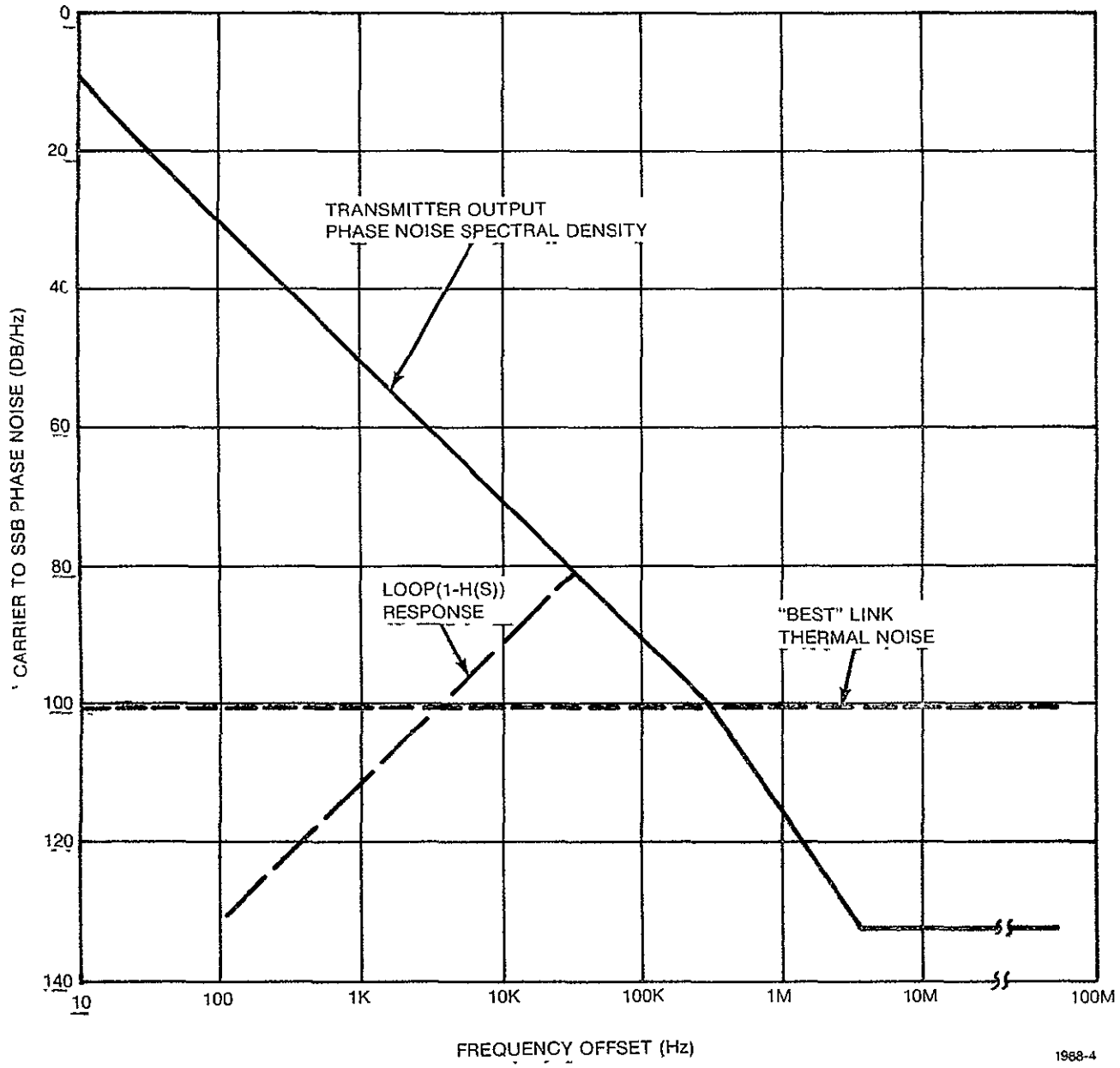

Figure 3-4. Phase Noise Spectral Density
$S_{\emptyset}$ (f)

Table 3-1. Parameter Summary

INDEPENDENT PARAMETERS	Noise Figure	$893^{\circ}K$	Equipment
	Acquisition Time	4 Sec	
	Frequency Uncertainty	± 1 MHz	Mission Requirements
	Strong Signal Freq Rate	35 kHz/Sec	Mission Requirements
	Data Symbol Rate (Max)	100 Mb/Sec	Mission Requirements
DEPENDENT PARAMETERS	Sweep Rate	556 kHz/Second	From Freq Uncertainty and Acquisition Time
	Acquisition Bandwidth (B_L)	2000 Hz	From Sweep Rate
	Acquisition Threshold	-112.6 dBw	From Predetection BW, Noise Figure and Acquisition BW
	Tracking Bandwidth (B_L)	500 Hz	Low Noise Reference
	Predetection Bandwidth	300 MHz	Data Rate Plus False Lock Considerations
	Data Rate Bandwidth Limit	800 kHz	Data detection considerations

be less than 1.5° rms and the requirements for acquisition and tracking will be met.

PARAMETER SUMMARY

From the foregoing example, it maybe seen that by choosing a limited number of parameters (Acquisition time, Frequency Uncertainty, Noise figure and strong signal tracking rate) the complete design of the loop is bounded. Choice of other independent parameters would yield other solutions. However, the frequency uncertainty and strong signal tracking rates are determined by the mission leaving only limited flexibility in the choice of acquisition time and noise figure. A summary is shown in Table 3-1.

2.3.2 High Data Rate Coding

The design for the high rate coding equipment is shown on Figure 3-5.

While this payload data source may be of any rate between 4 MBPS to 50 MBPS, for convenience it will here be referred to as the 50 MBPS data. The 50 MBPS data and 50 MHz clock will be received from the payload by MECL 10K receiver interface circuits. The clock is then routed to a clock regeneration circuit where it is regenerated in time and amplitude using phase-lock-loop synthesizer methods. The regenerated 50 MHz clock is then used to reclock the input 50 MBPS data in order to perform amplitude reconstruction and time synchronization of the input data.

The regenerated 50 MHz clock is routed to the encoder timing generator and the 50 MBPS data is routed to the input multiplexer of the encoder network in synchronism with the 50 MHz clock where the 50 MBPS data is serial-to-parallel converted on a 5 bit per byte basis at a 10 megabytes per second rate. Bits are formed into bytes as received.

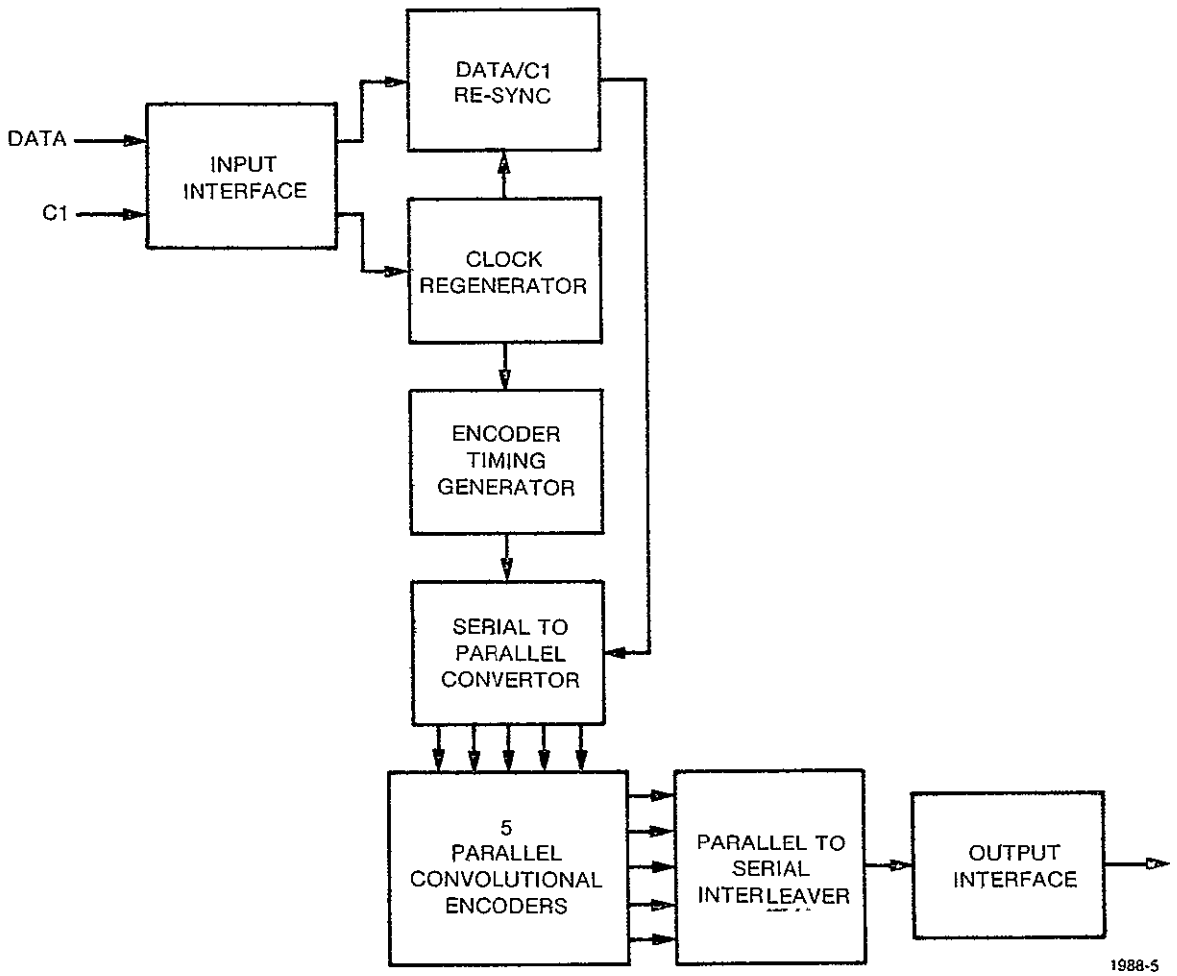

Figure 3-5. High Data Rate Coder

ORIGINAL PAGE IS
OF POOR QUALITY

Thus, the output of the data bit sorter is five 10-MBPS data sources. Each 10-MBPS data source is then convolutionally encoded with the rate $\frac{1}{2}$, constraint length 7 convolutional encoder. The resulting 20 MSPS data from each encoder is routed to an interleaver mux which performs a parallel-to-serial data conversion, again on a 5-bit per byte basis at 20 megabytes per second. Since one encoder symbol from each convolutional encoder is serially outputted every byte time, the resulting output from the interleaving multiplexer is 100 MBPS. Motorola has chosen this interleaving technique for a baseline as it spreads any burst error pattern of the channel to 5-bit spacings before they are decoded by Viterbi decoders that are to be used in the decoder configuration. This will provide some error control improvement should burst errors be encountered in the data transmission. If other requirements should dictate another interleaving pattern, this can also be implemented; however it may not result in the ease of implementation as does the straightforward approach Motorola has taken as the baseline.

The rates given above are all scaled down proportionally for rates less than 50 MBPS. For example, at 4 MBPS the corresponding rates are 4 MHz, 800 kHz, 1.6 MHz and 8 MHz.

The 50 MBPS data conditioning and convolutional encoding circuitry uses a mixture of MECL and LPSTTL logic devices. Whenever good design practices permit, LPSTTL circuitry is used in preference to MECL 10K, circuitry, thereby achieving the performance required without consuming the higher power levels that the MECL circuitry require.

An alternate approach to the baseline encoding configuration described above is presented in Appendix G. While this approach adds complexity to the Orbiter Ku-Band System, it could significantly reduce the complexity of the synchronization problem for the ground data processing of the received data. A relative bit structure of the baseline encoding scheme is also illustrated in Appendix G.

REFERENCE

(1) Weber, C.L., "Feasibility of Candidate Receivers for Ku-Band Communications Signals To and From Shuttle," Axiomatic Report No. R7510-4, October 31, 1975.

2.4 Task #4 - Investigation of Three Channel PM Mode

An approach for simultaneously accommodating three digital channels in the PM mode was selected after considering two different techniques. Each technique would provide for the transmission of the high rate channel (up to 50 Mbps) and two independent low rate channels up to 2 Mbps each.

The comparison of two schemes for implementing a three channel PM mode showed that either the QPSK/QPSK or the frequency multiplexing (Interplex) was satisfactory and that neither had distinctive performance advantages. Thus the selection of the QPSK/QPSK scheme as the preferred choice was made primarily on the basis of implementation. Details of the study are presented in Appendix H.

Additional effort has shown that by proper implementation of the hardware the transmitted signal can be a constant envelope four phase signal. The functional diagram for this scheme is shown on Figure 4-1. The difference between this diagram and Figure 1 of the Appendix is the bandpass filter on the output of the subcarrier QPSK modulator. The limiter is shown to indicate that the balanced modulator is switched by this signal. This is possible because the phase of the zero crossings carries the combined d_2 and d_3 information. Since the input to the quadrature modulator is now bilevel, the output combined with the high rate channel will be an unbalanced QPSK signal rather than the eight phase signal described in the appendix.

The fact that the subcarrier phase will carry the information is shown by writing expressions for the signals at the bandpass filter input:

$$e_1 = a_2\, d_2\, \frac{4}{\pi} \left[\sin \omega_{sc} t + \text{odd harmonics}\right]$$
$$+a_3\, d_3\, \frac{4}{\pi} \left[\cos \omega_{sc} t + \text{odd harmonics}\right]$$

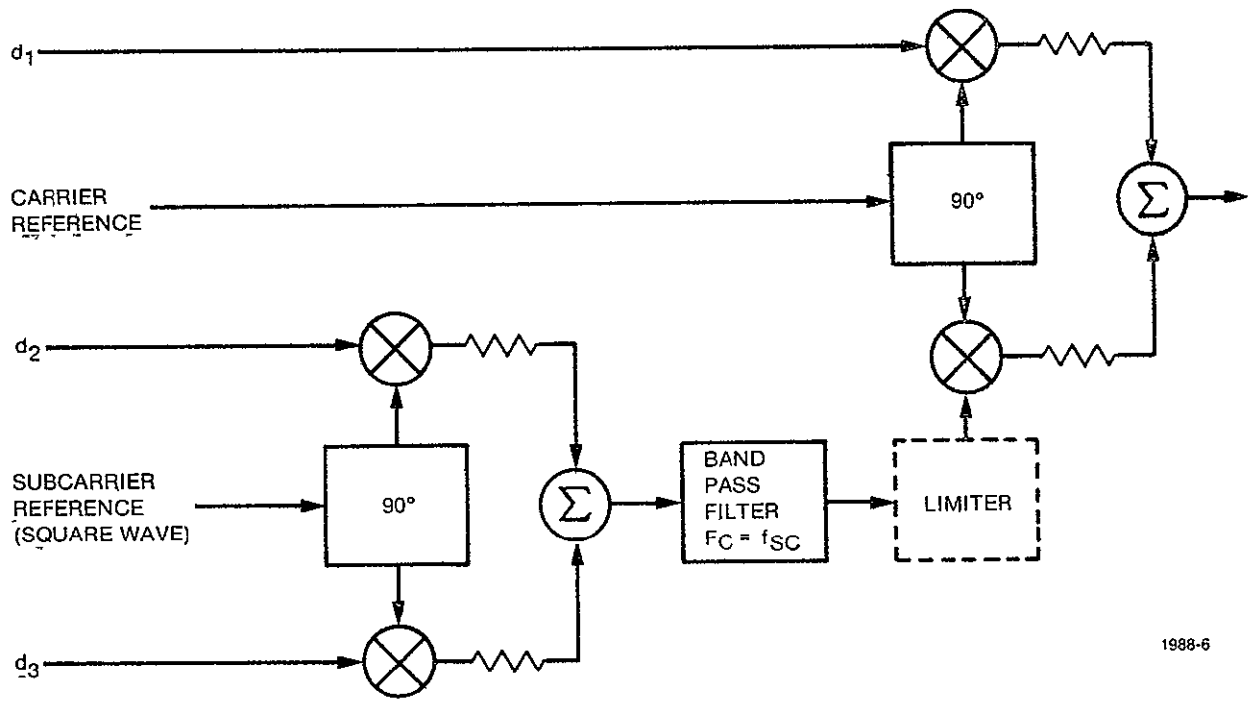

Figure 4-1. Functional Diagram: Modified QPSK/QPSK Mechanization.

ORIGINAL PAGE IS
OF POOR QUALITY

and at the limiter input:

$$e_2 = \frac{4}{\pi} \left[a_2 \, d_2 \sin \omega_{sc} t + a_3 \, d_3 \cos \omega_c t\right]$$

$$= c \sin (\omega_{sc} t + \emptyset)$$

where C is a constant amplitude because d_2 and d_3 have values ± 1 and $a_2^2 + a_3^2 = 1$. The phase $\emptyset = \tan^{-1} \frac{a_3 d_3}{a_2 d_2}$ now has the information from the two channels. Limiting this signal regenerates harmonics of the subcarrier but the zero crossings retain the data. Since the inputs for both are now bilevel, the modulators for the high rate channel and the subcarrier channel can be balanced modulators. If the bandpass filter is omitted, the d_2 and d_3 information is carried on the amplitude of the square wave subcarrier and not the phase which would require that the subcarrier channel use a linear modulator. Removing this requirement simplifies the hardware mechanization and retains the function common to the FM mode.

An additional advantage is that the output signal has no inherent AM. The transmitter output is an unbalanced four phase signal with a constant envelope. Any AM will be the result of bandlimiting rather than being introduced by the modulation scheme. An extension of the analysis of the QPSK/QPSK three channel modulation mechanization examined the effects of large AM/PM conversion coefficients on the high rate channel as well as the subcarrier channel. The results indicate that the amount of crosstalk caused by the AM/PM conversion in the high power TWTA will be small enough so as not to be significant. The values calculated indicate signal to distortion ratios in excess of 60 dB in the low rate channels and in excess of 40 dB in the high rate channel when the source of distortion is AM/PM at the level of 10°/dB.

During the examination of parameters to be included in the performance requirements for the return link equipment it was found that the high power TWTA units being developed would have an AM/PM conversion coefficient of nearly 10°/dB. Since this is larger than has previously been experienced and since its effect on the unbalanced QPSK links was unknown, the following analysis was undertaken. The results show that even with this large conversion coefficient neither the high rate channel nor the subcarrier channel is significantly degraded.

Previous paragraphs in this section showed that the three channel mode can be implemented using balanced modulators. If the diodes in these units could switch instantaneously, the output signal would have a constant envelope, however, the finite switching time causes some AM to appear. This can be examined analytically using the following expression for the output of the modulator:

$$e(t) = p_1 m_1 (t) \cos \omega_o t - p_2 m_2 (t) \sin \omega_o t$$

where

$$p_1^2 + p_2^2 = 1 \text{ and}$$

the power split between phases is $\frac{p_1^2}{p_2^2}$

The signal $m_1(t)$ is the high rate NRZ (± 1) bit stream and $m_2(t)$ is the unbalanced QPSK modulated subcarrier. Because the TWTA produces a phase shift in the signal proportional to the amplitude of the combined QPSK signal the input signal can be written as

$$e(t) = R(t) \cos (\omega_o t + \tan^{-1} (P_2 m_2 / P_1 m_1))$$

where

$$R(t) = (p_1^2 m_1^2 (t) + p_2^2 m_2^2 (t))^{\frac{1}{2}}$$

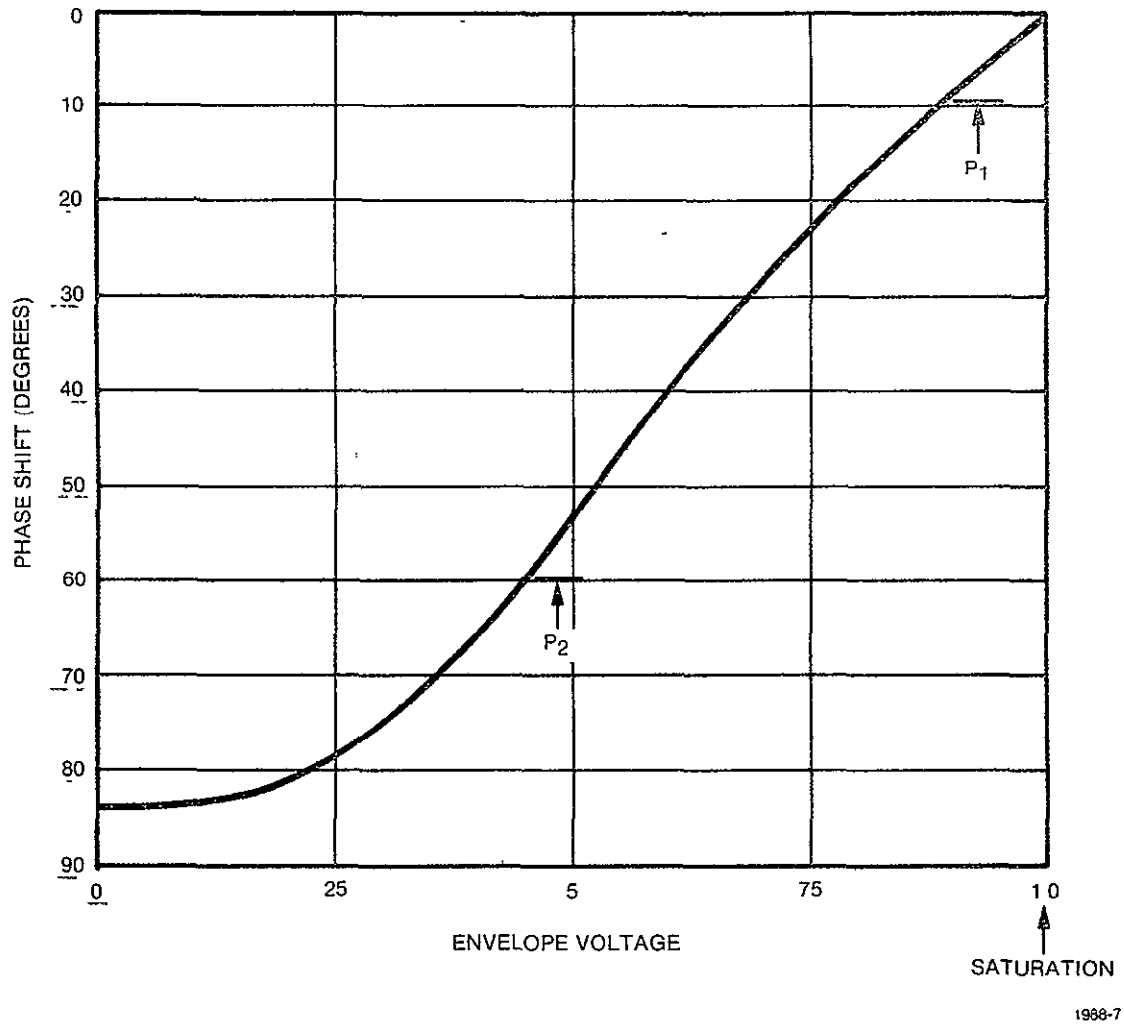

Figure 4-2. TWTA Phase Shift as a Function of Input Amplitude

Then the output of the TWTA can be written as

$$e_o(t) = R(t) \cos (\omega_o t + \tan^{-1} (\frac{p_2 m_2(t)}{p_1 m_1(t)}) + \theta (R(t)).$$

where θ (R(T)) is the phase angle introduced by the TWTA.

The phase shift with amplitude, θ (R(T)), can be estimated from typical TWTA characteristics as provided by manufacturers. Figure 4-2 shows phase shift versus amplitude with the amplitude of 1 being saturation of the TWTA. The effect of AM/PM conversion may then be approximated by considering the three cases:

(1) A transition in modulation $m_1(t)$ while $m_2(t)$ is constant.

(2) A transition in modulation $m_2(t)$ while $m_1(t)$ is constant.

(3) A transition in both $m_1(t)$ and $m_2(t)$ simultaneously.

For case (1) the envelope amplitude goes from 1 to p_2 and back to 1 as m_1 goes from 1 to 0 to -1. In case (2) the minimum envelope is p_1, while in case (3) the minimum envelope is zero.

Of these three, cases (1) and (2) are considered in the following paragraphs. Because case (3) is statistically improbable due to the asynchronous nature of the two modulating signals, its effect will be insignificant and hence is not considered further. Examination of the other situations is begun by writing expressions for the demodulated signals. These are given as:

$$e_i(t) = p_1 m_1(t) \cos \theta(R) - p_2 m_2(t) \sin \theta(r)$$

$$e_q(t) = p_2 m_2(t) \cos \theta(R) + p_1 m_1(t) \sin \theta(R)$$

where it has been assumed that limiting in the receiver will not contribute any significant additional AM/PM conversion.

The effect of case (1) is shown on Figure 4-3 which demonstrates that for each transition of the high rate channel $m_1(t)$ an interfering

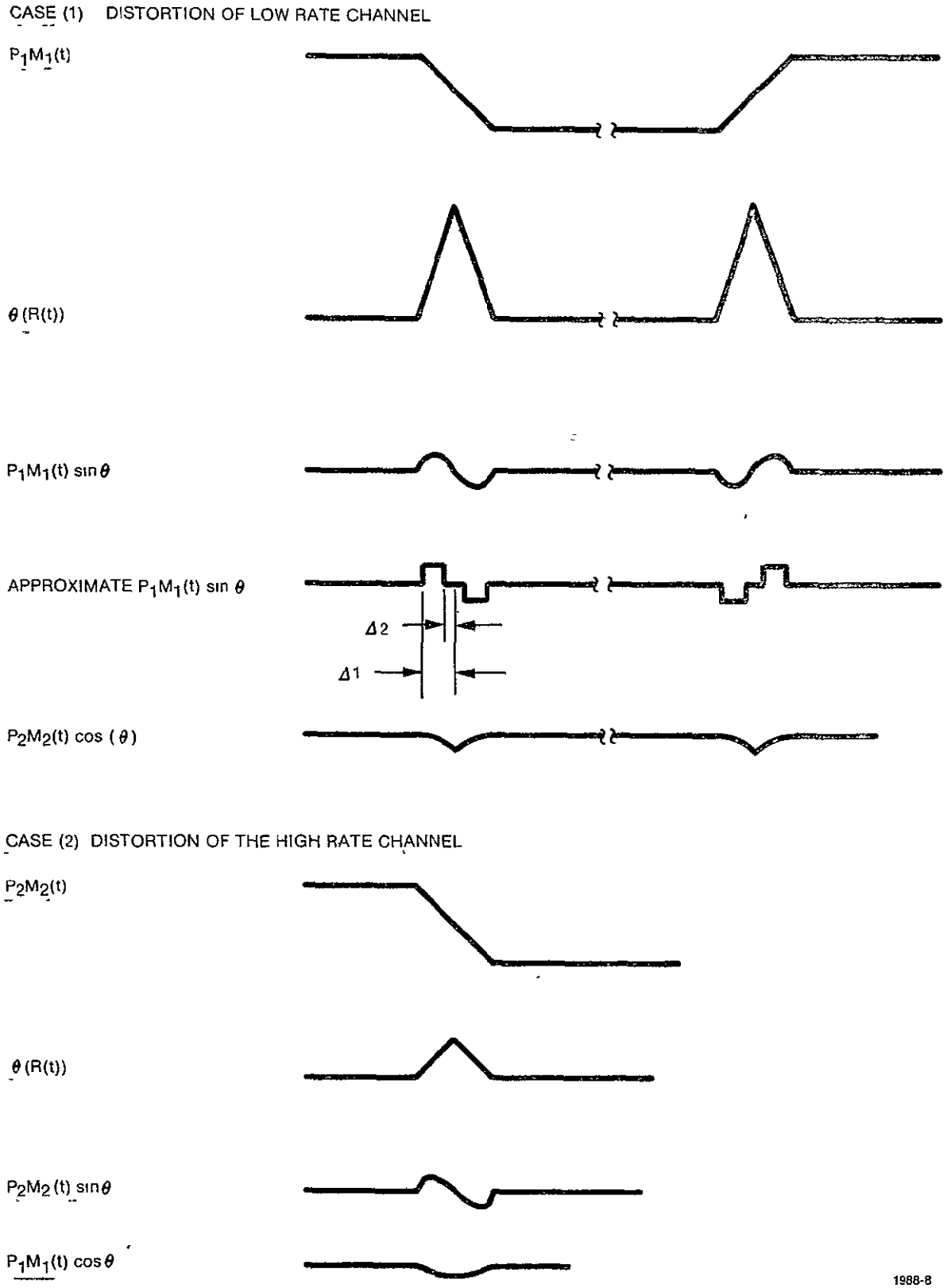

Figure 4-3. Distorting Waveforms

signal is generated in the subcarrier channel. This signal has been approximated as shown and can be written as

$$e_{iq}(t) = g(t+\Delta_1) - g(t+\Delta_2) - g(t-\Delta_2) + g(t-\Delta_1)$$

where $g\ (t+\Delta_1)$ is a delayed version of the data $m_1(t)$. Using this formulation of the crosstalk voltage the correlation function is written:

$$\begin{aligned} R_{e_{tq}}(\tau) = 4R_g(\tau) &- 2(R_g(\tau+\Delta_2 - \Delta_1)+R_g\ (\tau- \Delta_2 +\Delta_1)) \\ &- 2(R_g(\tau-\Delta_2 - \Delta_1)+R_g\ (\tau+ \Delta_2 +\Delta_1)) \\ &+ (R_g(\tau-2\Delta_1) + R_g\ (\tau+2\Delta_1)) \\ &+ (R_g(\tau-2\Delta_2) + R_g\ (\tau+2\Delta_2)) \end{aligned}$$

from which

$$S_{e_{iq}}\ (\omega) = G(\omega)\left[4\ \cos\ (\omega\Delta_1) - \cos\ (\omega\Delta_2)\right]^2$$

where

$$G(\omega) = K^2T\ \frac{\sin^2(\omega T/2)}{(\omega T/2)^2}$$ is the power

spectrum of the data. The magnitude of K is determined from the peak of the interfering term as approximately $0.5\ p_1\ \sin\ (\theta_{max}/2)$.

Evaluating $S_{e_{iq}}\ (\omega)$ at the subcarrier frequency gives the spectral density of this interference from which an equivalent E_b/N can be determined. The following values

$K = 0.5\ (.89)\ \sin\ (70^o/2)$

$T = 1/100$ Msps

$\Delta = 2$ nsec

$\Delta_1 = 7/8\Delta,\ \Delta_2 = 1/8\Delta$

$\omega_{sc} = 2\pi \cdot 8.5$ MHz

yield

$S_{e_{iq}}\ (\omega_{sc}) = -134$ dB/Hz relative to the total power.

In addition to the noise term described above, the signal will also suffer a loss during each transition as indicated on Figure 2. The amount of loss is calculated by integrating over the period of one bit and comparing that energy with the total amount available. The phase shift as shown on Figure 4-3 can be expressed as

$$\theta - \theta_{max} \left(1 - \frac{t}{\Delta} \right)$$

and the energy loss over a period of m_1 as

$$\text{loss} = \frac{2 \int_0^{\Delta} P_2^{\,2} \cos^2\theta(t)dt + \int_{\Delta}^{T-\Delta} P_2^{\,2} dt}{\int_0^T P^2 \, dt}$$

Evaluated for the constants previously listed

$$\text{loss} = 0.88$$

However, since transitions occur with about 50% probability the loss will statistically occur on only one of each pair of bits in the $m_1(t)$ stream so that

$$\text{loss} = \frac{1+.88}{2} \Rightarrow -0.3 \text{ dB}$$

Using the noise of -134 dB/Hz and the loss of 0.3 dB, the signal to noise in a bit rate bandwidth of 2 MHz will still exceed 60 dB as indicated below.

Noise density	-134 dB/Hz
Data rate 2×10^6	63
	- 71 dB
Subcarrier signal level (.2)	- 7 dB
	64 dB
data signal level (.8)	- 1 dB
signal loss	- .3
E_b/N	62.7 dB

Case (2) causes degradation in the high rate channel when a subcarrier transition occurs. In this case one transition will affect a single symbol of the high rate stream rather than several transitions affecting one symbol as was true of case (1). Thus the analysis calculates the desired energy to interfering energy on a single symbol. Approximating the interference in the same way as for case (1) the interfering energy

$$D = 2 \int_{\Delta/8}^{\frac{7}{\Delta 8}} \left(\frac{P_2}{2}\right)^2 \sin^2 (\theta_{max}/2)\, dt$$

and the desired energy $E = p_1^2 T$

The values used for evaluating the ratio E/D are

$P_2^2 = .2,\ P_1^2 = .8$

$T = 1/100$ Msps

$\Delta = 2$ ns

$\theta_{max} = 10^o$

$$\text{Thus } E/D = 10 \log \frac{.8T}{.5\, p_2^2 \sin^2(5^o)\, (\frac{3}{4})\, (.2T)} = 38.5 \text{ dB}$$

Since subcarrier transitions occur at a rate such that approximately 1/6 of the high rate symbols will be affected, the statistical E/D = 46.2 dB.

This signal will also suffer the loss due to the cosine term, however, this loss is less than .05 dB because the value of θ is less than 10°.

The results of analyzing cases (1) and (2) demonstrate that the links can tolerate AM/PM conversion coefficients as large as 10°/dB without significantly degrading the performance.

2.5 Task #5 - Mode Simplification

The feasibility of utilizing only a PM mode or only an FM mode to accommodate all transmission requirements was examined. This investigation demonstrated that a PM mode was feasible while an FM mode was not. The findings tend to reinforce the selection of a dual mode signal design.

2.5.1 PM Mode Investigation

Investigation of techniques which might be used to simplify the return link transmission modes began by considering the PM mode for sending those signals now planned for the FM mode. By using the three channel PM mode, the unbalanced QPSK modulated 8.5 MHz subcarrier will handle the two low rate channels while a digital version of the 4.5 MHz wideband signal will occupy the high rate channel. Since the two low rate channels are combined in the same way as for the 3 channel PM mode, the signal of concern is the video signal. The remainder of the investigation dealt with the problem of digitizing this analog signal and in particular with digitizing a color TV signal.

The simplest method for converting the signal would be direct PCM using a sampling rate in excess of 9M samples/sec. The number of bits per sample needed to assure a commercial grade signal can be found from the following formula (3)

$$S_{pk-pk}/N_{rms} = 10.8 + 6n \text{ dB}$$

where n is the number of bits per sample.

By setting this equation equal to 53 dB and solving for n, seven or more bits are shown to be necessary. This multiplied by the Nyquist rate of 9 Msps shows that data rates exceeding 63 Mbps would be required for direct PCM signaling. Since this is greater than the 50 Mbps capability of the high rate link, some form of data compression must be considered.

Two basic kinds of compression are available, source encoding and transform techniques. Each of these tries to exploit the signal "redundancies" in order to compress the bandwidth (hence, reduce the signalling rate). The result is that application of any technique causes some form of signal degradation. Because the ultimate output is a picture, the effect of this degradation cannot necessarily be measured. Thus the selection of any technique will include some subjective considerations. If the picture statistics are unknown, source encoding probably holds more promise for a high quality picture than the transform techniques. In this case the encoding is adaptive in the sense that for the complex active scene there will be little compression while for a simple quiet scene the most compression occurs. If the scene statistics are known and have a limited range, some specific transform technique may provide a more nearly optimum link, however in most techniques an active scene will overload the transform and the result is a distorted "smeary" picture.

The simplest form of source encoding is differential PCM (DPCM) which uses a linear first order predictor in the encoder. The number of bits per sample needed for this scheme is given by (3):

$$\frac{S_{pk-pk}}{N_{rms}} = 24 + 6n$$

which yields n = 5 for S_{pk-pk}/N_{rms} = 53 dB. This can be used to calculate the signaling rate of 45 Mbps required to transmit the video signals.

If the video signal is NTSC format color TV, a significant portion is devoted to transmitting sync information. Each line is 83% picture and each frame has 93% of the lines with video information. For comparison purposes these values can be used to translate the number of

bits per sample into an equivalent number of bits per pixel as follows:

$$\frac{(5b/\text{sample})\ (m \cdot n\ \frac{\text{sample}}{\text{frame}})}{(.83n\ \frac{\text{pixel}}{\text{line}})\ (.93m\ \frac{\text{line}}{\text{frame}})} = 6.5\ \frac{\text{bits}}{\text{pixel}}$$

which indicates a 30% cost to transmit the sync pattern.

Reports of the Bell System Picturephone (8) indicate that 4 bits/pixel are required to adequately encode the monochrome signal for this system. The direct addition of chrominance to this signal was done at the cost of 1 bit/pixel although another scheme using line average techniques is suggested which will provide color information within the original 4 bits/pixel. Thus a color version of Picturephone requires 4 to 5 bits/pixel. The picture statistics used to design this scheme are primarily portrait scenes which may account for the smaller number of bits/pixel than the 6.5 projected for the NTSC format.

The form of source encoding using the first order linear predictive coder was the only one examined. Other forms of coding which take advantage of the signal statistics might provide additional compression at the cost of more complicated equipment.

Motorola has been investigating the use of image processing using transform techniques and is a present developing equipment which will mechanize the Hadamard Transform. A summary of the study (5, 6) leading to the selection of this method is given on Table 5-1. The amount of signal compression which might be expected from using the H transform can be estimated by adding 30% to the reported 1 bit/pixel and then an additional 1 bit/pixel required for chrominance. This yields an estimated 2.3 bit/pixel or greater than 2 to 1 reduction in the data rate requirement. The cost of this reduction is the complication of transmitting and receiving equipment as well as the more subjective loss of picture quality.

TABLE 5-1. COMPARISON OF VARIOUS IMAGE CODING TECHNIQUES

TECHNIQUE	ADVANTAGES	DISADVANTAGES	B/P
* SVD	Maximum energy compaction	Prohibitive numerical complexity	0.05
KL	Statistically Optimal (MSE)	Numerically inefficient	0.30
* CØS/DPCM	Almost as good as KL Economical CZT/CCD implementation	CCD hardware problems yet to be solved. Successful in 1-2 years.	0.40
CØS/CØS	Slightly inferior to CØS/DPCM Economical CZT/CCD implementation	CCD problems. Success in 1-2 years. Large memory requirement.	0.50
F/F	Numerically efficient FFT algorithm	Memory requirement depending on block size. Slow-scan TV depending on multiply speed.	0.60
S/S	Numerically efficient FST algorithm	"	0.70
H/H	Numerically efficient FHT algorithm with only additions.	Memory requirement depending on block size, (H/DPCM does not have this disadvantage)	1.00
A/A	Numerically efficient FAT algorithm with few special multiplications.	Memory requirement depending on block size. Less noise immunity than H.	1.20
CAQ	Simple implementation	Sensitive to noise	1.20
DPCM	Simple implementation	Sensitive to noise	2.00
DM	Simplest implementation	Sensitive to noise. Needs to be sampled densely to overcome slope distortion (Adaptive DM possible)	3.00

*H. Whitehouse and R. Means of NUC claim that CØS/DPCM perform slightly better than CØS/CØS.

ORIGINAL PAGE IS
OF POOR QUALITY

TABLE 5-1. GLOSSARY

SVD	Singular Value Decomposition
KL	Karhunen - Loève
COS	Cosine Transform
DPCM	Differential Pulse Code Modulation
F/F	Fast Fourier Transform
S/S	Fast Slant Transform
H/H	Hadamard Transform
A/A	Haar Transform
CAQ	Constant Area Quantization
DM	Delta Modulation

The investigation of the use of the three channel PM mode for transmitting the FM mode signals has shown that all the services can be provided within the constraints assumed. In particular it was shown that a digitized version of the TV signal can be transmitted within the 50 Mbps capability of the link. If greater bandwidth compression is required there are several alternatives available. Whether or not any of these is adequate can be determined only by subjective testing of the resulting picture.

2.5.2 FM Mode Investigation

The feasibility of using the FM mode to accommodate all the requirements was examined in two ways. In the first, the parameters of the FM mode were used to determine the maximum rate at which data can be transmitted. In the second, the parameters of a multitone FSK system were computed and compared with PSK and DPSK systems.

Parameters of the FM mode are an RF bandwidth of 40 MHz, video baseband bandwidth of 4 5 MHz, and peak deviation due to the video of 11MHz. At the received carrier to noise density of 90 dB-Hz, the signal to noise ratio in the detected baseband will be 34.5 dB This is calculated from the strong signal FM analysis·

$$S/N = \frac{3}{2} \quad \frac{\Delta f^2}{f_m^3} \quad \cdot \quad \frac{C}{n}$$

Data can be transmitted as a video signal by using multilevel signals. The number of levels and the signal to noise ratio which determine the symbol error performance that can be expected are related by the expression (11)

$$P_e = \frac{n-1}{n} \left[1-\mathrm{erf} \left(\frac{3}{2(n^2-1)} \cdot \frac{S}{N} \right)^{\frac{1}{2}} \right]$$

where n is the number of levels. By appropriate coding, the relationship between symbol errors and bit errors at low error rates is given by $P_{eb} = P_e/\log_2 n$. **Figure 5-1** shows the number of levels which can be used if a bit error rate of 10^{-6} is to be achieved at a given signal to noise ratio. This data shows that the maximum value that the FM mode can use is 4 bits (i.e. 16 levels). Since the baseband bandwidth is restricted to 4.5 MHz, the Nyquist sampling rate is 9M samples/sec Thus, at 4 bits per symbol and 9M samples/sec, the maximum data rate will be 36 Mbps which falls short

ORIGINAL PAGE IS
OF POOR QUALITY

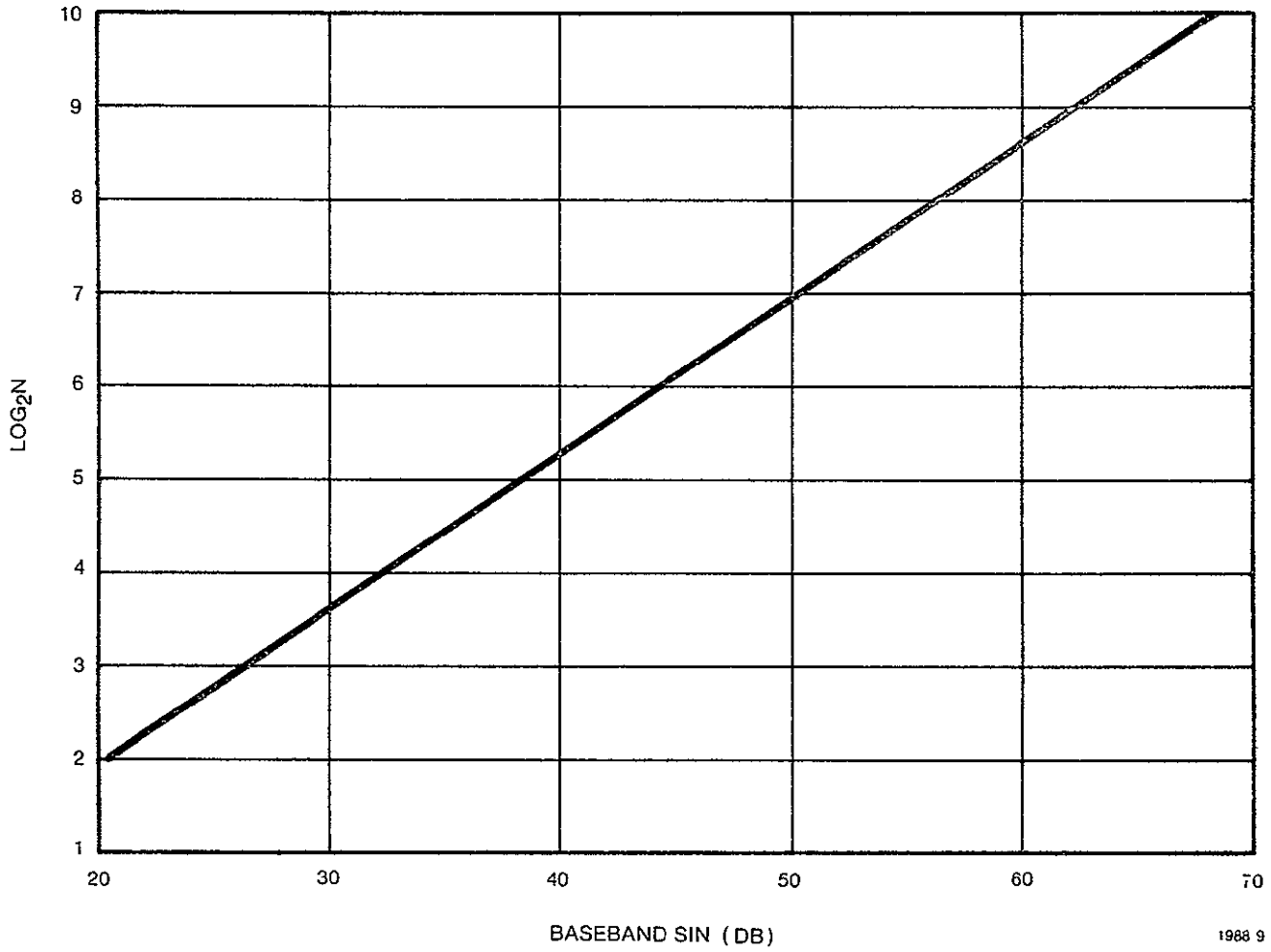

Figure 5-1. Number of Bits Allowable to Attain 10^{-6} BER at a Given S/N.

of the desired 50 Mbps rate. In addition some provision would have to be made for synchronizing each symbol so that the true information rate would be less than the 36 Mbps. Hence, in order for this form of signaling to be useful, some form of encoding would have to be applied which would remove any data redundancies

Orthogonal multitone FM was also examined. For this portion of the analysis, the FM mode parameters were not used. The results of the analysis are shown on Figure 5-2 which plots the data of Table 5-2. This shows that orthogonal multitone FSK using 4, 8, or 16 tones would meet the requirements of the Shuttle link It also indicates the additional bandwidth needed as the number of tones increases Data for this curve is derived from the expression for symbol error probability (12)

$$P_e = \sum_{k=1}^{M-1} (-1)^{k-1} \binom{M-1}{k} \frac{1}{k+1} \exp(-\gamma k/k+1)$$

where M is the number of tones and γ is the signal to noise ratio per symbol. This expression can be evaluated for E_b/N_o using the relationship $E_b/N_o = \gamma/\log_2 M$. Because a symbol error results strictly in any other symbol as the output, the bit error rate is related to the symbol error rate as:

$$P_{eb} = \frac{1}{2} \frac{P_e}{1-(1/M)}$$

The bandwidth requirement for this form of signaling is given by

$$B = \frac{M}{T_b \log_2 M} \quad \text{or } BT_b = M/\log_2 M$$

Tabulating P_{eb} and BT_b for values of $\log_2 M$ ranging from 1 through 5 yields Figure 5-2. Thus at a given E_b/N_o and data rate the amount of margin can be seen for any number of tones For example, the Shuttle link

ORIGINAL PAGE IS
OF POOR QUALITY

TABLE 5-2. SYSTEM COMPARISON

		E_b/N_o at $P_{eb}=10^{-6}$		
k	$M=2^k$	Coherent PSK	DPSK	Multitone FSK
1	2	10.5 dB	11.2 dB	13.9 dB
2	4	10.5	12.8	11.2
3	8	14.0	16.8	9.6
4	16	18.4	21.4	8.6
5	32	23.4	26.4	7.8
BT_b		1/k	1/k	$2^k/k$

B = signaling bandwidth

T_b= time per data bit

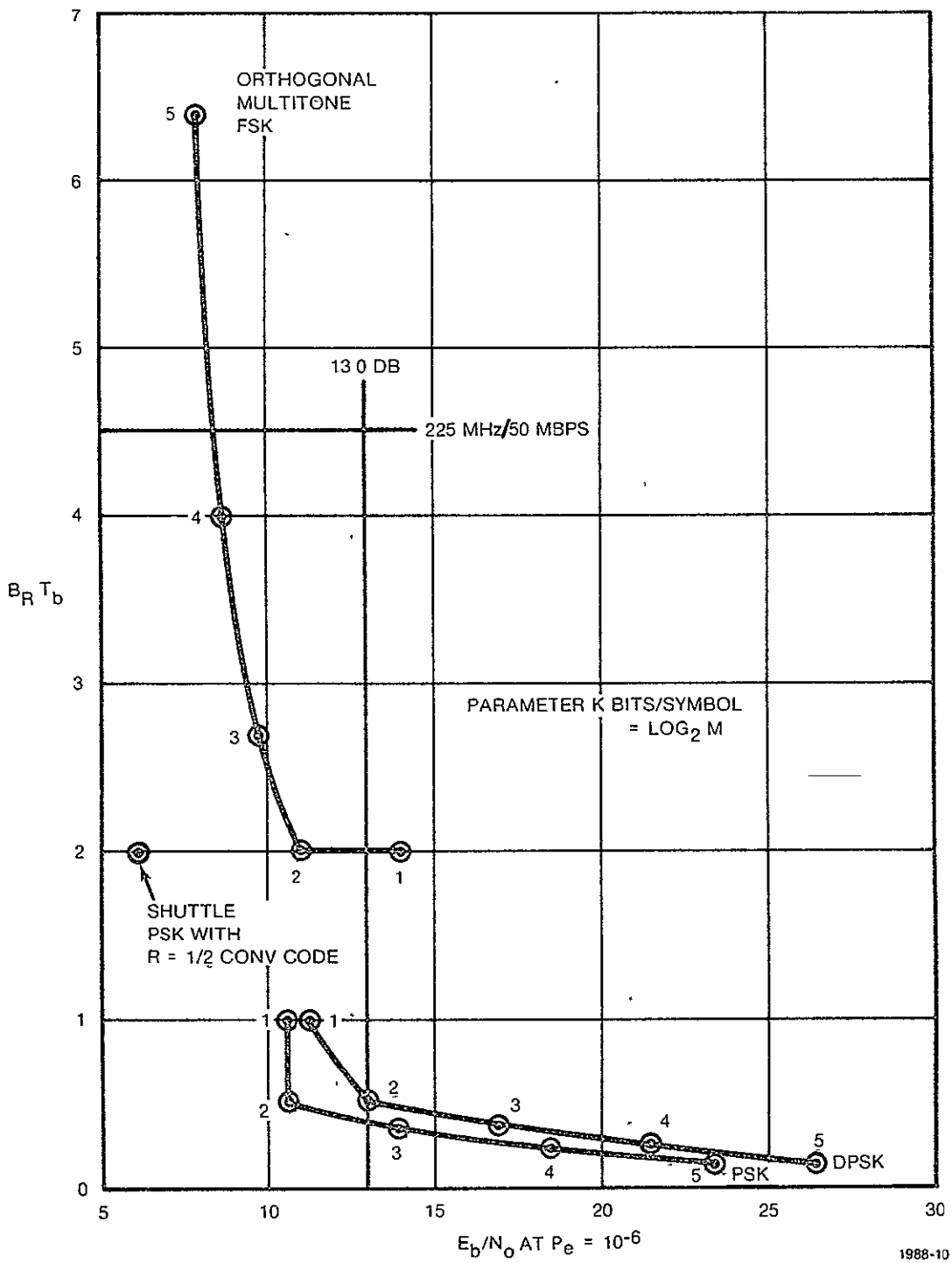

Figure 5-2. System Comparison

ORIGINAL PAGE IS
OF POOR QUALITY

E_b/N_o at 50 Mbps is about 13 dB, thus this link will support signal structures requiring less than this value as indicated for values of $\log_2 M \geqslant 2$. The bandwidth restriction of 225 MHz, however, eliminates the k=5 (32 tones) system, leaving systems of 4, 8, or 16 tones as possibilities. Of note is the small gain in margin for large bandwidth increases in going from the small number of tones to the larger number.

For purposes of comparison both M-ary PSK and DPSK systems are shown on the same chart. The expressions used for computing the data are

$$\text{for PSK}: \quad P_e = 1 - \frac{1}{2\pi} \int_{-\pi/m}^{\pi/m} \exp(-\gamma) \left[1 + \sqrt{4\pi\gamma}\, \cos\theta \exp(\gamma \cos^2\theta)\, \Phi(\sqrt{2\gamma}\cos\theta)\right] d\theta$$

$$\text{where } \Phi(X) = \frac{1}{\sqrt{2\pi}} \int_{-\infty}^{x} \exp(-X^2/2)\, dx$$

and M and γ are as previously defined

$$\text{for DPSK}: \quad P_e = \frac{1}{2} e^{-\gamma}, \quad M=2$$

$$P_e = \operatorname{erfc}(\sqrt{2\gamma} \sin \pi/2M), \quad M > 2$$

In these cases E_b/N_o is related to γ as given before, but $P_{eb} = P_e/\log_2 M$. Data for both are listed on Table 5-1 where the E_b/N_o to achieve a P_{eb} of 10^{-6} is given for several values of M. The comparative bandwidth is given by

$$B = 1/T_b \log_2 M \text{ or } BT_b = 1/\log_2 M$$

By including these two systems on the same graph with the FSK system, the trade off between bandwidth and signal energy is very apparent. FSK gives improved sensitivity at the expense of bandwidth, while PSK and DPSK conserve bandwidth at the expense of signal level.

One additional data point is also included on the graph, showing the operating point for the PM mode of the Shuttle baseline design. This demonstrates that the effect of the convolutional encoder is to significantly increase the signaling margin using the same bandwidth as a 4 tone FSK system.

BIBLIOGRAPHY

1. Poo, Zung, "Study of Efficient Video Compression Algorithms for Space Shuttle Applications," Linkabit Corp. June 1975.

2. Landau, H. J., and D. Slepian, "Some Computer Experiments in Picture Processing for Bandwidth Reduction," BSTJ, Vol. 50., No. 5, May-June 1971.

3. O'Neal, J. B. Jr., "Predictive Quantizing Systems (Differential Pulse Code Modulation) for the Transmission of Television Signals, BSTJ, Vol. 45, No. 5, May-June 1966.

4. Perkins, F. A., and G. C. Clark, "Performance of a Digital TV System, Part 1: Source Encoding, Part II: Channel Encoding" National Telemetering Conference Record, Dec. 1972.

5. Daniel, A.M., "Definition of an RPV Bandwidth Compression System," Final Report for Motorola ESP No. 510-294, Dec. 1975.

6. ----, "Survey of Image Coding Techniques," Final Report for Motorola ESP No. 510-270, June 1975.

7. Golding, L.D., and R.K. Garlow, "Frequency Interleaved Sampling of a Colar Television Signal" IEEE Transactions on Communication Technology, Vol. COM-19, No. 6, Dec. 1971.

8. Limb, J.O., C.B. Rubinstein, and K.A. Walsh, "Digital Coding of Colar Picturephone Signals by Element - Differential Quantization," IEEE Transactions on Communications Technology, Vol. COM-19, No. 6, Dec. 1971.

9. ----, "The Picturephone System," BSTJ, Vol. 50, No. 2, February 1971.

10. ----, "Video Processing," IEEE Transactions on Communication Technology, Vol. COM-19, No. 6, December 1971.

11. Bennett, W. R., and J.R. Davey, Data Transmission, Chapter 11, McGraw Hill, 1965.

12. Stein, S., and J. J. Jones, Modern Communication Principles, Chapter 14, McGraw Hill, 1967.

APPENDIX A

LINK MARGIN

DEC 1976
RECEIVED
NASA STI FACILITY
INPUT BRANCH

INPUT PARAMETER LIST

1.	ORBITER TRANS POWER (WATTS)	50.000	RI ORBITER DESIGN SPEC
2.	ORBITER TRANS LOSS (DB)	2.7000	ANALYSIS, MOTOROLA
3.	ORBITER TRANS ANT GAIN (DB)	38.400	ANALYSIS, MOTOROLA
4.	ORBITER TRANS FREQ (GHZ)	15.080	SPECIFICATION
5.	PATH LENGTH (NAUTICAL MILES)	22786.	TDRSS USER'S GUIDE
6.	TDRS ANT POINTING LOSS (DB)	.50000	TDRSS USER'S GUIDE
7.	POLARIZATION LOSS (DB)	.50000	TDRSS USER'S GUIDE
8.	TDRS RECEIVE ANT GAIN (DB)	52.600	TDRSS USER'S GUIDE
9.	TDRS AUTO TRACK LOSS (DB)	1.0000	RI ORBITER DESIGN SPEC
10.	TDRS SYSTEM NOISE TEMP (DEG K)	708.00	RI ORBITER DESIGN SPEC
11.	TDRS S/N DEGRADATION (DB)	2.0000	TDRSS USER'S GUIDE
12.	FM THRESHOLD (DB)	10.000	ANALYSIS, MOTOROLA
13.	PREDETECTION BANDWIDTH (MHZ)	36.000	ANALYSIS, MOTOROLA
14.	TV BANDWIDTH (MHZ)	4.5000	BASELINE SPECIFICATION
15.	TV MODULATION DEVIATION (MHZ)	11.000	ANALYSIS, MOTOROLA
16.	TV REQUIRED OUTPUT S/N RATIO (DB)	26.000	RI DESIGN GOAL
17.	DATA SUBCXR FREQ (MHZ)	8.5000	BASELINE SPECIFICATION
18.	DATA SUBCXR DEVIATION (MHZ)	6.0000	ANALYSIS, MOTOROLA
19.	192 KBPS SUBCXR POWER SHARE (%)	20.000	RI ORBITER DESIGN SPEC
20.	2 MBPS SUBCXR POWER SHARE (%)	80.000	RI ORBITER DESIGN SPEC
21.	BER FOR 192 KBPS CHAN	.10000E-03	RI ORBITER DESIGN SPEC
22.	BER FOR 2 MBPS MODE 2 CHAN	.10000E-05	RI ORBITER DESIGN SPEC
23.	DISC S/N DATA CHAN DEGRADATION (DB)	1.0000	ANALYSIS, MOTOROLA
24.	TV CROSSTALK LOSS IN DATA CHAN (DB)	2.0000	ANALYSIS, MOTOROLA
25.	192 KBPS BIT SYNC LOSS (DB)	2.5000	RI ORBITER DESIGN SPEC
26.	2 MBPS BIT SYNC LOSS (DB)	3.0000	RI ORBITER DESIGN SPEC
27.	BER FOR 2 MBPS MODE 1 CHAN	.10000E-03	RI ORBITER DESIGN SPEC
28.	BER FOR 50 MBPS MODE 1 CHAN	.10000E-05	RI ORBITER DESIGN SPEC
29.	50 MBPS BIT SYNC LOSS, (DB)	4.5000	RI ORBITER DESIGN SPEC
30.	CODING GAIN (V=2, K=7), (DB)	4.0000	RI ORBITER DESIGN SPEC
31.	POWER SHARE 50 MBPS CHAN (%)	80.000	BASELINE SPECIFICATION
32.	POWER SHARE 2 MBPS CHAN (%)	20.000	BASELINE SPECIFICATION
33.	BANDPASS LOSS 50 MBPS, (DB)	.70000	ANALYSIS, MOTOROLA

13:24 NOV 15,'76

ORIGINAL PAGE IS OF POOR QUALITY

ORIGINAL PAGE IS
OF POOR QUALITY

CIRCUIT MARGIN SUMMARY FOR KU-BAND 50 MBPS CHANNEL, MODE 1, RETURN LINK

1	ORBITER TRANSMIT POWER (50 WATTS), DBW	17.0	
2	ORBITER TRANSMIT LOSS, DB	-2.7	
3	ORBITER TRANSMIT ANT GAIN, DB	38.4	
4	ORBITER EIRP, DBW		52.7
5	SPACE LOSS(15.08 GHZ, 22786. N. MI.), DB	-208.5	
6	TDRS ANT POINTING LOSS, DB	-.5	
7	POLARIZATION LOSS, DB	-.5	
8	TDRS RECEIVE ANT GAIN, DB	52.6	
9	CIRCUIT LOSS (INCLUDED IN ANT GAIN)		
10	TDRS AUTO-TRACK LOSS, DB	-1.0	
11	TOTAL REC POWER, DBW		-105.2
12	CHANNEL MODULATION LOSS(80% PWR), DB	-1.0	
13	RECEIVED CHANNEL POWER(50MBPS CHAN), DBW		-106.2
14	TDRS SYSTEM NOISE TEMP (10LOG 708 DEG K), DB-K	28.5	
15	BOLTZMANN'S CONSTANT (10LOG 1.38E-23), DBW/K-HZ	-228.6	
16	TDRS NOISE SPECTRAL DENSITY, DBW/HZ		-200.1
17	TOTAL REC PWR/NOISE SPECTRAL DENS, DB-HZ		93.9
18	BIT-RATE BANDWIDTH (10 LOG(50 MBS), DB-HZ	77.0	
19	S/N IN BIT-RATE BANDWIDTH, DB		16.9
20	THEORETICAL EB/NO FOR 1.E-06 BER, DB	10.5	
21	BANDLIMITING EFFECT DEGRADATION, DB	-.7	
22	BIT SYNC DEGRADATION, DB	-4.5	
23	CODING GAIN (V=2, K=7), DB	4.0	
24	TDRS S/N DEGRADATION, DB	-2.0	
25	REQUIRED EB/NO, DB		13.7
26	CIRCUIT MARGIN, DB		3.2
27	DESIRED MARGIN, DB	3.0	
28	UNALLOCATED CIRCUIT MARGIN, DB		.2

13:24 NOV 15,'76

CIRCUIT MARGIN SUMMARY FOR KU-BAND 2 MBPS CHANNEL, MODE 1, RETURN LINK

1	ORBITER TRANSMIT POWER (50 WATTS), DBW	17.0	
2	ORBITER TRANSMIT LOSS, DB	-2.7	
3	ORBITER TRANSMIT ANT GAIN, DB	38.4	
4	ORBITER EIRP, DBW		52.7
5	SPACE LOSS(15.08 GHZ, 22786. N. MI.), DB	-208.5	
6	TDRS ANT POINTING LOSS, DB	-.5	
7	POLARIZATION LOSS, DB	-.5	
8	TDRS RECEIVE ANT GAIN, DB	52.6	
9	CIRCUIT LOSS (INCLUDED IN ANT GAIN)		
10	TDRS AUTO-TRACK LOSS, DB	-1.0	
11	TOTAL REC POWER, DBW		-105.2
12	CHANNEL MODULATION LOSS(20% PWR), DB	-7.0	
13	RECEIVED CHANNEL POWER(2MBPS CHAN), DBW		-112.2
14	TDRS SYSTEM NOISE TEMP (10LOG 708 DEG K), DB-K	28.5	
15	BOLTZMANN'S CONSTANT (10LOG 1.38E-23), DBW/K-HZ	-228.6	
16	TDRS NOISE SPECTRAL DENSITY, DBW/HZ		-200.1
17	TOTAL REC PWR/NOISE SPECTRAL DENS, DB-HZ		87.9
18	BIT-RATE BANDWIDTH (10 LOG(2 MBS), DB-HZ	63.0	
19	S/N IN BIT-RATE BANDWIDTH, DB		24.9
20	THEORETICAL EB/NO FOR 1.E-04 BER, DB	8.4	
21	BIT SYNC DEGRADATION, DB	-3.0	
22	TDRS S/N DEGRADATION, DB	-2.0	
23	REQUIRED EB/NO, DB		13.4
24	CIRCUIT MARGIN, DB		11.5
25	DESIRED MARGIN, DB	3.0	
26	UNALLOCATED CIRCUIT MARGIN, DB		8.5

13:24 NOV 15,'76

CIRCUIT MARGIN SUMMARY FOR KU-BAND CARRIER THRESHOLD, MODE 2, RETURN LINK

1	ORBITER TRANSMIT POWER (50 WATTS), DBW	17.0	
2	ORBITER TRANSMIT LOSS, DB	-2.7	
3	ORBITER TRANSMIT ANT GAIN, DB	38.4	
4	ORBITER EIRP, DBW		52.7
5	SPACE LOSS(15.08 GHZ, 22786. N. MI.), DB	-208.5	
6	TDRS ANT POINTING LOSS, DB	-.5	
7	POLARIZATION LOSS, DB	-.5	
8	TDRS RECEIVE ANT GAIN, DB	52.6	
9	CIRCUIT LOSS (INCLUDED IN ANT GAIN)		
10	TDRS AUTO-TRACK LOSS, DB	-1.0	
11	TOTAL REC POWER, DBW		-105.2
12	TDRS SYSTEM NOISE TEMP (10LOG 708 DEG K), DB-K	28.5	
13	BOLTZMANN'S CONSTANT (10LOG 1.38E-23), DBW/K-HZ	-228.6	
14	TDRS NOISE SPECTRAL DENSITY, DBW/HZ		-200.1
15	TOTAL REC PWR/NOISE SPECTRAL DENS, DB-HZ		94.9
16	TDRS S/N DEGRADATION, DB	-2.0	
17	NET USEABLE REC PWR/NOISE DENS, DB-HZ		92.9
18	FM THRESHOLD, DB	10.0	
19	PREDETECTION BW (36 MHZ), DB-HZ	75.6	
20	FM THRESHOLD MARGIN, DB		7.3
21	DESIRED MARGIN, DB	3.0	
22	UNALLOCATED THRESHOLD MARGIN, DB		4.3

13:24 NOV 15,'76

ORIGINAL PAGE IS
OF POOR QUALITY

CIRCUIT MARGIN SUMMARY FOR KU-BAND TV CHANNEL, MODE 2, RETURN LINK

1	ORBITER TRANSMIT POWER (50 WATTS), DBW	17.0	
2	ORBITER TRANSMIT LOSS, DB	-2.7	
3	ORBITER TRANSMIT ANT GAIN, DB	38.4	
4	ORBITER EIRP, DBW		52.7
5	SPACE LOSS(15.08 GHZ, 22786. N. MI.), DB	-208.5	
6	TDRS ANT POINTING LOSS, DB	-.5	
7	POLARIZATION LOSS, DB	-.5	
8	TDRS RECEIVE ANT GAIN, DB	52.6	
9	CIRCUIT LOSS (INCLUDED IN ANT GAIN)		
10	TDRS AUTO-TRACK LOSS, DB	-1.0	
11	TOTAL REC POWER, DBW		-105.2
12	TDRS SYSTEM NOISE TEMP (10LOG 708 DEG K), DB-K	28.5	
13	BOLTZMANN'S CONSTANT (10LOG 1.38E-23), DBW/K-HZ	-228.6	
14	TDRS NOISE SPECTRAL DENSITY, DBW/HZ		-200.1
15	TOTAL REC PWR/NOISE SPECTRAL DENS, DB-HZ		94.9
16	TDRS S/N DEGRADATION, DB	-2.0	
17	NET USEABLE REC PWR/NOISE DENS, DB-HZ		92.9
18	PREDETECTION BW (36 MHZ), DB-HZ	75.6	
19	PREDETECTION C/N RATIO, DB		17.3
20	FM IMPROVEMENT (B=4.5 MHZ, DEV=11.0 MHZ), DB	18.6	
21	OUTPUT SIGNAL/NOISE RATIO, DB		35.9
22	REQUIRED OUTPUT SIGNAL/NOISE RATIO, DB	26.0	
23	TV MARGIN, DB		9.9
24	DESIRED MARGIN, DB	3.0	
25	UNALLOCATED TV MARGIN, DB		6.9
26	UNALLOCATED LINK MARGIN (FM THRESHOLD), DB		4.3

CIRCUIT MARGIN SUMMARY FOR KU-BAND 2 MBPS CHANNEL, MODE 2, RETURN LINK

1	ORBITER TRANSMIT POWER (50 WATTS), DBW	17.0	
2	ORBITER TRANSMIT LOSS, DB	-2.7	
3	ORBITER TRANSMIT ANT GAIN, DB	38.4	
4	ORBITER EIRP, DBW		52.7
5	SPACE LOSS(15.08 GHZ, 22786. N. MI.), DB	-208.5	
6	TDRS ANT POINTING LOSS, DB	-.5	
7	POLARIZATION LOSS, DB	-.5	
8	TDRS RECEIVE ANT GAIN, DB	52.6	
9	CIRCUIT LOSS (INCLUDED IN ANT GAIN)		
10	TDRS AUTO-TRACK LOSS, DB	-1.0	
11	TOTAL REC POWER, DBW		-106.2
12	TDRS SYSTEM NOISE TEMP (10LOG 708 DEG K), DB-K	28.5	
13	BOLTZMANN'S CONSTANT (10LOG 1.38E-23), DBW/K-HZ	-228.6	
14	TDRS NOISE SPECTRAL DENSITY, DBW/HZ		-200.1
15	TOTAL REC PWR/NOISE SPECTRAL DENS, DB-HZ		94.9
16	TDRS S/N DEGRADATION, DB	-2.0	
17	NET USEABLE REC PWR/NOISE DENS, DB-HZ		92.9
18	DISC FM IMPROVEMENT, DB	-6.0	
19	TOTAL SUB-CXR PWR/NOISE SPECTRAL DENS, DB-HZ		86.8
20	CHANNEL MODULATION LOSS(80% PWR), DB	-1.0	
21	POST DETECTION CHAN SIG/NOISE DENS, DB-HZ		85.9
22	BIT-RATE BANDWIDTH (10 LOG(2 MBS), DB-HZ	63.0	
23	S/N IN BIT-RATE BANDWIDTH, DB		22.8
24	THEORETICAL EB/NO FOR 1.E-06 BER, DB	10.5	
25	DISC S/N DEGRADATION, DB	-1.0	
26	TV CROSSTALK LOSS, DB	-2.0	
27	BIT SYNC DEGRADATION, DB	-3.0	
28	REQUIRED EB/NO, DB		16.5
29	DATA LINK MARGIN, DB		6.3
30	DESIRED MARGIN, DB	3.0	
31	UNALLOCATED DATA MARGIN, DB		3.3

13:24 NOV 15,'76

CIRCUIT MARGIN SUMMARY FOR KU-BAND 192 KBPS CHANNEL, MODE 2, RETURN LINK

1	ORBITER TRANSMIT POWER (50 WATTS), DBW	17.0	
2	ORBITER TRANSMIT LOSS, DB	-2.7	
3	ORBITER TRANSMIT ANT GAIN, DB	38.4	
4	ORBITER EIRP, DBW		52.7
5	SPACE LOSS(15.08 GHZ, 22786. N. MI.), DB	-208.5	
6	TDRS ANT POINTING LOSS, DB	-.5	
7	POLARIZATION LOSS, DB	-.5	
8	TDRS RECEIVE ANT GAIN, DB	52.6	
9	CIRCUIT LOSS (INCLUDED IN ANT GAIN)		
10	TDRS AUTO-TRACK LOSS, DB	-1.0	
11	TOTAL REC POWER, DBW		-105.2
12	TDRS SYSTEM NOISE TEMP (10LOG 708 DEG K), DB-K	28.5	
13	BOLTZMANN'S CONSTANT (10LOG 1.38E-23), DBW/K-HZ	-228.6	
14	TDRS NOISE SPECTRAL DENSITY, DBW/HZ		-200.1
15	TOTAL REC PWR/NOISE SPECTRAL DENS, DB-HZ		94.9
16	TDRS S/N DEGRADATION, DB	-2.0	
17	NET USEABLE REC PWR/NOISE DENS, DB-HZ		92.9
18	DISC FM IMPROVEMENT, DB	-6.0	
19	TOTAL SUB-CXR PWR/NOISE SPECTRAL DENS, DB-HZ		86.8
20	CHANNEL MODULATION LOSS(20% PWR), DB	-7.0	
21	POST DETECTION CHAN SIG/NOISE DENS, DB-HZ		79.8
22	BIT-RATE BANDWIDTH (10 LOG(192 KBS), DB-HZ	52.8	
23	S/N IN BIT-RATE BANDWIDTH, DB		27.0
24	THEORETICAL EB/NO FOR 1.E-04 BER, DB	8.4	
25	DISC S/N DEGRADATION, DB	-1.0	
26	TV CROSSTALK LOSS, DB	-2.0	
27	BIT SYNC DEGRADATION, DB	-2.5	
28	REQUIRED EB/NO, DB		13.9
29	DATA LINK MARGIN, DB		13.1
30	DESIRED MARGIN, DB	3.0	
31	UNALLOCATED DATA MARGIN, DB		10.1
32	UNALLOCATED LINK MARGIN (FM THRESHOLD), DB		4.3

13:24 NOV 15,'76

STOP 0

APPENDIX B

BIT DETECTION PERFORMANCE DEGRADATION PARAMETERS

APPENDIX B

Bit Detection Performance Degradation Parameters

Several of the parameters which have been identified as degrading factors in the list detection performance have been examined parametrically. The results of these analyses are presented in the following paragraphs.

1. Sync Jitter

The degradation in performance of an optimum detector operating with a noisy sync reference is described in detail in Chapter 9 of "Telecommunication Systems Engineering" by Lindsey and Simon. The results of their analysis of this problem for the specific cases of NRZ and biphase L signaling are presented in graphical form. Figures B-1 and B-2 show the average P_E for NRZ and biphase L, respectively, with the rms jitter as a parameter. These are computed by numerically integrating

$$P_E = \int_\lambda P(\lambda)\ P_E\ (\lambda)\ d\lambda$$

The appropriate probability density and error rate functions are:

for NRZ

$$p(\lambda) = \frac{\exp\left[\cos 2\pi\lambda/(2\pi\sigma_y)^2\right]}{I_o\left[(1/2\pi\sigma_y)^2\right]}\ ;\ |\lambda| \leq \tfrac{1}{2}$$

$$P_E(\lambda) = \tfrac{1}{4}\ \{\mathrm{erfc}(\sqrt{R_d}) + \mathrm{erfc}\ [\sqrt{R_d}(1-2|\lambda|)]\}$$

for biphase L

$$p(\lambda) = \frac{2\exp\left[\cos 4\pi\lambda/(4\pi\sigma y)^2\right]}{I_o\left[(1/4\pi\sigma y)^2\right]}$$

$$P_E(\lambda) = \tfrac{1}{4}\ \{\mathrm{erfc}[\sqrt{R_d}(1-2|\lambda|)] + \mathrm{erfc}[\sqrt{R_d}(1-4|\lambda|)]\}$$

where R_d = energy per bit to noise density ratio

λ = fractions of a bit period

$\sigma_{\ddot{y}}$ = rms jitter

$I_o[\cdot]$ = zero order modified Bessel function

This same data plotted in Figure B-3 as rms sync jitter as a function of E_b/No to maintain a particular bit error probability shows the amount of additional signal level required to maintain the performance equivalent to the jitter-free case.

The effect of sync jitter combined with a static offset in the carrier tracking loop was also considered in a similar manner. The data presented on Figure B-4 for NRZ signaling was computed by numerically integrating the following expression.

$$P_E(\phi_s) = \int_\lambda p(\lambda) P_E(\phi_s, \lambda) d\lambda$$

where $P_E(\phi_s, \lambda) = \frac{1}{4}\{\mathrm{erfc}(\sqrt{R_d}\cos\phi_s) + \mathrm{erfc}[\sqrt{R_d}(1-2|\lambda|)\cos\phi_s]\}$

with $p(\lambda)$ as given above and ϕ_s representing the static offset.

Curves are plotted of the difference between E_b/N_o at the conditions noted and the E_b/N_o for ideal conditions to achieve error rates of 10^{-4} and 10^{-6}.

NRZ SIGNALING

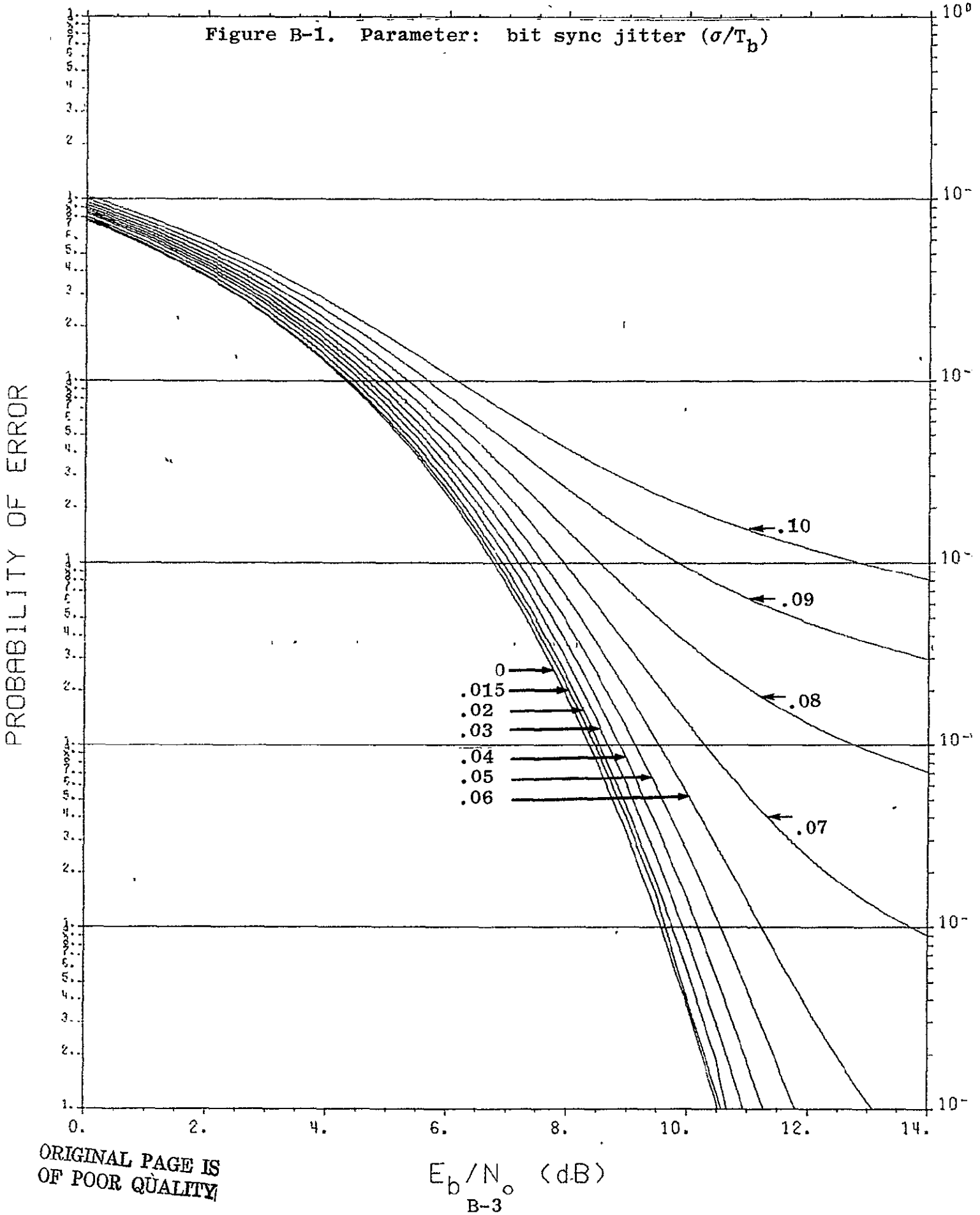

Figure B-1. Parameter: bit sync jitter (σ/T_b)

ORIGINAL PAGE IS
OF POOR QUALITY

BIPHASE L SIGNALING

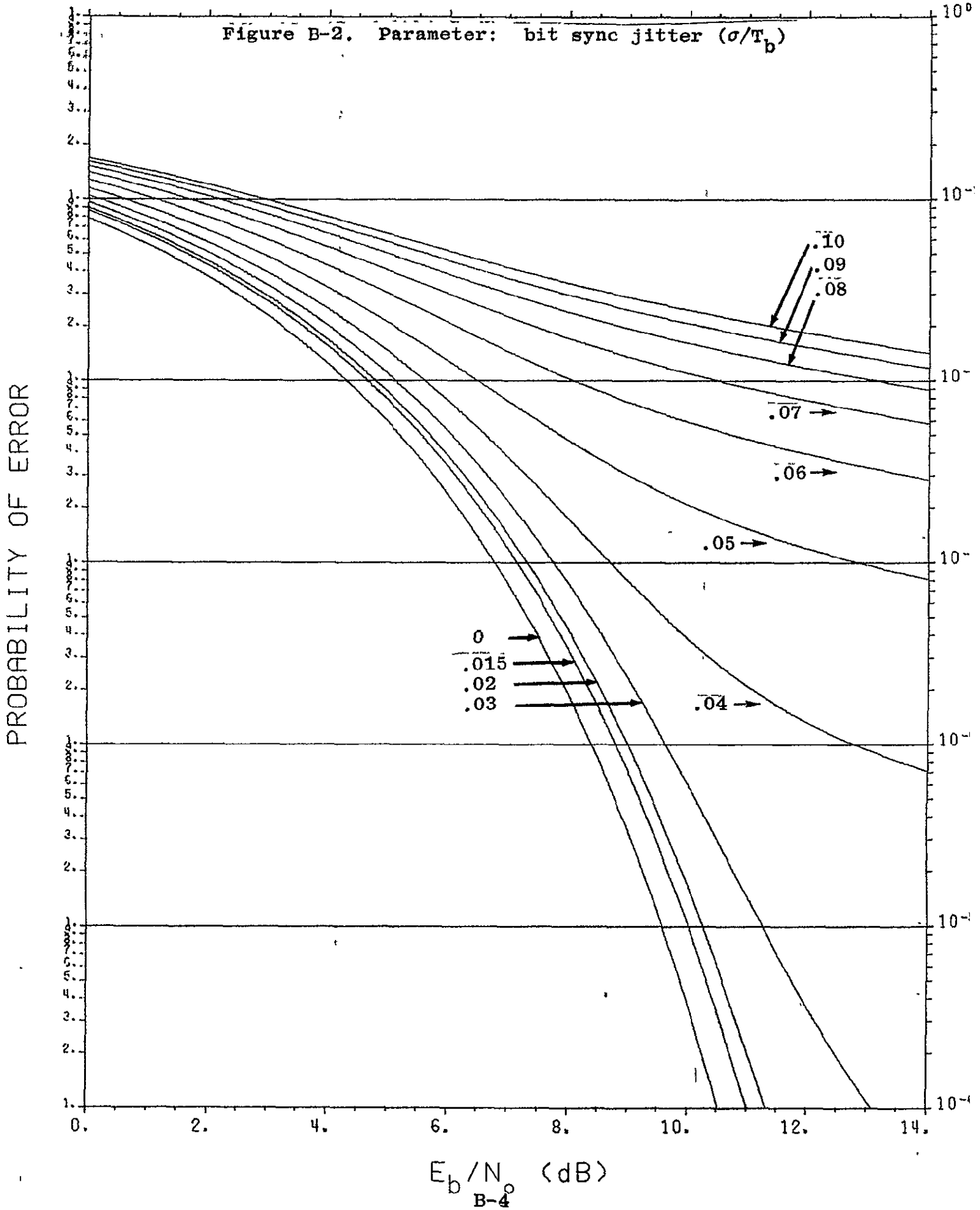

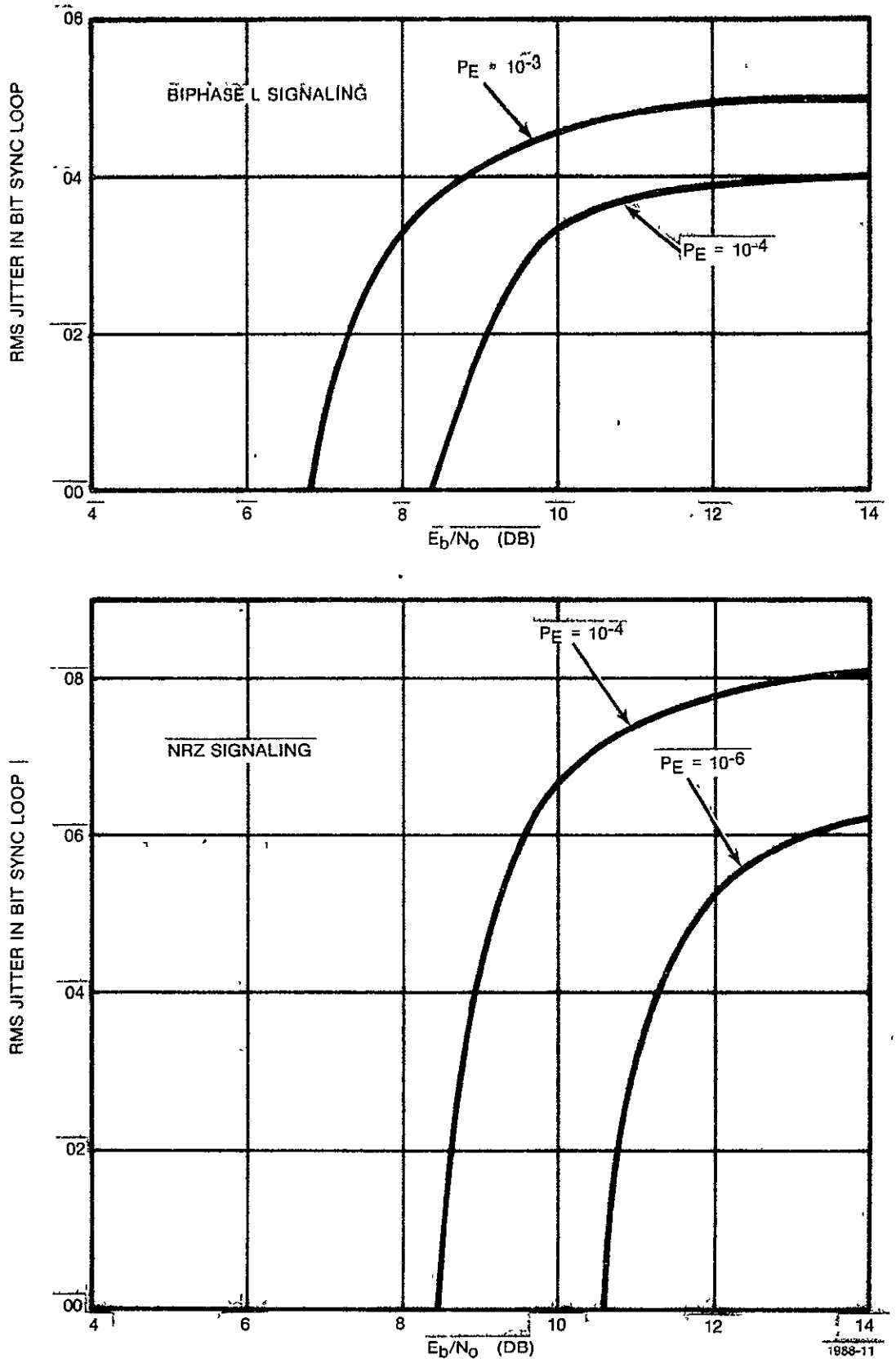

Figure B-3. Degradation Due to Sync Jitter

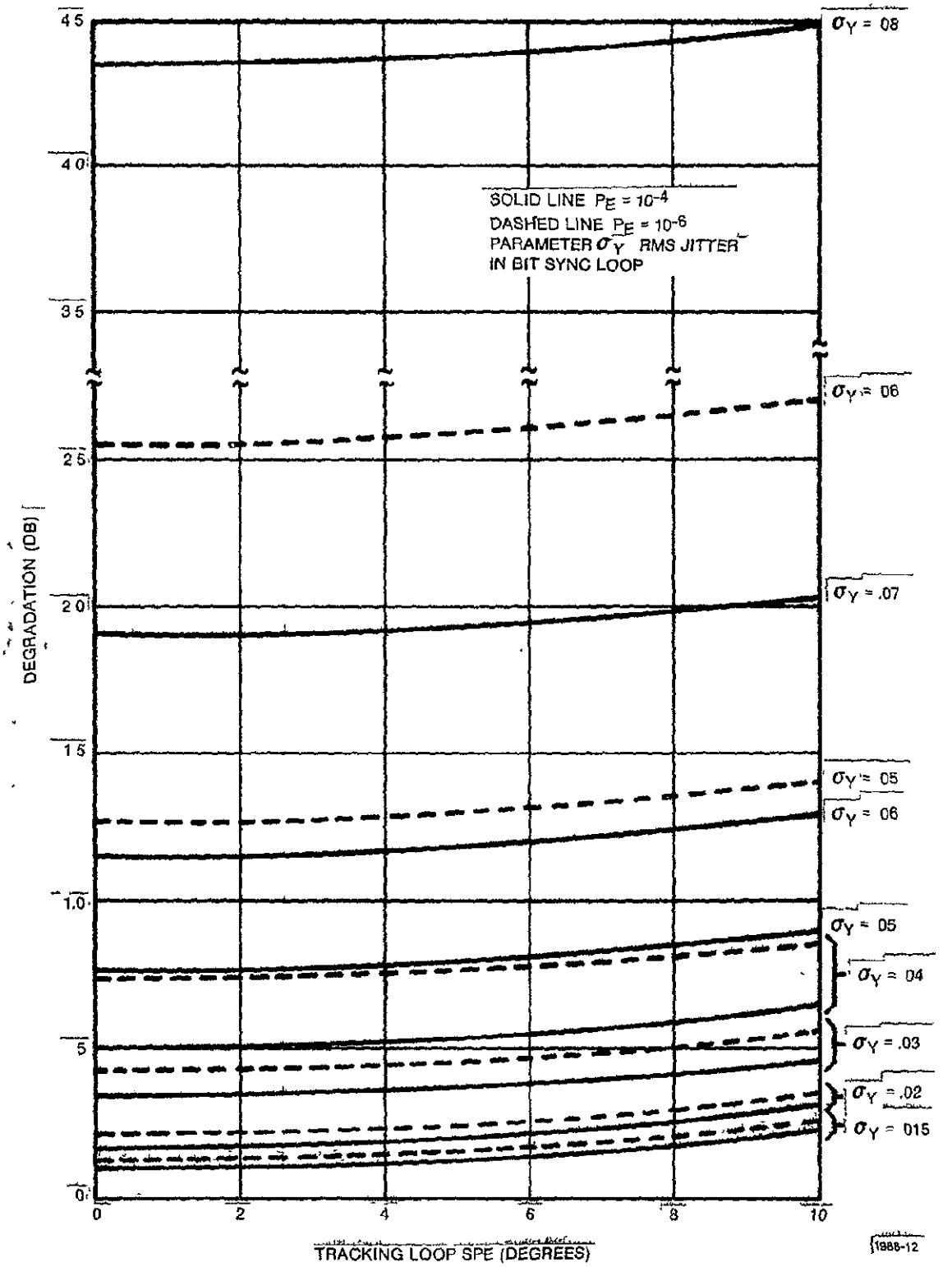

Figure B-4. Additional E_b/N_o(dB) Required to Maintain Given P_E(NRZ Signaling).

2. Pulse width asymmetry

Different durations for ones and zeroes cause a form of intersymbol interference. The effect of this interference on error probability for rectangular pulses is expressed as

$$P_E = \frac{1}{2} \{ P_E [(1+\delta) E_b/N_o] + P_E [(1-\delta) E_b/N_o] \}$$

where δ is the asymmetry factor. From this function the degradation in performance can be computed as shown in Figure B-5. When the pulses are modelled as trapezoidal waveforms which have rise times greater than the assymmetry factor, the degradation is reduced by $\frac{1}{2}$.

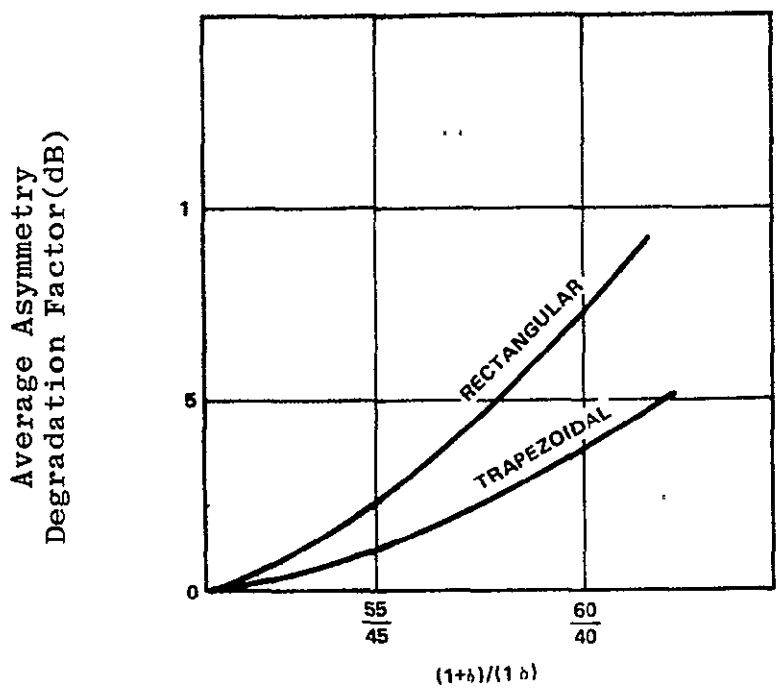

Figure B-5. Asymmetry Degradation as a Function of the Asymmetry Factor, i.e., Relative widths of Zeros and Ones

3. DC Offsets in Matched Filter Mechanization

The first offset considered is one of threshold bias. The result of such a bias is the favoring of one bit decision at the expense of the other. The decision process is shown graphically on Figure B-6 where Gaussian voltage probability densities are indicated as the matched filter output. From this representation, the bit error probability can be expressed as:

$$P_E = \frac{1}{2}\left\{\frac{1}{\sqrt{2\pi}} \int_{-\infty}^{-A} \exp(-x^2/2)\,dx + \frac{1}{\sqrt{2\pi}} \int_{-\infty}^{-B} \exp(-x^2/2)\,dx\right\}$$

where $A = m/\sigma\,(1+e_b/m)$

$B = m/\sigma\,(1-e_b/m)$

σ = rms noise voltage

m = signal voltage

This allows the calculation of P_E at any desired E_b/N_o using the ratio e_b/m as a parameter. Performance degradation from the ideal is then plotted as shown in Figure B-7.

A similar effect results from a decision uncertainty region. In any practical zero detecting circuit, an input region exists in which the output polarity is uncertain. By assuming that if the voltage falls within this region an error will occur half the time, the following expression defines the total error probability.

$$P_e = \frac{1}{\sqrt{2\pi}} \int_{-\infty}^{-\epsilon} \exp\left[\frac{(y-m)^2}{2\sigma^2}\right] dy + \frac{1}{2}\left\{\frac{1}{\sqrt{2\pi}\,\sigma} \int_{-\epsilon}^{\epsilon} \exp\left[\frac{(y-m)^2}{2\ 2}\right] dy\right.$$

where $\pm\epsilon$ defines the uncertainty region and the threshold bias e_b is assumed to be zero. Using these assumptions, the bit error probability can be evaluated using the bias analysis with the following substitutions:

$A = m/(1+\epsilon/M)$

$B = m/(1-\epsilon/m)$

Figure B-7 thus shows the effect of either bias offsets or decision uncertainty.

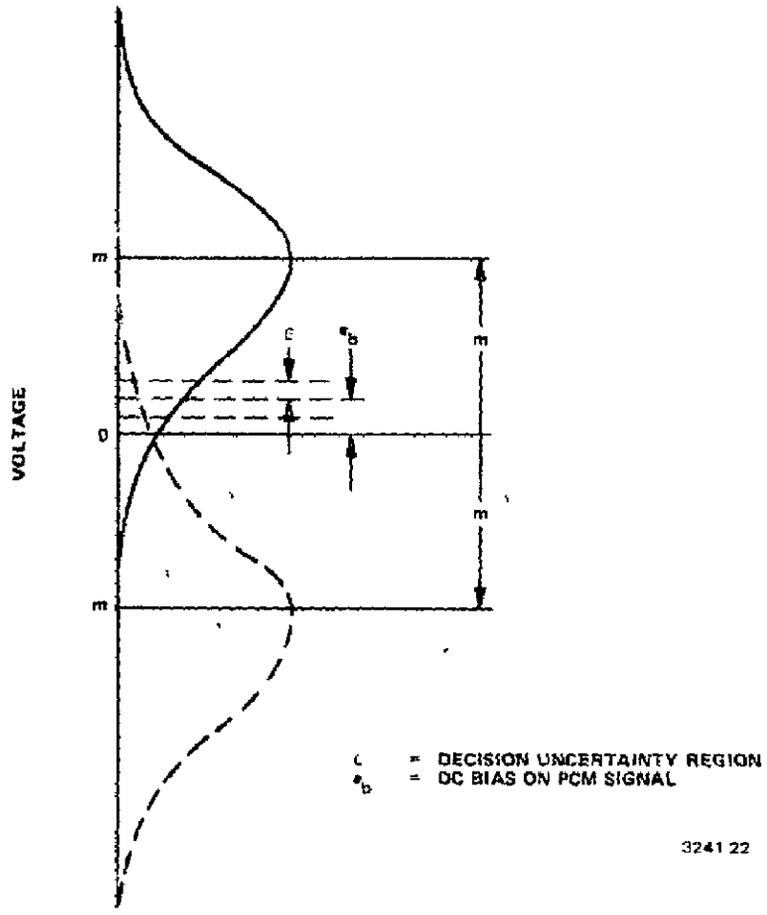

Figure B-6. Voltage Probability Density Function for Integrator Output

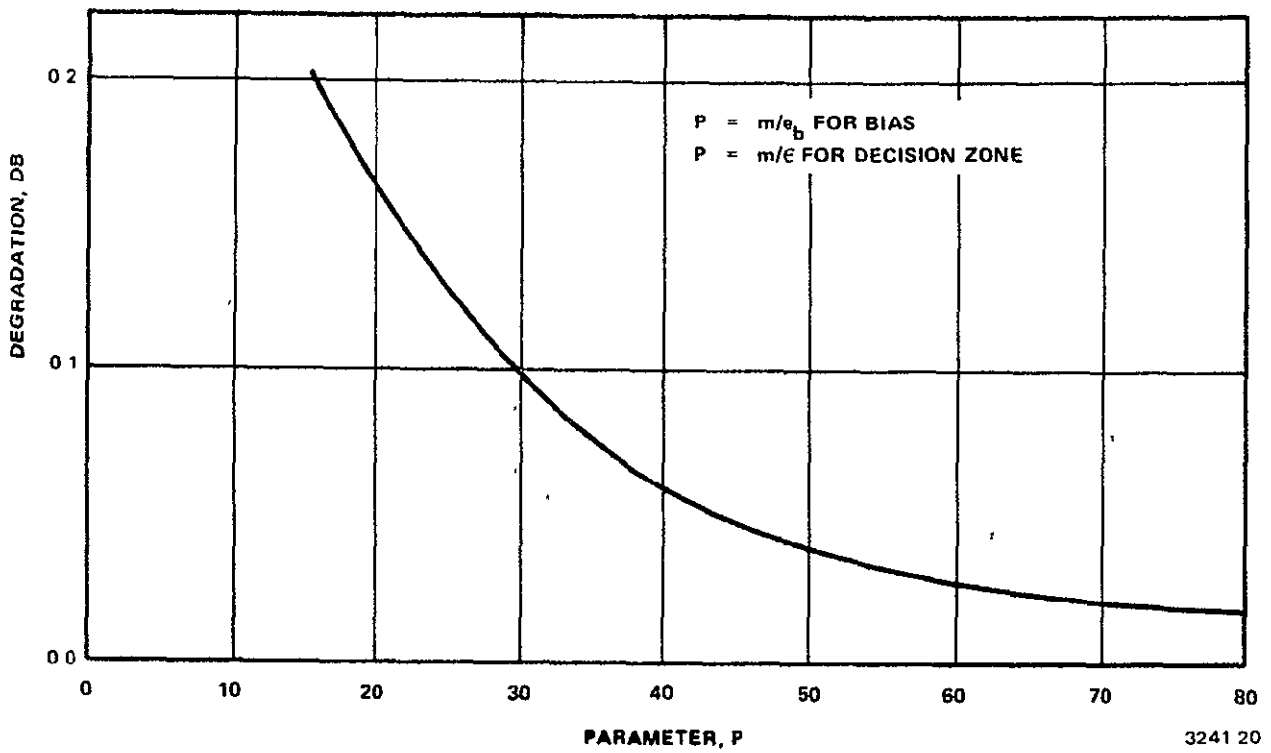

Figure B-7. Performance Degradation in Matched Filter Detection Due to Decision Window Effect and Bias

4. Reset Integrator Implementation

Most reset integrator implementations have a finite constant relative to the bit interval. The signal-to-noise ratio degradation for a single time constant integrator is given by

$$D = \frac{2}{(T/\tau)} \quad \frac{1-\exp(-T/\tau)}{1+\exp(-T/\tau)}$$

where T/τ is the ratio of bit interval to integrator time constant. Figure B-8 shows the amount of degradation as a function of this parameter.

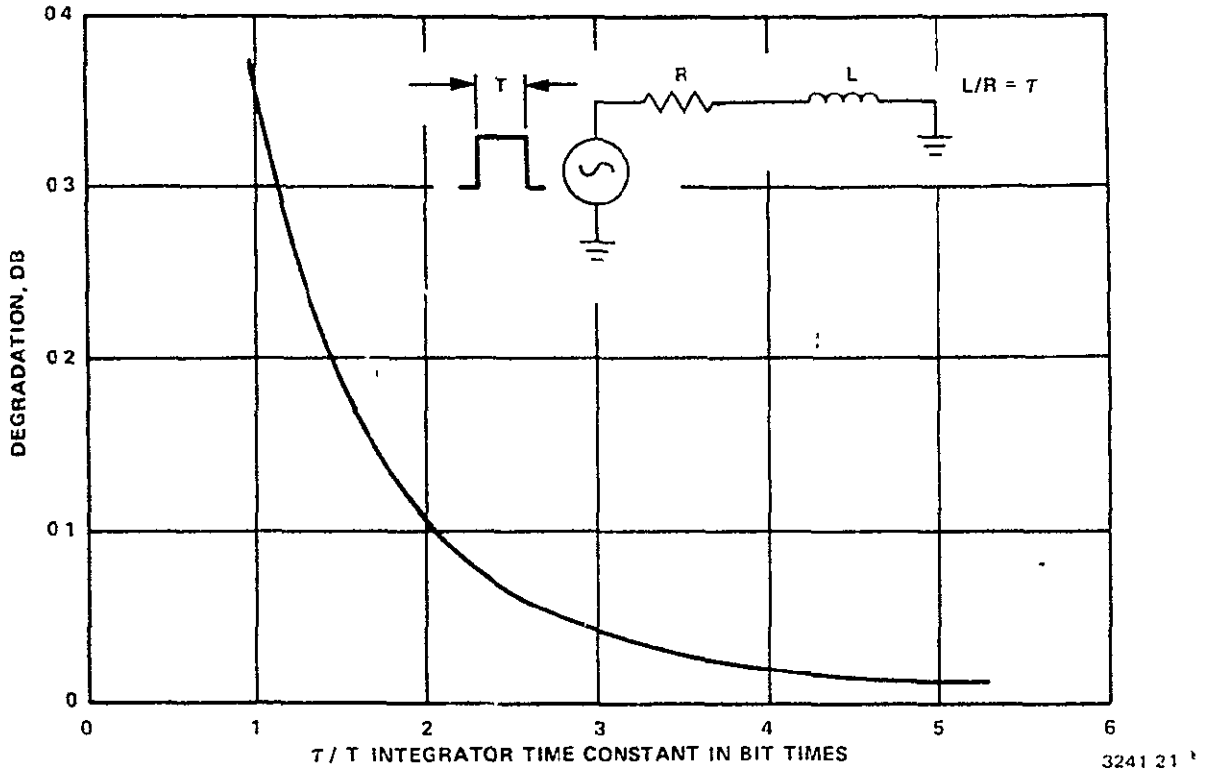

Figure B-8. Reset Integrator S/N Degradation as a Function of Integrator Time Constant

APPENDIX C

FM SIMULATION

In any angle modulation system, transmission impairments can cause frequency components to appear in the received baseband spectrum which were not in the original modulating signal. These undesirable components must be considered as noise contributors to the received signal. One method used to measure the amount of this noise is the NPR (noise power ratio) test which is shown in Figure C-1. This test provides an "end-to-end" system measurement which is an excellent figure of merit. It is, therefore, desirable to determine what factors cause distortion noise to fall in the notched-out slot. In general, these can be classified as deviations from constant gain and constant time delay as a function of frequency.

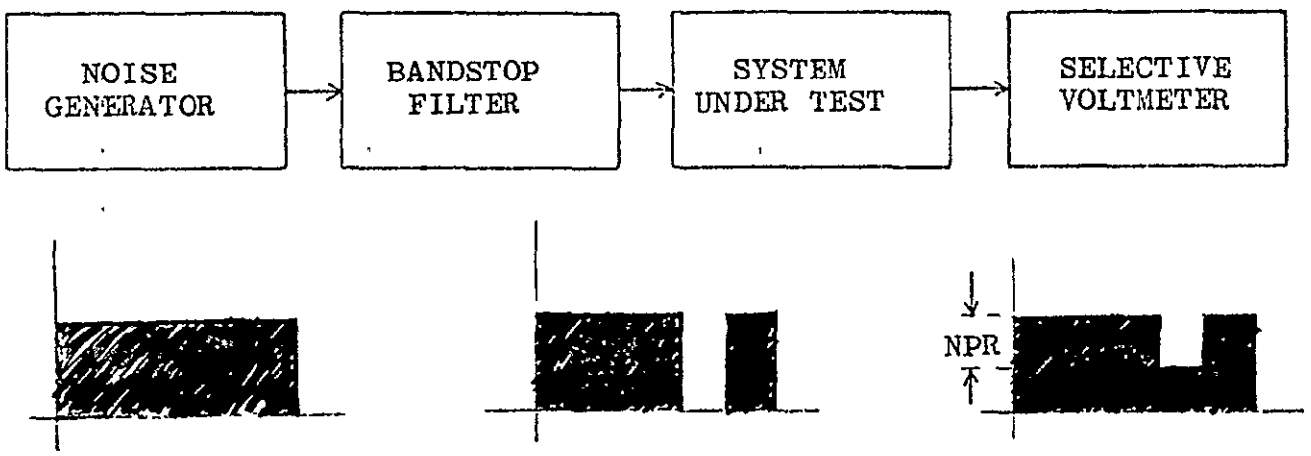

Figure C-1. Noise Power Ratio

The problem which arises is the determination of, first, the amount of distortion due to any one deviation and, second, the total due to combinations of the deviations. One solution to this problem is a simulation of the FM system from which the NPR can be calculated. In this solution, it is possible to model system components in terms of

analytical functions or test data as well as a power series representation. Because of this capability, the solution is useful in designing a system using idealized parameters and in evaluating a system using measured data.

Initially the system is characterized in three major blocks (Figure C-2) each of which contains some transmission deviations. The baseband signal is represented by an integer number of tones equally spaced in frequency which have equal magnitude and random phase.

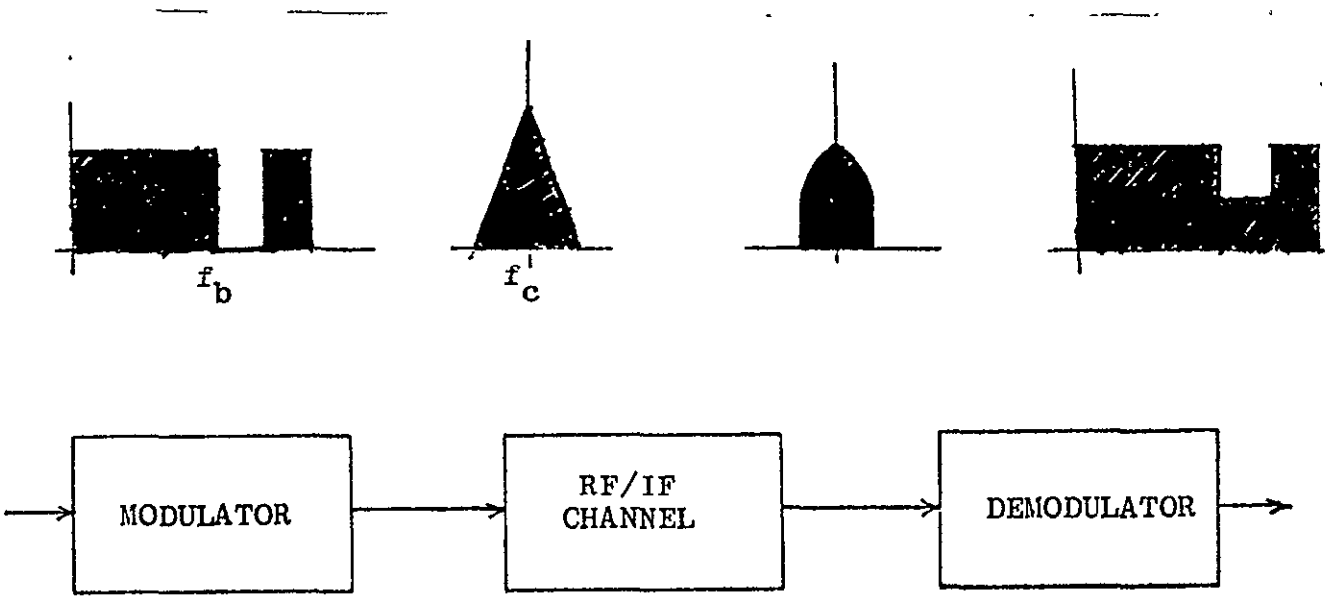

Figure C-2. Basic Simulation

Setting the amplitude of any tone to zero simulates notching a slot. The composite waveform resulting from this baseband spectrum is the signal to be processed by the modulator block. The function of this system component is to determine the instantaneous phase and magnitude of the carrier from the modulating voltage waveform at the input. This phase and amplitude will contain the effects of deviations resulting from the modulation mechanism. The second component lumps all the IF and RF portions of the system into a

single block. Included here is the modification of the IF spectrum by the amplitude and delay characteristics of the channel and the distortion of the carrier phase by the AM to PM conversion preceding the demodulator. The amplitude and delay characteristics of the channel can include upconverters, down-converters, filters, the transmission medium, and any other factor which can be modeled as gain and time delay, or phase, as a function of frequency. Any AM caused by band-limiting and by deviation from constant amplitude within the band is converted to a distorting phase through the AM to PM conversion factor. Thus, the second block processes the bandpass spectrum and yields the instantaneous carrier phase which is present at the demodulator input. At this point the carrier amplitude has been set to a constant value by a limiter. In the third block, the demodulator, instantaneous phase is processed to yield a received baseband signal from which the NPR can be computed. The output from this device will contain deviations resulting from the demodulation process.

By replacing the flat input spectrum described in the preceeding paragraphs with one which simulates a composite of TV and data, signal to distortion ratios can be computed for both services. This is accomplished by generating a simulated baseband spectrum, notching out selected frequencies, measuring the amount of energy in these notches at the output, and then calculating the appropriate signal to distortion noise ratios.

The baseband signal generation is done in a manner similar to that used for the usual NPR testing. The difference occurs in shaping the spectrum so that the video spectrum approximates an "average" TV signal and the data spectrum has the appropriate envelope for biphase L modulation. The video shaping is given by the expression[1] :

---

[1] Bruce, R. A., COM Sept. '64.

$$S(f) = (140)^2 \left\{ \frac{1/30.3}{1 + (f/.06)^2} + \frac{1/945}{1 + \left(\frac{f-3.58}{.06}\right)^2} \right\} \quad f \text{ in MHz}$$

The data shaping is given by[2]:

$$S(f) = \frac{\sin^4 (\pi fT/2)}{(\pi fT/2)^2}$$

This data spectrum is then translated to the subcarrier frequency and summed with the video to form the composite baseband signal which is then subjected to the transmission impairments of the link.

Measurement of the TV distortion noise is done by notching out two frequencies within the input TV bandwidth, then measuring the power appearing at these frequencies in the output. Experience with these measurements has shown that the noise spectrum of the video baseband can be approximated as a straight line on semilog scale between the noise powers expressed in dB at each of the notch frequencies. This characterization of the noise spectrum allows the total distortion noise to be computed by integrating over the baseband bandwidth.

The TV signal power is measured by summing the power at all frequencies except those notched out which are within the video baseband. Thus the TV channel signal to distortion noise ratio is determined.

Measurement of the signal to distortion noise ratio in the data subcarrier channel occurs in nearly the same manner. The distortion noise density is determined from the amount of energy appearing at the subcarrier frequency which is nulled by the QPSK modulation. Total distortion noise in the data channel is calculated by first assuming that the noise density is flat across this bandwidth then integrating over the data subcarrier bandwidth. Total signal is determined by integrating the signal spectrum

---

[2] Lindsey & Simon, Telecomm Systems Eng. p20

across the subcarrier bandwidth. The ratio of the two calculated values is the data channel signal to distortion noise ratio.

Some results of this simulation are shown in Figures A and B. The parameter under consideration for these calculations was channel bandwidth, thus the only transmission impairments are those introduced by the predetection filtering. For the data shown the filter chosen was a 5 pole, 0.1 dB ripple, Chebyshev design with a ripple bandwidth of 36 MHz. All other link elements have ideal characteristics. Figure A shows the effect of varying the composite peak deviation while retaining the nominal ratio between the TV deviation and the data deviation. Signal to noise ratios for both TV and data channels are indicated and show 12 dB increase per octave increase in deviation. In addition, the signal to thermal noise ratio is also shown for both TV and data channels. These values are based on the same data as the nominal link margin calculations. By combining the distortion noise and the thermal noise, a total signal to noise plus distortion ratio has been plotted to indicate the performance expected for a link in which the predetection filtering is the dominant factor.

The effects of changing the ratio between the data and TV deviations are shown on Figure C-4. For these calculations, the peak deviation of 17 MHz was held constant while the $\Delta f_{tv}/\Delta f_{data}$ ratio was varied from .9 to 3.6. These plots show that the TV channel signal to distortion is virtually independent of this ratio, while the data channel improves slightly as the amount of data signal is increased.

These two figures are examples of the kinds of data that can be derived from the simulation.

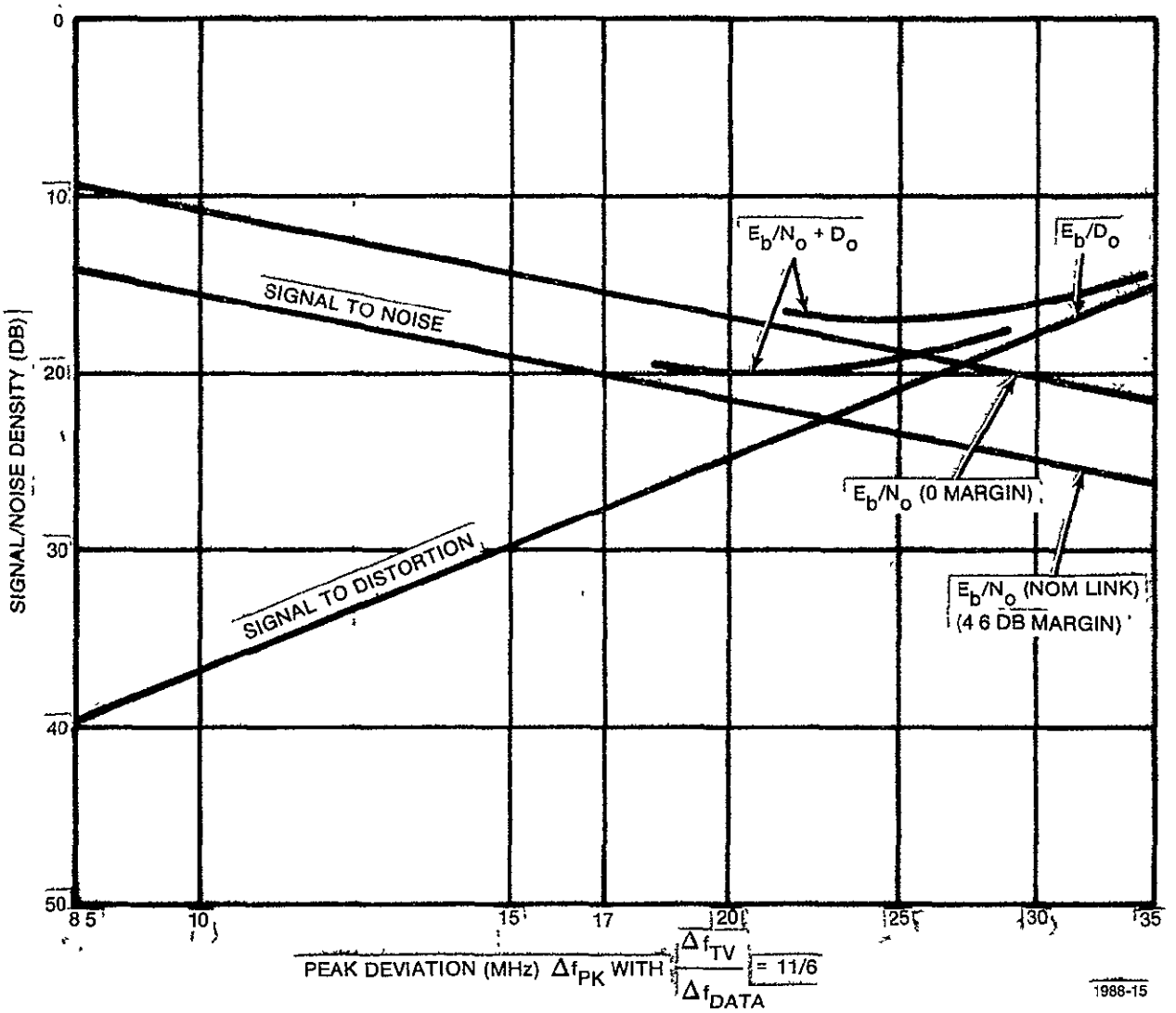

Figure C-3. Signal to Noise vs Deviation: Mode 2, 2 Mbps Channel.

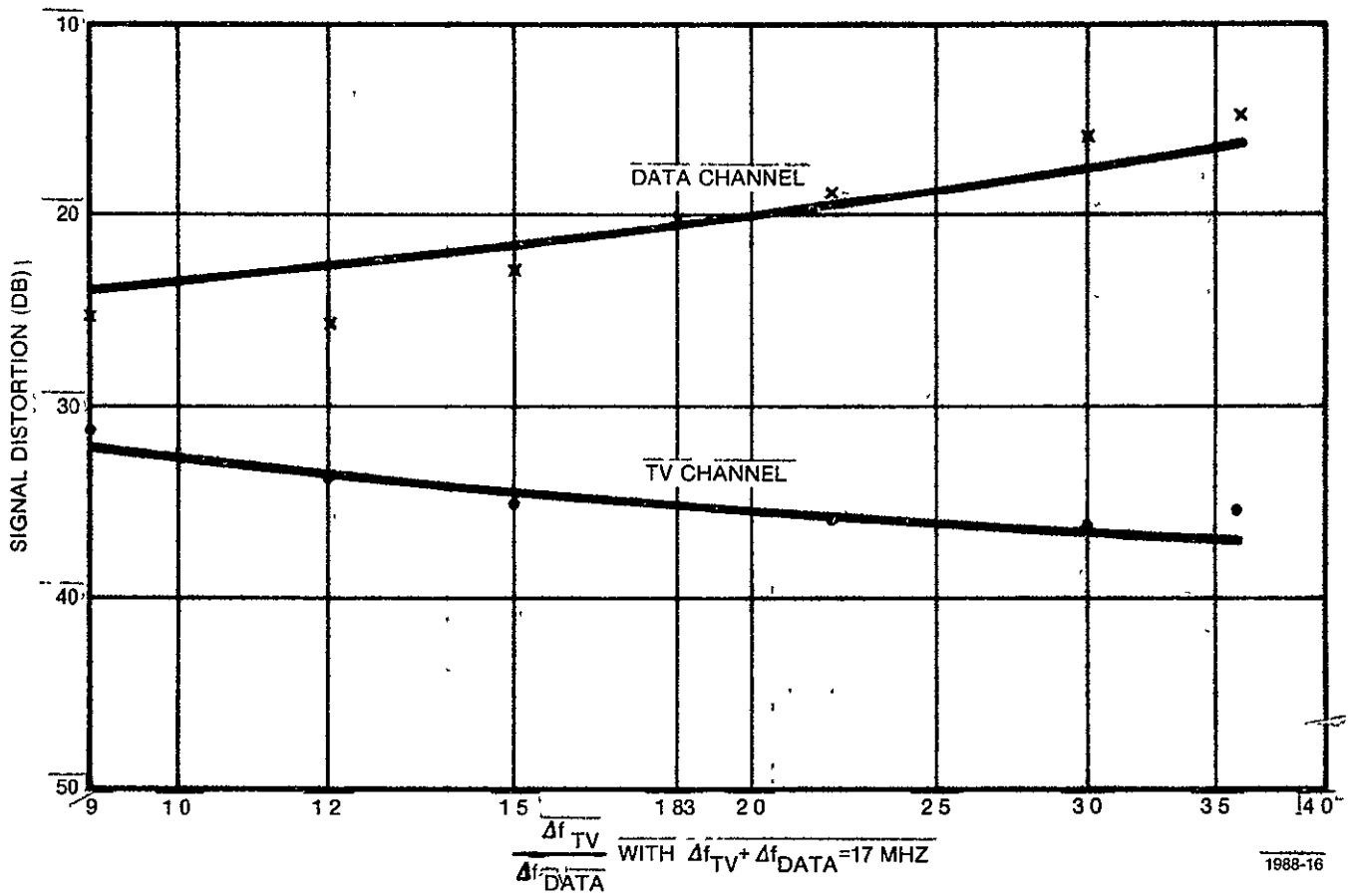

Figure C-4. Signal to Distortion Ratio in TV and Data Channels.

APPENDIX D

TRANSMITTER SPECIFICATION

APPENDIX D

SPECIFICATION FOR ORBITER/TDRSS KU-BAND RETURN LINK TRANSMITTER

1.0 SCOPE

This specification defines the detailed requirements for the transmitter hardware associated with the Orbiter/TDRSS Ku-Band return links. This equipment will accept data from the signal processor unit and modulate it on the carrier in either of two fashions:

Mode 1: Unbalanced QPSK modulation

Channel 3 (80%): 8 to 100 Msps encoded data

Subcarrier (20%): unbalanced QPSK modulated by:

Channel 2 (80%) 16 kbps to 2 Mbps data

Channel 1 (20%) 192 kbps data

Mode 2: FDM/FM modulation

Channel 3: 4.5 MHz wideband data or analog signal

Channel 2: 16 kbps to 2 Mbps data

Channel 1: 192 kbps data

Channels 2 (80%) and 1 (20%) are unbalanced QPSK modulated on a 8.5 MHz subcarrier then frequency division multiplexed with Channel 3.

Only one of these modes will be operational at a time. Mode selection will be accomplished by control signal.

The modulated signal will be amplified as necessary to the desired output signal level.

2.0 APPLICABLE DOCUMENTS

The following documents, of the exact issue shown, form a part of this specification to the extent specified herein:

Federal	TBS
Military	TBS
NASA	TBS
Motorola	TBS

3.0 REQUIREMENTS

3.1 PERFORMANCE

3.1.1 FUNCTIONAL CHARACTERISTICS

The equipment shall consist of a power amplifier and high voltage power supply, an exciter, a QPSK modulator, and an FM modulator whose functional characteristics are detailed in the following paragraphs.

3.1.1.1 Input Signals

3.1.1.1.1 Mode 1

Channel 1: Data rate: 192 kbps

Waveform: Biphase - L

Input Voltage: high level = 3.5 to 5.0 V

low level = 0 to 0.4 V

Impedance: TBD

Rise Time: TBD

Fall Time: TBD

Channel 2: Data rate: 16 kbps to 2 Mbps

Waveform: biphase - L or NRZ - L

Input Voltage: high level = 3.5 to 5.0 V

low level = 0 to 0.4 V

Impedance: TBD

Rise Time: TBD

Fall Time: TBD

Channel 3: Data rate: 8 to 100 Msps

Waveform: NRZ-L

Input Voltage: Binary 1 = ECL compatible

Binary 0 = ECL compatible

Channel 3: (Cont'd)

Source impedance: TBD

Rise Time: TBD

Fall Time: TBD

3.1.1.1.2 Mode 2

Channel 1: Same as Mode 1, Channel 1

Channel 2: Same as Mode 1, Channel 2

Channel 3: one of the following

(1) Data rate: 16 kbps to 4 Mbps

Waveform: NRZ-L

Input Voltage: Binary 1 - 3.5 to 5.0 V

Binary 0 - 0. to 0.4 V

Impedance: TBD

Rise Time: TBD

Fall Time: TBD

(2) Analog input

Bandwidth: 3 Hz to 4.5 MHz

Waveform: Analog or TV

Amplitude: TBD

Impedance: TBD

Channel 4: Narrow band Payload Subcarrier:

3.1.1.2 Output Signals

The output will be an angle modulated carrier with one of the following sets of characteristics.

3.1.1.2.1 Mode 1. Simultaneous transmission of three data channels shall be accomplished by unbalanced QPSK modulation. The I Channel input is the channel 3 data. The Q channel input is the 8.5 MHz subcarrier which has been unbalanced QPSK modulated by Channel 2 data (80%) and Channel 1 data

(20%). The power division between Channel 3 and the subcarrier shall be:

Channel 3 (I channel): 80 ± 5%

Subcarrier (Q channel): 20% (nominal)

3.1.1.2.2 Three Channel Mode 2. Three information channels shall be transmitted simultaneously by FM modulating the carrier with a FDM signal format. The FDM format is the composite of Channel 3 and the 8.5 MHz subcarrier which has been unbalanced QPSK modulated by channels 1 and 2. The power division for the QPSK is: Channel 2 = 80% and Channel 1 = 20%.

Nominal frequency deviation will be ±6 MHz peak by the modulated subcarrier and +11 MHz peak by Channel 3.

Two Channel Mode 2. Two information channels shall be transmitted simultaneously by FM modulating the carrier with the composite of Channel 3 and the 8.5 MHz subcarrier which has been phase modulated by Channel 4, the Narrowband Payload Subcarrier signal. Characteristics for this mode are TBD.

3.1.1.3 Control Signals

Signals controlling the state of the transmitter shall include:

a. Mode 1 select
b. Mode 2 3/2 Channels select
c. High voltage enable
d. High voltage inhibit
e. Standby power select
f. Comm. power select

Each shall have the following characteristics:

Waveform: pulse
Amplitude: TBD
Pulse Width: TBD
Rise Time: TBD
Fall Time: TBD
Source Impedance: TBD
Load Impedance: TBD

3.1.1.4 Telemetry Signals

Signals monitoring the status of the transmitter shall be provided as follows:

Analog Signals

a. Transmitter temperature

b. Power output

Bilevel Signals

a. Operational status

b. Self Test Status

Each shall have the following characteristics

	ANALOG	BILEVEL
Voltage range:	0 to +5 V	TBD
Source impedance	10K ohms (max)	TBD
Load impedance	100 K ohms (min)	TBD

3.1.1.5 Input Power

Power for the transmitter shall be derived from the TBD supply. The continuous power shall not exceed TBD watts.

3.1.1.6 Transmitter

Requirements for the transmitter are as follows:

a. Transmit frequency: 15.0085 GHz $\pm$ .003%

b. Operating frequency band: The frequency range containing information is from 14.896 to 15.121 GHz. The transmitter 3 dB bandwidth shall be 300 MHz (min) centered at 15.0085 GHz.

c. Output power: not less than 50 watts at the power amplifier output.

d. Spurious output levels: Any spurious level shall be at least 60 dB below the unmodulated carrier measured in a 4 kHz bandwidth.

e. Harmonic output levels: Any harmonics of the output frequency shall be at least 50 dB below the unmodulated carrier for frequencies up to 20 GHz.

f. Output power variation vs. frequency: Peak to peak ripple within the information frequency band shall be within ± 1.0 dB. The change in power shall not exceed .4 dB in any 10 MHz segment of the operating frequency band.

g. Frequency stability: $\pm 1 \times 10^{-6}$ per hour.
Aging: $\pm 5 \times 10^{-6}$ per year.

h. Phase stability: The phase noise shall not exceed 3 degrees rms when measured in a 10 MHz bandwidth using a 5 kHz ($2 B_L$) tracking phase lock loop.

i. Incidental AM: IAM shall not exceed 3%

j. Incidental FM: With no modulating signal present at the input, IFM shall not exceed 5 kHz rms in any 1 MHz bandwidth from 500 kHz to 12.5 MHz.

k. Modulation Mode 1: The following characteristics apply when Mode 1 is selected.

1. Modulation: unbalanced QPSK
2. Power division: Channel 3: $80 \pm 5\%$
   Subcarrier: 20% (nominal) with at least 3% of the total transmitted power in Channel 1.
3. Orthogonality: Phase of Q channel relative to the I channel shall be $90 \pm 5^{\circ}$.
4. Carrier suppression: With modulation applied the carrier shall be at least 30 dB below the unmodulated carrier.
5. Output Signal-to-Noise ratio: The minimum ratio shall be 20 dB measured in 100 MHz noise bandwidth.

6. Subcarrier Modulation: Unbalanced QPSK

   a. Subcarrier frequency: 8.5 MHz (nominal)

   b. Subcarrier frequency Stability: ±TBD parts in 10

   c. Modulation power division: Channel 2: 80%

      Channel 1: 20%

   d. Orthogonality: Phase of Q subcarrier channel relative to the I subcarrier channel shall be 90 ±5°.

7. Subcarrier Modulation: Same as Mode 1.

1. Modulation Mode 2: The following characteristics apply when three channel Mode 2 is selected.

   1. Carrier Modulation: FDM/FM

   2. FM Polarity: An increased modulating voltage will increase the carrier frequency.

   3. FM Deviation sensitivity: The deviation sensitivity of the transmitter shall be 20 MHz per volt ±10% for deviations up to ±20 MHz

   4. Modulation bandwidth: The modulation response shall be within ±1 dB from dc to 12.5 MHz at deviations up to ±17 MHz.

   5. Linearity: The differential gain of the modulator shall not exceed .3 dB peak to peak and the differential phase of the modulator shall not exceed 3 degrees peak to peak within ±18 MHz of the carrier frequency.

   6. Intermodulation: With two tones of equal level applied at the modulator input such that the peak deviation is 1 MHz, the intermodulation between the two shall be at least 40 dB below either tone.

      The following characteristics apply when two channel Mode 2 is selected.

TBD

m. Modulation input impedances:

Each input shall have the following characteristics:

Zin shall be 50 ohms ±20% for both Mode 1 and Mode 2 inputs.

n. Transmitter RF Output impedance:

The transmitter shall meet all requirements while operating into a load which has 1.5:1 VSWR (max).

o. Protection: The transmitter shall be protected from damage due to open or short circuit conditionson either input or output.

p. Self test provisions: The following self test features shall be provided: TBD

q. Test Points: The following test points shall be provided: TBD

3.2 ENVIRONMENTAL CONDITIONS

TBD

3.3 DESIGN AND CONSTRUCTION

TBD

3.4 ELECTROMAGNETIC COMPATIBILITY

MIL STD 461A as modified for Shuttle.

APPENDIX E

SIGNAL PROCESSOR SPECIFICATION

SPECIFICATION FOR SIGNAL PROCESSOR
FOR ORBITER/TDRSS KU-BAND RETURN LINK

1.0 SCOPE

This specification defines the requirements for the return link signal processor. This equipment accepts signals from the orbiter and from the payload, conditions or encodes the signals if necessary, then routes the desired signals to the appropriate transmitter modulator.

2.0 APPLICABLE DOCUMENTS

The following documents, of the exact issue shown, form a part of this specification to the extent specified herein:

Federal	TBS
Military	TBS
NASA	TBS
Motorola	TBS

3.0 REQUIREMENTS

3.1 PERFORMANCE

3.1.1 Functional Characteristics

The signal processor will accept the signals listed in 3.1.1.1 and the control signals listed in 3.1.1.3. On the basis of the control signal states a Mode selection will be made and the appropriate signals will be routed to the signal processor output. Paragraph 3.1.1.2 details the output characteristics. This signal processing is shown functionally on Figure 1.

ORIGINAL PAGE IS
OF POOR QUALITY

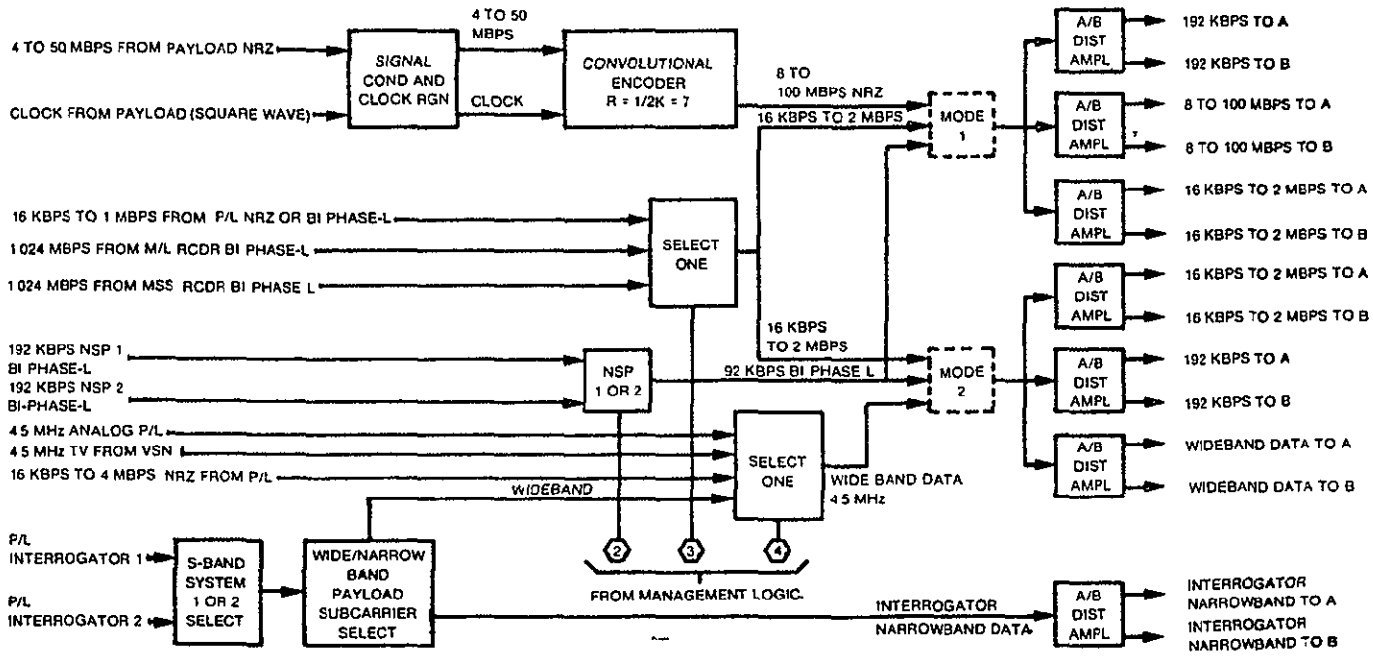

Figure 1. Functional Block Diagram Return Link Signal Processor

3.1.1.1 Input Signals

The following list details the characteristics of the information signals. In parenthesis is the output to which it may be routed.

a. 50 Mbps data and clock input (Mode 1, Channel 3)

Data rate: 4 to 50 Mbps

Clock rate: same as data rate

Waveform: data:NRZ-L

clock:square wave

Amplitude: 0 to 5 V ± 10%

Source impedance: TBD

Rise time: TBD

Fall time: TBD

b. 16 kbps to 2 Mbps payload data (Mode 1, Channel 2 or Mode 2, Channel 2)

Data rate: 16 kbps to 2 Mbps

Waveform: NRZ-L or Biphase - L

Amplitude: 0 to 5 V ± 10%

Source impedance: 75 ohms ± 10%

Rise time: TBD

Fall time: TBD

c and d. M/L and MSS Recorder data (Mode 1, Channel 2 or Mode 2, Channel 2)

Data rate: 1.024 Mbps

Waveform: Biphase-L

Amplitude: 3 to 9 volts peak to peak

± 2 % asymmetry

Source Impedance: 75 ohms ± 10%

Rise time: Less than 10% of bit cell time

Fall time: Less than 10% of bit cell time

e. Orbiter data (Mode 2, Channel 1 or Mode 1, Channel 1 or Mode 2, Channel 2)

Data rate: 192 kbps

Waveform: Biphase - L

3.1.1.1 Input Signals (Cont'd)

e. (Cont'd)

Amplitude: 5.25 volts peak to peak ± 2V

Source impedance: 71 ohms ±10%

Rise time: 390 ns max

Fall time: 390 ns max

f. 4.5 MHz Analog or TV from payload (Mode 2, Channel 3)

Bandwidth: 3 Hz to 4.5 MHz (information bandwidth)

Waveform: analog

Amplitude: 0 to 1 volt peak ±10%

Source impedance: 75 ohms ±10%

g. Orbiter TV input (Mode 2, Channel 3)

Signal: composite TV video waveform per EIA RS 330, Figure 1

Bandwidth: dc to 4.5 MHz

Level: 0 to 1 volt peak ± 10% with the sync tip of white reference at 0 volts.

Source impedance: 75 ohms ± 5%

h. 16 kbps to 4 Mbps payload data (Mode 2, Channel 3)

Data rate: 16 kbps to 4 Mbps

Waveform: NRZ-L

Amplitude: 0 to 5 volts peak ± 10%

Source Impedance: 75 ohms ± 10%

Rise time: TBD

Fall time: TBD

i. Payload interrogator signal: compatible with f.

3.1.1.2 Output Signals

The following list details the characteristics of the output information signals.

3.1.1.2.1 Mode 1 Outputs

a. Channel 3: 8 to 100 Msps data

Data rate: 8 to 100 Msps

Source: Convolutionally encoded from input (a)

Waveform: NRZ-L

Amplitude: MECL Compatible

Source impedance: TBD

Rise and fall times: less than 10% of bit period

b. Channel 2: 16 kbps to 2 Mbps data

Data rate: 16 kbps to 2 Mbps

Source: selected from inputs (b), (c), (d), and (e)

Waveform: NRZ-L or Biphase L

Amplitude: TTL Compatible

Source impedance: TBD

Rise and Fall times: less than 10% of bit period

c. Channel 1: 192 kbps return link operational data

Data rate: 192 kbps

Source: Input (e)

Waveform: Biphase-L

Amplitude: TTL Compatible

Source impedance: 75 ohms $\pm$10%

Rise and Fall times: TBD

3.1.1.2.2 Mode 2 Outputs

a. Channel 1: Same as Mode 1, Channel 1 (3.1.1.2.1b)

b. Channel 2: Same as Mode 1, Channel 2

c. Channel 3: Wideband Analog or data

Source: Selected from inputs (f), (g), (h), and (i)

Characteristics: see 3.1.1.1 (f), (g), (h)

Amplitude: Analog: 0 to 1 volt
Data: TBD

Source Impedance: 75 ohms ±10%

Rise and fall times: TBD

d. Narrowband Payload Subcarrier Signal: TBD

3.1.1.3 Control Signals

The following control signals are used to configure the return link signal.

a. Orbiter TV signal

b. 4 to 50 Mbps data

c. 192 kbps operational data

d. Payload digital data

e. MSS recorder data

f. Payload analog data

g. Payload digital data

h. Payload interrogator signal

i. M/L recorder data

j. S-band system 1

k. S-band system 2

l. network signal processor (NSP) 1

m. NSP 2

n. Narrowband Payload Subcarrier

The status of these signals is used to generate only one of the following control signals:

a. Mode 1 select

b. Mode 2 select

Output characteristics of these signals are TTL Compatible.

3.1.1.4 Input Power

Power for the signal processor shall be derived from the +28 VDC supply. The maximum power required shall not exceed TBD watts.

3.1.1.5 Convolutional encoder

The 4 to 50 Mbps channel data shall be encoded at rate 1/2 into an encoded channel at up to 100 Mbps. The encoded channel shall consist of 5 interlaced convolutional coders (R = 1/2, K = 7) operating in parallel at output symbol rates up to 20 Msps each. The five encoder outputs shall be the inputs to a parallel - to - serial data buffer and decommutator for assembly into a serial bit stream. The generator coefficients for each of the five encoders shall be

$g_1 = (171)_8$ and $g_2 = (133)_8$.

3.1.1.6 Protection Circuits

The signal processor shall be protected so that open or short circuit conditions on inputs or outputs shall not cause damage to the equipment. A short or open condition on any input or output shall not degrade the performance of any other signal path.

3.1.1.7 Test Points

The following test points shall be included:

Digital Data

100 Msps Data

WidebandData

Others: TBD

3.2 ENVIRONMENTAL CONDITIONS

TBD

3.3 DESIGN AND CONSTRUCTION

TBD

APPENDIX F

COSTAS LOOP TRACKING SIGNAL TO NOISE RATIO

The error signal plus noise in the Costas loop can be written as (1):

$$e(t) = \frac{(P_A - P_B)}{2} \sin 2\phi + \sqrt{P_A P_B}\, a\, b \cos 2\phi$$
$$+ n_c(t)\, n_s(t)$$
$$+ n_c(t) \left[P_A\, a(t) \sin\phi + P_B\, b(t) \cos\phi \right]$$
$$+ n_s(t) \left[P_A\, a(t) \cos\phi - P_B\, b(t) \sin\phi \right]$$

where P_A is the power in the high rate channel

P_B is the power in the subcarrier channel

$a(t)$ is the high modulation = ± 1

$b(t)$ is the modulated subcarrier = ± 1

From this expression the correlation function of the noise terms can be written:

$$R_{neq}(\tau) = R_N^2(\tau)$$
$$+ R_N(\tau) \left[P_A R_A(\tau) + P_B R_B(\tau) \right]$$
$$+ P_A P_B R_A(\tau) \cos^2 2\phi$$

Since $a(t)$ is an NRZ data stream,

$$R_A(\tau) = 1 - \frac{|\tau|}{T_a} \qquad |\tau| \le T_a$$
$$= 0 \qquad |\tau| > T_a$$

For the three channel PM mode

$$b(t) = \mathrm{sgn} \left[a_2 d_2(t) \sin \omega_{sc} t + a_3 d_3(t) \cos \omega_{sc} t \right]$$

This can be approximated using the fundamental term as

$$b(t) = \frac{4}{\pi} \left[a_2 d_2(t) \sin \omega_{sc} t + a_3 d_3(t) \cos \omega_{sc} t \right]$$

$$R_B(\tau) = \left(\frac{4}{\pi}\right)^2 \left[P_{a_2 d_2} R_{a_2 d_2}(\tau) \cos \omega_{sc}\tau + P_{a3} R_{d3}(\tau) \cos \omega_{sc}\tau \right]$$

where for NRz signaling $R_{d2}(\tau) = 1 - \frac{|\tau|}{T_{d2}}$, $|\tau| \le T_{d2}$

$= 0$ $|\tau| > T_{d2}$

or for biphase L signaling

$$R_{d2}(\tau) = 1 - \frac{3|\tau|}{T_{d2}} \qquad |\tau| \le T_{d2/2}$$

$$= \frac{|\tau|}{T_{d2}} - 1 \qquad \frac{T_{d2}}{2} < |\tau| \le T_{d2}$$

$$= 0 \qquad |\tau| > T_{d2}$$

Similarly $R_{d3}(\tau)$ is the biphase L function.

Using these functions the noise spectrum can be found as the Fourier transform:

$$S(\omega) = F\left[R_{neq}(\tau)\right]$$

Because the noise near the carrier will be nearly flat, it is considered as a density function therefore, the $S(\omega)$ will be evaluated for $\omega = o$.

The $R_N^2(\tau)$ term contributes $\frac{N_o^2 B_1}{2}$

and $R_N(\tau)\left[P_A R_A(\tau) + P_B R_B(\tau)\right]$ contributes $\frac{N_o}{2}(P_A + P_B)$

The remaining term is calculated as

$$R_A(\tau) R_B(\tau) = \left(\frac{4}{\pi}\right)^2 \left(1 - \frac{|\tau|}{T_a}\right)\left[P_{a2}\left(1 - \frac{|\tau|}{T_{d2}}\right)\cos \omega_{sc}\tau\right.$$

$$\left. + P_{a3}\left(1 - \frac{3|\tau|}{T_{d3}}\right)\cos \omega_{sc}\tau\right]; |\tau| \le T_a$$

$$= o; \quad |\tau| > T_a$$

Since T_a is always significantly less than T_{d2} or T_{d3} and $P_{a2} + P_{a3} = 1$

$$R_A(\tau)\, R_B(\tau) \approx \left(1 - \frac{\tau}{T_a}\right)\left(\frac{4}{\pi}\right)^2 \cos \omega_{sc}\tau \qquad ; \quad |\tau| \leq T_a$$

$$= o \qquad ; \quad |\tau| > T_a$$

The transform of this term is

$$\left(\frac{4}{\pi}\right)^2 \frac{T_a}{2} \left[\frac{\sin^2 (\omega+\omega_{sc})\, T_a/2}{(\omega + \omega_{sc})\, T_a/2)^2} + \frac{\sin^2 (\omega - \omega_{sc})\, T_a/2}{(\omega - \omega_{sc})\, T_a/2)^2}\right]$$

Thus the remaining term contributes

$$\left(\frac{4}{\pi}\right)^2 \quad P_A\, P_a\, T_a\, \frac{\sin^2 \omega_{sc}\, T_a/2}{((\omega_{sc}\, T_a/2)^2}$$

The tracking signal to noise in the loop bandwidth can be written:

$$P = \frac{P_c}{N_{oeq}\, B_L}$$

$$= \frac{(P_A - P_B)^2}{4B_L\left[\frac{N_o^2 B_1}{2} + \frac{N_o}{2}(P_A + P_B) + \left(\frac{4}{\pi}\right)^2 P_A\, P_B\, T_a\, \frac{\sin^2 \omega_{sc}\, T_a/2}{((\omega_{sc}\, T_a/2)^2}\right]}$$

Using the relationships: $P_A = P_T$ and $P_B = (1-\alpha)P_T$

$$B_{IF} = 2\, B_1$$

$$\rho = \frac{(20(-1)^2\, (2P_T/N_o\, B_{IF})^2}{4\left(\frac{2\, B_L}{B_{IF}}\right)\left[1 + \frac{2\, P_T}{N_o\, B_{IF}} + \left(\frac{4}{\pi}\right)^2\left(\frac{2\, P_T}{N_o\, B_{IF}}\right)\left(\frac{P_T\, T_a}{N_o}\right)\alpha(1-\alpha)\, \frac{\sin^2 \omega_{sc}\, T_a/2}{((\omega_{sc}\, T_a/2)^2}\right]}$$

Because of the values chosen for ω_{sc} and T_a, the last term is quite small so that

$$\beta \approx \frac{(2\alpha - 1)^2 \quad (2P_T/N_o\ B_{IF})^2}{4\left(\frac{2B_L}{B_{IF}}\right)\left(1 + \frac{2P_T}{N_o B_{IF}}\right)}$$

This approximation seems reasonable since the use of the subcarrier for transmitting data from the two low rate channels has moved their information spectrum away from the carrier frequency leaving only spectrum from the high rate channel in that region.

REFERENCE

(1) Weber, C. L., "Feasibility of Candidate Receivers for Ku-Band Communications Signals To and From Shuttle," Axiomatic Report No. R 7510 - 4, October 31, 1975.

APPENDIX G

METHODS FOR HANDLING THE HIGH RATE RETURN LINK DATA

APPENDIX G

METHODS FOR HANDLING THE HIGH RATE RETURN LINK DATA

INTRODUCTION

The baseline design for handling the up to 50 Mbps return link Payload data is presented in Task #3 description. While this provides the lowest-risk, most straight-forward implementation on the Orbiter, it may present some difficult problems for the ground data handling equipment. Of primary concern is the capability required by the ground equipment to acquire and maintain data synchronization lock with a continuum of encoded data rates from 8 Mbps to 100 Mbps. If some preprocessing of the data could be performed onboard the Orbiter, it might significantly reduce the complexity of the ground data handling problem. This should be accomplished without excessive additional complexity introduced to the Orbiter equipment and with a reasonable restriction to the number of encoded data rates. Such a tradeoff might be favorable for a Communication Signal Processor modification.

Before discussing a proposed modification of the signal processor to reduce the processing burden on the ground equipment, alternatives to the present baseline encoding concept will be briefly reviewed. This short discussion supports the baseline approach of five multiplexed encoders.

Figure G-1 illustrates the bit arrangement of the data as it is being processed in the baseline design. Note that all timing is scaled in proportion to the input data rate. Any uncoded data rate from a 4 Mbps to 50 Mbps can be accommodated.

Figure G-2 shows an alternate encoder which uses a single 31-stage linear feedback shift register, instead of multiplexing five standard 7-stage linear feedback shift registers. Implementation with the 31-stage shift register removes the requirement for the signal processor multiplexers and demultiplexers, but will require some data formatting, either on the Orbiter as shown in G-2, or on the ground to prepare the encoded data for the five Viterbi decoders. As shown, the formatted data is identical to that of the baseline design (see Figure G-1).

The tap or connection polynominals $G_1(X)$ and $G_2(X)$ for the 31-stage encoder are related to the tap polynominals $g_1(X)$ and $g_2(X)$ for the 7-stage encoder by $G_1(X) = g_1(X)^5$ and $G_2(X) = g_2(X^5)$. The first two symbols at the output of the long encoder correspond to the first branch of the first (of five) short encoder; the second two symbols correspond to the first code branch of the second short encoder, etc.

Implementation of the 31-stage encoder would eliminate the logic required for the demultiplexing and multiplexing, but would require additional logic for the longer shift register. As the baseline approach allows a very simple serial-to-parallel and parallel-to-serial implementation for the demultiplexer and multiplexer, respectively, only a single standard MSI integrated circuit is required for each. The 31-stage shift register requires an addition of three standard MSI integrated circuits (longer shift register ICs are not applicable, as the output from each stage is required). Also, the long shift register would have to operate at the 50 Mbps rate, requiring MECL logic devices, which consume considerably more power than do the LPSTTL devices used in the baseline 10 Mbps encoder design. Finally, the data still needs to be formatted for the five Viterbi decoders, requiring MECL logic to operate at the 100 Mbps

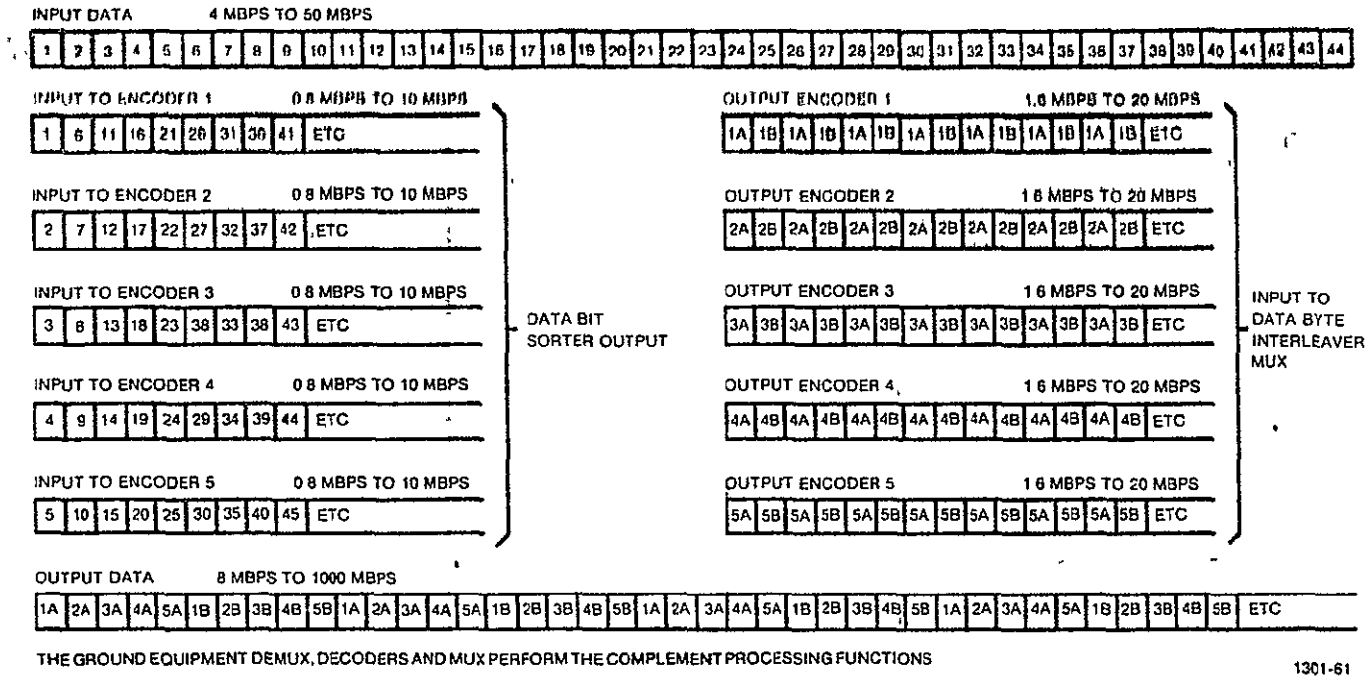

Figure G-1. Signal Processor Data Processing of the 50 Mbps Data

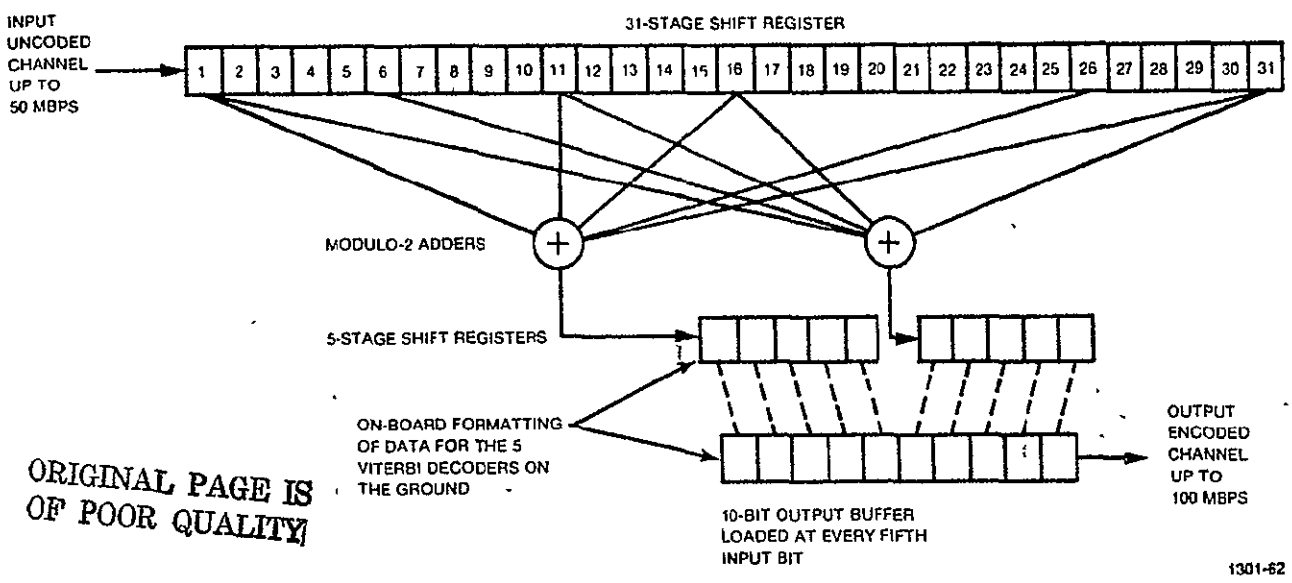

ORIGINAL PAGE IS OF POOR QUALITY

Figure G-2. Alternate KuSP 50 Mbps Convolutional Encoder

rate. Thus, while the 31-stage encoder appears to be the less complex approach in concept, actual implementation favors the multiplexed five 7-stage encoder approach.

A single 7-stage encoder operating at the 100 Mbps encoder rate could also be used in the signal processor. However, to operate with the five Viterbi decoders on the ground, the data would need to be blocked. This means that a number of information bits are encoded and blocked by finishing off the data for each decoder with a tail of six additional data zeros. These six data zeros are required to bring the encoder (and decoder) back to the all-zeros state to reinitialize the encoder-decoder for each new block. There is a corresponding loss in E_b/N_o (several tenths of a dB), depending on the percentage of overhead required. Other modifications to the Viterbi decoders to insure all-zero state initialization may also be required (such as resetting all the state metrics and forced branch synchronization). Clearly, this approach introduces more risk for only a marginal decrease in encoding complexity on the Orbiter.

FIXED ENCODED DATA RATES FOR RETURN LINK

To reduce the data handling problems for the ground equipment introduced by a continuum of data rates between 8 Mbps to 100 Mbps, a rate buffering technique is proposed here as a possible alternative. This scheme apportions the continuum of Payload data rates to five fixed rates. These are: 10 Mbps, 20 Mbps, 30 Mbps, 40 Mbps, and 50 Mbps. The apportionment is as follows:

PAYLOAD DATA RATES	BUFFER OUT RATES	ENCODED RETURN LINK RATE
4 Mbps to 10 Mbps	10 Mbps	20 Mbps
10.000001 Mbps to 20 Mbps	20 Mbps	40 Mbps
20.000001 Mbps to 30 Mbps	30 Mbps	60 Mbps
30.000001 Mbps to 40 Mbps	40 Mbps	80 Mbps
40.000001 Mbps to 50 Mbps	50 Mbps	100 Mbps

While this buffering concept could have several implementations, an example of one implementation is presented here. Implementation of this proposed alternate data handling scheme is shown by the functional block diagram of Figure G-3. A random access memory (RAM) buffer would be required to rate-buffer the slower rate input Payload data and, when added to fill data, produce the higher rate uncoded return link data. The clock regeneration circuits which consist of amplitude and frequency synthesizing techniques, using multiple taps from the feedback divider timing network and multiple phase detectors, will re-clock and synchronize the data as is done in the baseline design. The re-generated clock would be counted in a 10-bit counter for a period of approximately 16 μs. The 16 μs interval would be obtained from a 64 kHz clock sent to the signal processor from the Electronic Assembly. Clock stability would have to meet or exceed that of the Payload data timing. The 10-bit counter allows the input Payload data rate to be resolved to 100 kHz increments. The resultant count is read into a 4096 bit read-only-memory (ROM), used as a table look-up. The ROM's output number (3-bits) is used to determine the return link data range by preset command of the encoding timing and control logic. The 10-bit number itself is sent to the control and displays (or GCILC) to report the exact Payload data rate received (within 100 kHz). The

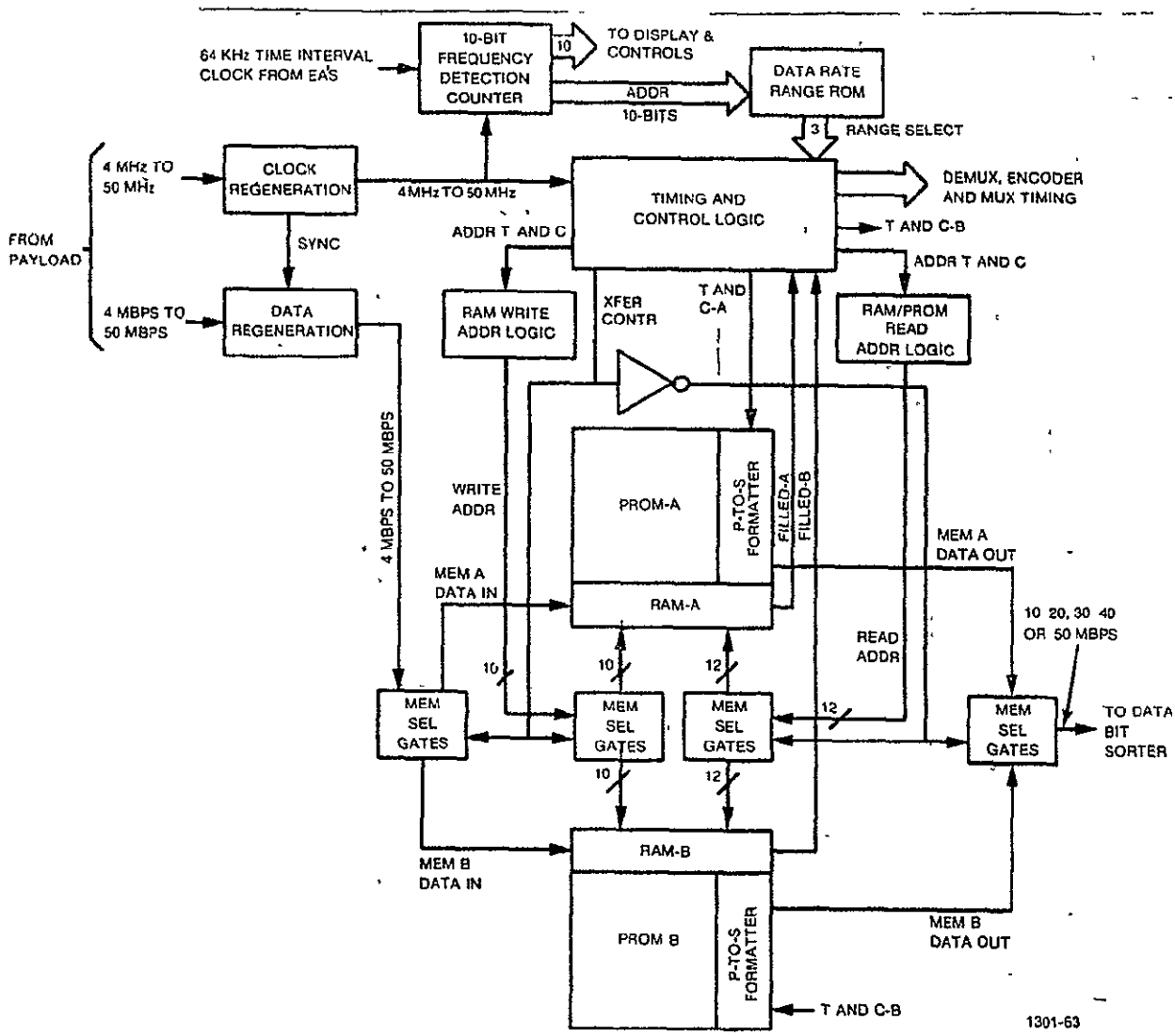

Figure G-3. High Rate Data Buffer

ORIGINAL PAGE IS OF POOR QUALITY

ground would thus set its ground processing rate to the appropriate return link rate from one of the five return link rates available.

The buffer itself would consist of two memory halves, which would alternate in performing the buffer input and buffer output functions. The exact size of these memories would require a detailed timing analysis of all the requirements, and tradeoffs of performance versus cost will have to be considered. The example implementation uses a 3584-bit memory (one 1024-bit RAM, one 2048-bit PROM, and one 512-bit PROM for each buffer half. The RAM is used for the buffered Payload data and the PROM are used for the fill data. Relative memory sizes are dictated by the limiting condition of a 4 Mbps Payload data rate with the 10 Mbps buffered data rate. In this condition, the output rate is 2.5 times the input rate. Thus the fill data block needs to be 2.5 times the Payload data block in memory. This corresponds to 1024 bits of Payload data and 2560 bits of fill data. In other cases, the reverse conditions exists; for example; a 40.000001 Mbps Payload data rate results in a 80% memory requirement for Payload data and 20% for fill data. Thus, in most cases only a small portion of the fill data PROM will be used (204 bits for the above case). The fill data may consist of any pattern desired; all ones, all zeros, alternate ones and zeros, or random data are all possibilities. The PROM implementation allows some flexibility in fill data selection. The fill data may require 30 trailing zeros to initialize the five Viterbi decoders on the ground for the next Payload data block. This would not be required if the fill data is removed after the decoding process.

The memory that is functioning as the fill buffer half controls the functional switchover between the buffer halves. When the functioning input buffer reaches overflow, it signals the timing and control logic

to immediately switch over the function of the buffer halves. The functioning output buffer will at that time be outputting fill data from some portion of the PROM. Actually, the switchover initiation could start a few bit-times earlier, such as at 1020-bits, to insure a timely switchover. Also, the last few bits in RAM (e.g. 15-bits) could be used as a signal to the ground that a switchover (Payload to fill or fill to Payload) is about to occur. As shown in Figure G-3, when switchover occurs, the I/O timing and data I/O for the buffer halves are switched.

In addition to supplying the buffer I/O timing, the timing and control logic supplies the five timing signal sets for the Data Bit Sorter, the five convolutional encoders, and the Data Byte Interleaving Multiplexer. Selection of the signal sets to be used is controlled by the data rate range ROM described earlier.

Note that while not all the convolutional encoders are needed for Payload data rates $\leq$40 Mbps, the demultiplexing, encoding, and multiplexing implementation is the simplest and most straight forward for the signal processor by using all encoders and scaling the demultiplexing, encoding, and multiplexing timing accordingly. Thus, this portion of the high rate data handling would be identical to that used for the baseline approach. Little is gained in the signal processor by using fewer numbers of the encoders, data rate permitting, as the hardware for all five still needs to be incorporated in the design. As the design consists mostly of flip-flop elements, power dissipation is the same, whether processing data or in a standby state.

ADDITIONAL MODIFICATION

If the ground equipment requires the flexibility of not using all five of the Viterbi decoders when the high rate Payload data permits, an additional modification could be incorporated in the signal processor encoding logic. For the 4 Mbps to 10 Mbps data, only a single convolutional encoder would be used; 10.000001 Mbps to 20 Mbps would require two convolutional encoders, and so forth until the 40.000001 Mbps to 50 Mbps would require all five convolutional encoders. The timing and control logic would have to be redesigned to supply five different types sets of timing signals, one 5 set type for each forward link encoded data rate range. The pre-encoding demultiplexing (i.e. Data Bit Sorter) and post-encoding multiplexing (i.e. Data Byte Interleaver Mux) would also need to be reconfigured for each forward link encoded data rate range in order to accommodate the changing byte structure. The tradeoff required would be the flexibility of the ground data handling equipment versus increased high speed MECL 10K logic in the signal processor. The additional power could be as high as 2 to 3 W of prime 28 V power.

ADDITIONAL POWER AND HARDWARE REQUIRED FOR MAIN MODIFICATION

The example implementation would require approximately 29 additional integrated circuits, including 8 LSI memory devices. The majority of the additional logic is needed in the added timing and control that this required, plus the memory addressing, and data I/O's. The additional power requirement would be approximately 10W of prime 28V power.

APPENDIX H

INVESTIGATION OF A 3-CHANNEL PM MODE

1.0 INVESTIGATION OF A THREE CHANNEL PM MODE

The problem of transmitting three asynchronous data channels without resorting to some form of time division multiplexing of the bit streams can be solved by using an eight phase PSK modulation scheme. Because the data rates are widely different, the signal energy allotted for each channel should be proportional to these rates. This leads to unbalanced modulation in the sense that the angles between phase states representing the eight different combinations of the data are not equal. Hence, the mechanization of an eight phase PSK system in the usual sense becomes difficult. For this reason two other schemes for generating an 8 phase PSK signal were examined. In the first, the two lower rate data channels are QPSK modulated on a subcarrier which then becomes one input channel to a second QPSK modulator which has as its second input the high rate data. Details of the analysis of this system are given in section 2.0. The second scheme frequency multiplexes the two lower rate channels by first biphase modulating a subcarrier with the lowest rate data then summing the subcarrier and the middle rate channel. This composite then forms the quadrature channel while the high signal becomes the in-phase channel for transmission. This system is detailed in section 3.0.

The results of these two analyses indicate that the two systems are very similar in terms of signal design. The second scheme does have some inherent crosstalk between the two channels which are frequency multiplexed, but the level is not high enough for the link performance to be seriously impaired. Thus hardware implementation becomes a key factor in determining which of the two is a better overall solution. The study results indicate that the first scheme is preferred because it uses the QPSK modulated subcarrier, a function which is common the FM mode, and because the total number of hardware functions is fewer.

2.0 PHASE MULTIPLEXED MECHANIZATION

The functional implementation for this scheme is shown on Figure H-1. In this mechanization data channels d_2 and d_3 are unbalanced QPSK modulated on a subcarrier. This signal then modulates the quadrature term of the carrier reference. The in-phase term is biphase modulated by data channel d_1. The composite of the two results in an unbalanced 8 phase PSK modulated signal. This can be visualized by assuming a square wave subcarrier reference then writing the modulated output as follows:

$$e(t) = \sqrt{2P}\ b_1\ d_1 \cos \omega_c t + \sqrt{2P}\ b_2\ (a_3 d_3 s_3 + a_2 d_2 s_3 \angle 90^\circ) \quad \sin\ \omega_c t$$

where d_1, d_2, and d_3 are the respective data streams each with a value of ±1,

a_2 and a_3 are the gains necessary to properly apportion the subcarrier power,

b_1 and b_2 are the gains necessary to apportion the carrier power,

and s_3 and $s_3 \angle 90^\circ$ are the in-phase and quadrature components of the square wave subcarrier with levels of ±1.

Evaluating the carrier term coefficients at each of the possible states yields the eight carrier phases indicated on Figure H-2. This shows that this mechanization is a form of unbalanced 8 phase PSK modulation.

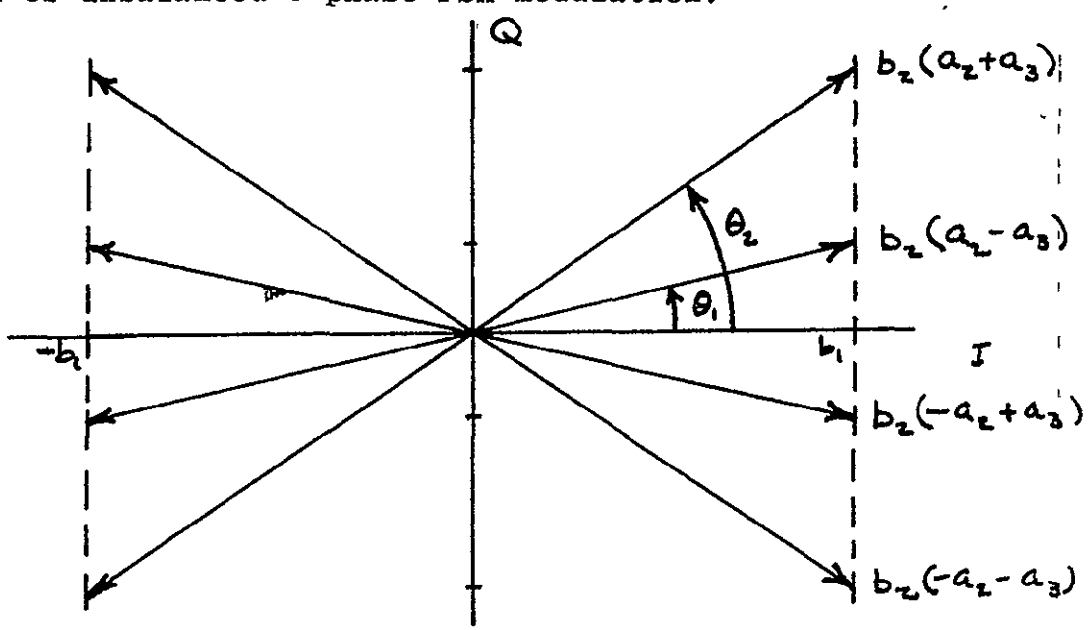

Figure H-2. The eight output phases of the QPSK/QPSK Modulator

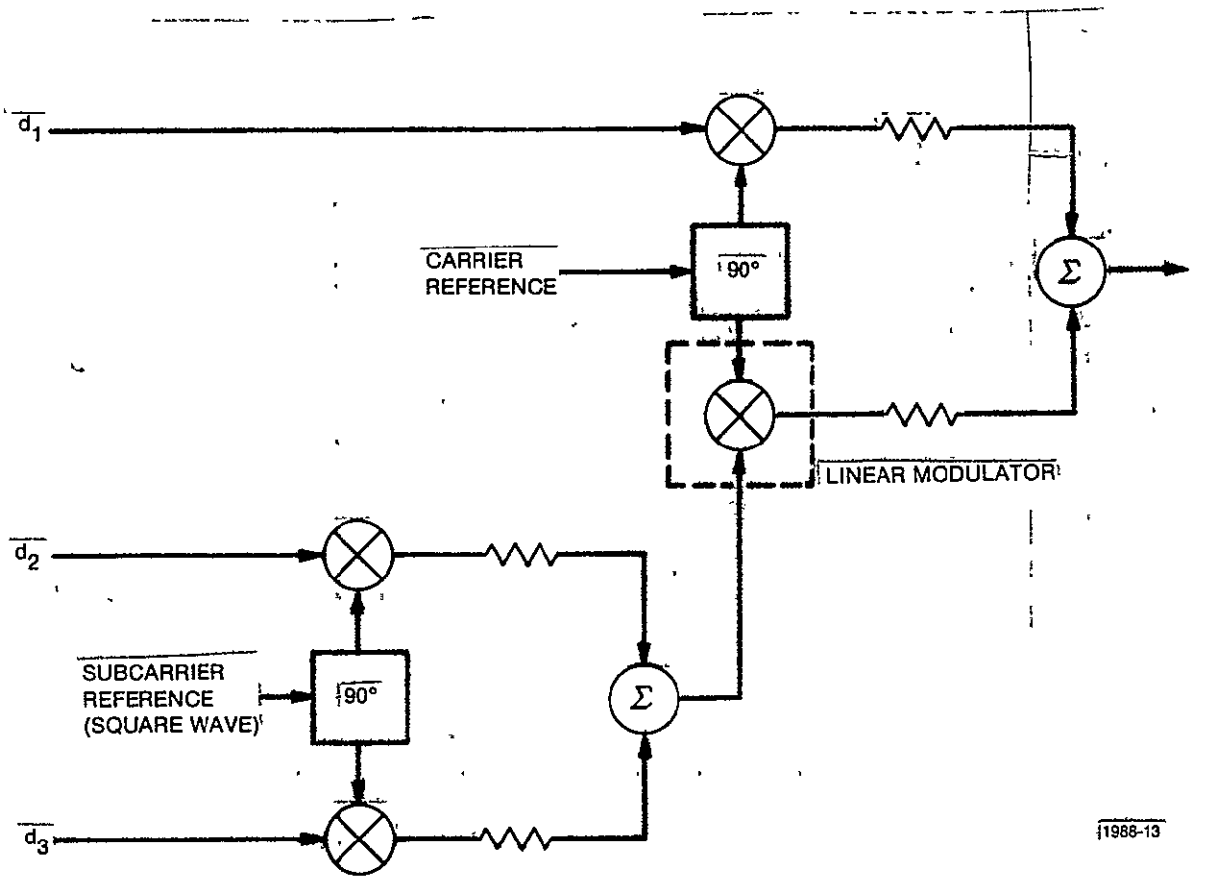

Figure H-1. Functional Block Diagram QPSK/QPSK Mechanization.

ORIGINAL PAGE IS
OF POOR QUALITY

The power apportionment among the data channels can be used to solve for the coefficients b_1, b_2, a_2, and a_3. By defining R_1 as the ratio of in-phase to quadrature carrier power and R_2 as the ratio of in-phase to quadrature subcarrier power, the following expressions can be written:

$$b_1^2 + b_2^2 = 1 \qquad \text{and} \qquad a_2^2 + a_3^2 = 1$$

$$R_1 = \frac{b_1^2}{b_2^2} \qquad \text{and} \qquad R_2 = \frac{a_2^2}{a_3^2}$$

These lead to expressions for the basic modulation angles θ_1 and θ_2:

$$\tan \theta_1 = \frac{(\sqrt{R_2} - 1)}{\sqrt{R_1 (R_2 + 1)}}$$

$$\tan \theta_2 = \frac{(\sqrt{R_2} + 1)}{\sqrt{R_1 (R_2 + 1)}}$$

Evaluated for $R_2 = R_1 = 4$; $\theta_1 = 12.6^\circ$ and $\theta_2 = 33.8^\circ$.

Evident from Fig. H-2 is that this signal contains some inherent amplitude modulation. This AM will be removed by amplitude limiting system elements following the modulator. The effects of the limiting are shown graphically on Fig. H-3 for the first quadrant vectors of the eight phase output. The result of the limiting will be to distort the intended signal.

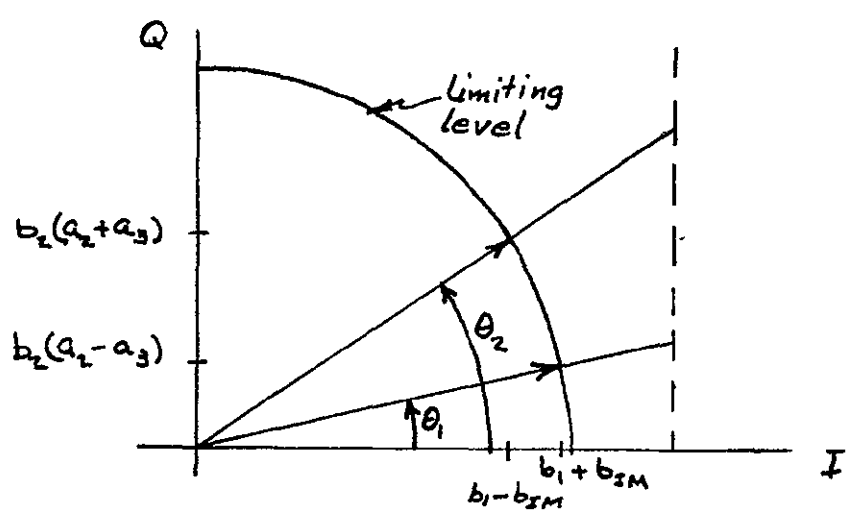

Figure H-3. Vector diagram of the limited signal

The effect of the distortion will be: (1) to alter the ratio of power between the two low rate signals which are in quadrature on the subcarrier, (2) to alter the ratio of power between I and Q channels of the carrier, and (3) to introduce an AM term on the high rate data which will cause an increase in the average probability of error. The effects can be seen numerically using the phase angles θ_1, and θ_2 calculated previously. For these values, the signals available for demodulation are:

$$\sin \theta_2 = b_2 (a_2 + a_3) = .56$$

$$\sin \theta_1 = b_2 (a_2 - a_3) = .22$$

$$\cos \theta_2 = b_1 - b_{IM} = .83$$

$$\cos \theta_1 = b_1 + b_{IM} = .98$$

where b_{IM} has been introduced as the intermodulation term. These can be solved for the amounts of power available in the output and are shown in comparison with the input allocation in Table H-1. The data in this table shows the alteration of the power ratios established by the input criteria.

Table H-1. Data Channel Power Allocation Before and After Limiting

Data Channel	Input	Output	E_b/N_o Degradation
d_1 (b_1)	80%	81.6%	.4 dB
d_2 (b_2 a_2)	16%	15.0%	.3 dB
d_3 (b_2 a_3)	4%	2.9%	1.4 dB
IM	--	.5%	----

The effect on data channels d_2 and d_3 will be a signal loss and the concomitant degradation in bit error performance. The effect on d_1 is significantly different. In this channel the signal level will be changing at a rate much slower than the maximum symbol rate so that the detector will see a signal which has two values of E_b/N_o. Half the time it will see a signal level proportional to $b_1 + b_{IM}$ and half the time it will be $b_1 - b_{IM}$. In terms of the values indicated on Tab. H-1 the variation will be approximately ±0.7 dB about the nominal b_1 value. By assuming the nominal value consistant with a $P_E = 10^{-6}$, the variation

described will cause a degradation in bit error performance equivalent to an E_b/N_o degradation of about 0.5 dB. This is offset slightly because of the increased average power of 0.1 dB shown on the Table. The net result is, however, a degradation of 0.4 dB.

If the degradations in the low rate channels are too severe, the input angles can be predistorted. For example, the angles θ_1 and θ_2 can be adjusted so that the output ratio between channels d_2 and d_3 is the desired 4 to 1. First quadrant vectors for the angles required to achieve this are shown on Fig. H-4. Solving for the output allocation of power for this predistorted signal in the same way described above yields the values shown in Tab. H-2. Note that all the degradation has been allocated to the high rate channel. Again this degradation is due to the AM resulting from the intermodulation term which causes a variation in E_b/N_o of about ±0.9 dB. This causes an average degradation in bit error performance at $P_e = 10^{-6}$ equivalent to an E_b/N_o loss of 0.6 dB. Thus by redistributing the modulation slightly the output of the limiter very closely approximates the desired signal structure.

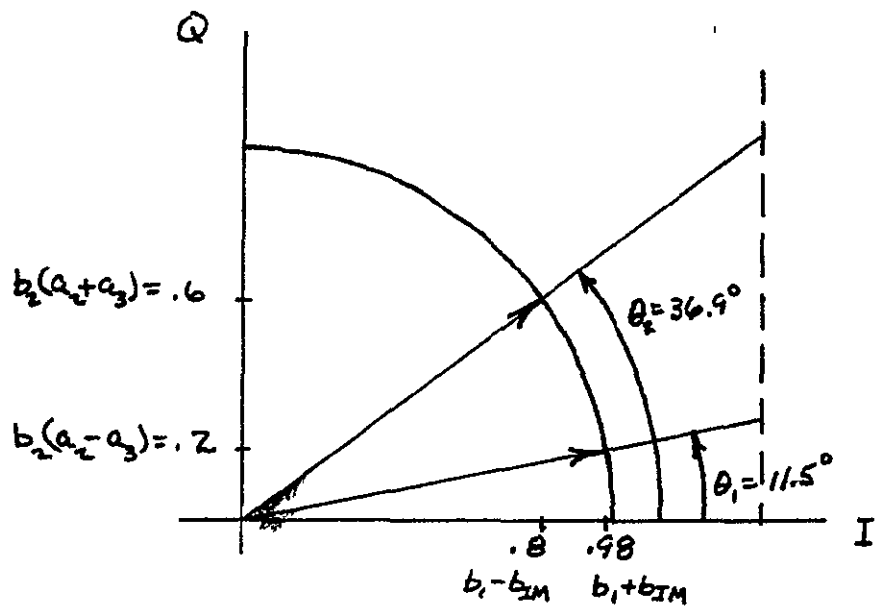

Figure H-4. Vector diagram for a predistorted input signal

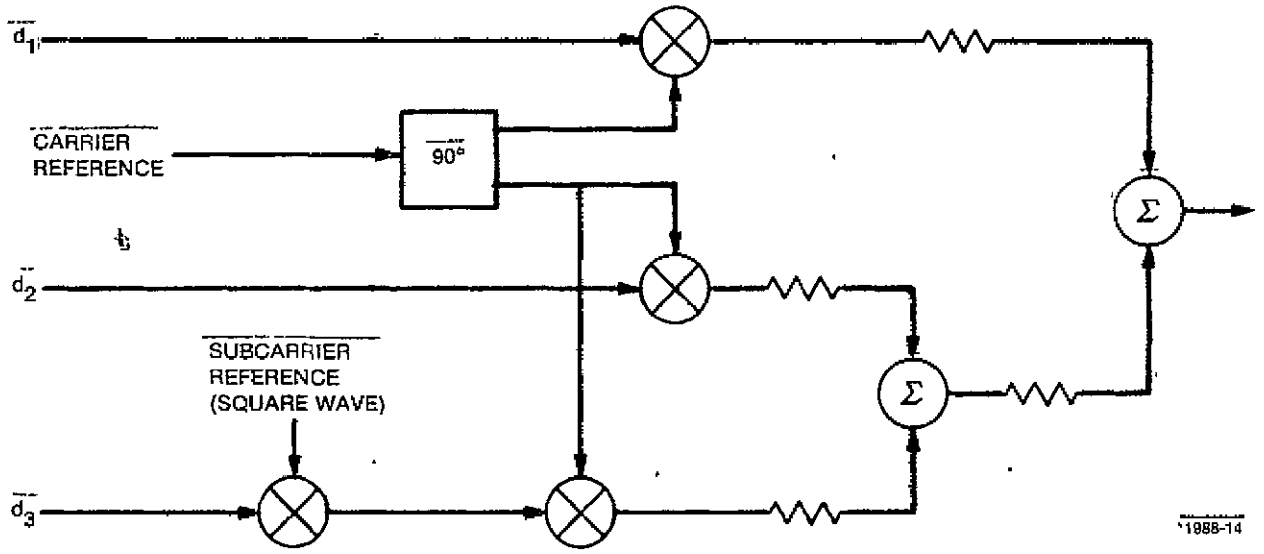

Figure H-5. Functional Block Diagram: FDM/QPSK Mechanization.

Table H-2. Data Channel Power Allocation Before and After Limiting Using Predistorted Modulation

Data Channel	Input	Output	E_b/N_o Degradation
d_1 (b_1)	80	79.2%	0.6dB
d_2 (b_2 a_2)	16%	16%	0
d_3 (b_2 a_3)	4%	4%	0
IM	--	0.8%	---

3.0 FREQUENCY MULTIPLEXED MECHANIZATION

The functional mechanization for this scheme is shown on Figure H-5. This system has evolved through examination of the Interplex system described in the JPL documentation (1)-(8). In the block diagram shown the low rate data channels are combined by modulating d_3 on a subcarrier then adding d_2 and the subcarrier after they have both been PSK modulated on the quadrature phase of the carrier reference. This effectively frequency division multiplexes the two low rate signals. Channel d_1 is PSK modulated on the in-phase carrier component then summed with the quadrature term to form the unbalanced QPSK signal. The output waveform can then be written as follows:

$$e_o(t) = \sqrt{2P}\, b_1 d_1 \cos \omega_c t + \sqrt{2P}\, b_2 (a_2 d_2 + a_3 s_3 d_3) \sin \omega_c t$$

where d_1, d_2, d_3, and s_3 all have values of ±1 and b_1, b_2, a_2, and a_3 are the appropriate gain coefficients for apportioning the power in each channel. From this expression it is obvious that this scheme also generates eight unique phases similar to those generated by the QPSK/QPSK system. This difference between the two mechanizations lies in the methods used for making the low rate signals orthogonal. In the first it was a phase orthogonality while in this scheme orthogonality is achieved by placing the lowest rate signal in an unused portion of the spectrum.

The nominal performance of this scheme will then be just as previously described for the first mechanization. The effects of amplitude limiting the signal will also be the same. Thus by predistorting the angles of modulation to those shown on Figure 4, the limited output will be exactly that of the Interplex modulation scheme described in the literature and the results listed on Table H-2 apply.

Crosstalk between channels is caused by the errors in orthogonality. In the QPSK portions of each of these schemes the orthogonality is controlled by the quadrature relationship of subcarrier references. This frequency multiplexing scheme depends on spectrum occupancy for the orthogonality between channels d_2 and d_3. The assumption was made that by modulating d_3 on a subcarrier, it could be placed in a portion of the spectrum where no significant energy from d_2 existed. The validity of this assumption

was tested by calculating the signal to crosstalk levels as a function of channel d_2 bit rate. The signal in channel d_3 is calculated as

$$E_3 = \frac{E_2}{4} = \frac{1}{4}\int_0^{\infty} \frac{\sin^4 (\frac{\pi}{2} f T_2)}{(\frac{\pi}{2} f T_2)^2} \, df = \frac{1}{4} \cdot \frac{1}{2 T_2}$$

where d_2 is a biphase L signal with bit period T_2. The crosstalk is calculated as the energy from d_2 existing in a matched filter detecting d_3 at the subcarrier frequency. Thus, energy from d_2 in d_3 bandwidth is calculated as

$$C_r = \int_{f_{sc} - 4B_3}^{f_{sc} + 4B_3} \frac{\sin^4 (\frac{\pi}{2} f T_2)}{(\frac{\pi}{2} f T_2)^2} \cdot \frac{1}{2} \frac{\sin^4 (\frac{\pi}{2} f_x T_3)}{(\frac{\pi}{2} f_x T_3)^2} \, df$$

where B_3 is the frequency in Hz equivalent to the d_3 data rate, T_3 is the d_3 bit period, and $f_x = f - f_{sc}$.

The ratio of E_3/C_r is plotted on Fig. H-6 as a function of the d_2 data rate. For purposes of this plot the d_3 rate was fixed at 192 kbps modulated on a 8.5 MHz subcarrier with a power ratio of 4 to 1 between d_2 and d_3. The undulations are caused by the subcarrier occuring at peaks or nulls of the d_2 data spectrum depending on the specific data rate. The plot shows that for this set of assumptions the E_b to crosstalk distortion in channel d_3 will be at least 22 dB. This then verifies the assumption that the frequency multiplexing provides adequate orthogonality between d_2 and d_3.

Comparing these two mechanizations has demonstrated that they are virtually alike in the expected performance. The one which offers the most economical mechanization will thus be better suited for inclusion in the orbiter system. Evaluation of the hardware required shows that the QPSK/QPSK scheme appears to be better. First, it shares the QPSK subcarrier function with the FM mode, and, second, it contains fewer functions that have to be accomplished by the hardware.

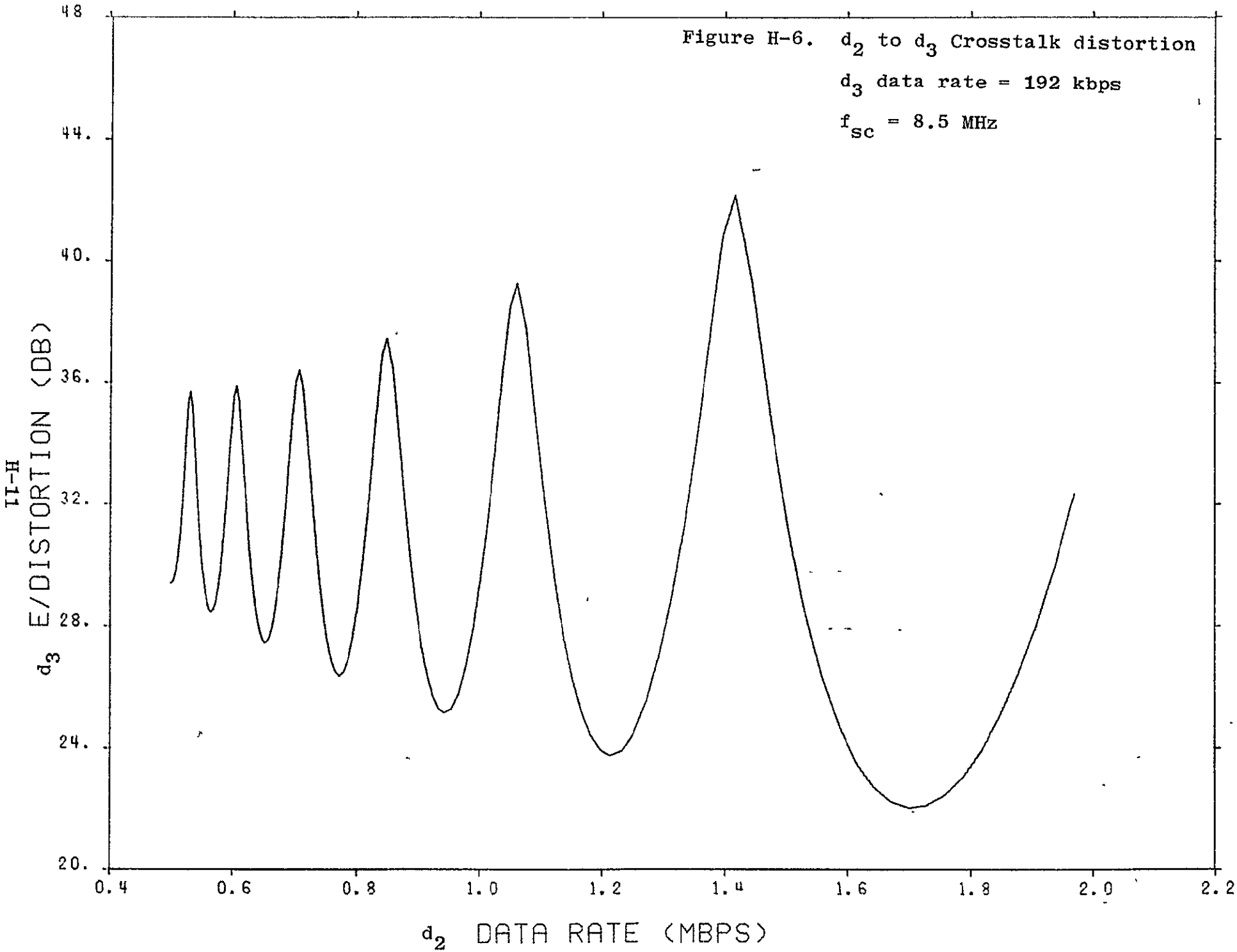

Figure H-6. d_2 to d_3 Crosstalk distortion

d_3 data rate = 192 kbps

f_{sc} = 8.5 MHz

REFERENCES

(1) Butman, S., and U. Timor, "Interplex - An Efficient Two-Channel Telemetry System for Space Exploration," JPL Space Programs Summary 37-62, Vol. III.

(2) --, "Efficient Multichannel Space Telemetry," JPL Space Programs Summary 37-63, Vol. III.

(3) La Frieda, J., "Optimum Modulation Indexes and Maximum Data Rates for the Interplex Modem," JPL Space Programs Summary 37-64, Vol. III.

(4) Butman, S., and U. Timor, "Suppressed-Carrier Two Channel Interplex Modulation System," JPL Space Programs Summary 37-64, Vol. III.

(5) Timor, U., "Efficiency of Biphase - Modulated Subcarriers, N-Channel Telemetry Systems," JPL Space Programs Summary 37-65, Vol. III.

(6) La Frieda, J., "Optimum Performance of Two Channel High-Rate Interplex Systems," JPL Space Programs Summary 37-65, Vol. III.

(7) Timor, U., "Optimum Configurations for PSK/PM Systems," JPL Space Programs Summary 37-66, Vol. III.

(8) Butman, A., and U. Timor, "Interplex Modulation," JPL Quarterly Technical Review, Vol. I, No. 1, April 1971.

APPENDIX I

MOTOROLA SPONSORED IMAGE CODING DEVELOPMENT STUDIES

a) Definition of an RPV Bandwidth Compression System

b) Survey of Image Coding Techniques

DEFINITION OF AN RPV BANDWIDTH COMPRESSION SYSTEM

REPORT 510-294

MOTOROLA, INC. - GED

S.M. Daniel
Systems Analysis Group

J.E. Greenwood
Drone Electronics Section

December 31, 1975

TABLE OF CONTENTS

Section	Title	Page
1.0	INTRODUCTION	
2.0	SYSTEM OBJECTIVES	
	2.1 Business Objectives	
	2.2 Method of Processing	
	2.3 Tools for Future Work	
3.0	IMAGE CODING APPROACH	
	3.1 Transform Options	
	3.1.1 Hadamard/DPCM	
	3.1.2 Hadamard/Hadamard	
	3.2 Coding Schemes	
	3.3 System Block Diagram	
4.0	SYSTEM DEVELOPMENT PLAN	
	4.1 Analysis	
	4.2 Computer Simulation	
	4.3 Hardware Realization	
5.0	REMARKS	

1.0 INTRODUCTION

The final report on ESP 510-270 [1] constitutes a fairly extensive survey of the most important image coding techniques useful for video bandwidth compression. As discussed there, the purpose of image coding is redundancy removal via an energy compaction transformation and optimal bit allocation by means of a quantization rule that guarantees minimum distortion in view of statistics involved. The net result of this process is a bit train of a desired bit rate corresponding to some tolerable distortion.

Bandwidth compression efficiency is directly related to the energy compaction capability of the particular transformation employed. However, it is by means of optimal quantization [2] that this compaction property is exploited to give rise to bandwidth compression.

Image coding techniques studied in ESP 510-270 included differential and transform techniques. Of the differential methods, we examined Delta Modulation (DM) [3], a special case of Differential Pulse Code Modulation (DPCM) [4]. Such techniques were noted to be susceptible to noise. Transform techniques considered included such transformations as the statistically optimal Karhunen-Loève (KL) [5], the Fourier (F) [6], the Slant (S) [7], the Hadamard (H) [8] and the Haar (A) [9], listed

according to their respective energy compaction capability. In addition, the newest method in the literature, Singular Value Decomposition (SVD) [10], [11], a deterministic transformation characteristically related to the image transformed, was also discussed. Although computationally prohibitive as it stands, this method is useful for surveillance purposes and continues to receive Air Force support [12].

image coding techniques mentioned above are conveniently compared in Table I indicating advantages, disadvantages and information densities (bits/pixel, B/P) required by each method that would guarantee less than 1% mean-square distortion error upon reconstruction. We have included three additional techniques, the CØS/CØS, CØS/DPCM [13], [14], [15] and the Constant Area Quantization (CAQ) [16] method.

Based on the best combination of hardware simplicity and expected performance, it has been recommended that Motorola pursue the development of a Hadamard-based bandwidth compression system. The present report is intended to outline the IDP effort during 1976 for the development of such a system. Section 2.0 gives specific system objectives further justifying the present

image coding choice. Section 3.0 describes the H/H and H/DPCM options available to us. Optimal quantization is discussed and system block diagrams included. Section 4.0 outlines the proposed development plan consisting of analysis, computer simulation and hardware realization.

2.0 SYSTEM OBJECTIVES

The purpose of bandwidth compression of video signals in a remotely piloted vehicle (RPV) is to reduce the data bit rate to a level such that an acceptable amount of A/J processing of the video bit rate can be accomplished. Bandwidth compression also reduces the transmitter power in the RPV to a level commensurate with size, weight, prime power and cost objectives.

The proposed IR and D project is to design and build a digital bandwidth compression processor that will:

a) be aligned with a known future business objective.
b) Provide a technical understanding of the details of bandwidth compression processing.
c) Allow engineering to accurately assess tradeoffs regarding the method of processing, i.e., digital versus analog.
d) Provide the engineering tools to do further work in this technology.

Each of the above objectives can be met by the proposed approach. Figure 2-1 illustrates the bandwidth compressed A/J video link with representative video bandwidths shown. During this IR&D project it is proposed to buy a sensor (TV camera) and sensor display (CRT monitor). The bandwidth reduction processor and its inverse processor on the ground will be designed, fabricated and tested. The IRDP will buy/design and fab the SCAN conversion.

TABLE I. COMPARISON OF VARIOUS IMAGE CODING TECHNIQUES

TECHNIQUE	ADVANTAGES	DISADVANTAGES	B/P
* SVD	Maximum energy compaction	Prohibitive numerical complexity	0.05
KL	Statistically Optimal (MSE)	Numerically inefficient	0.30
* CØS/DPCM	Almost as good as KL Economical CZT/CCD implementation	CCD hardware problems yet to be solved. Successful in 1-2 years.	0.40
CØS/CØS	Slightly inferior to CØS/DPCM Economical CZT/CCD implementation	CCD problems. Success in 1-2 years. Large memory requirement.	0.50
F/F	Numerically efficient FFT algorithm	Memory requirement depending on block size. Slow-scan TV depending on multiply speed.	0.60
S/S	Numerically efficient FST algorithm	"	0.70
H/H	Numerically efficient FHT algorithm with only additions.	Memory requirement depending on block size, (H/DPCM does not have this disadvantage)	1.00
A/A	Numerically efficient FAT algorithm with few special multiplications.	Memory requirement depending on block size. Less noise immunity than H.	1.20
CAQ	Simple implementation	Sensitive to noise	1.20
DPCM	Simple implementation	Sensitive to noise	2.00
DM	Simplest implementation	Sensitive to noise. Needs to be sampled densely to overcome slope distortion (Adaptive DM possible)	3.00

*H. Whitehouse and R. Means of NUC claim that CØS/DPCM perform slightly better than CØS/CØS. See [15].

The proposed IRDP will integrate the five functional blocks shown in Figure 2-1.

2.1 Business Objectives

Two known customer requirements will be investigated before selecting the bandwidth compression system and sensor. The Army will use a laser designator with Martin Marietta's 155-mm cannon-launched guided projectile (CLGP) anti-tank round. An engineer at ECOM has indicated that the Lockheed Aquila mini-RPV will be evaluated for the CLGP mission, but, he does not expect the Aquila to be satisfactory for the CLGP mission. Therefore, GED needs to understand the CLGP target acquisition and designation requirement before selecting a sensor (TV camera) and its associated resolution and data rates. Obviously, this understanding is desired prior to selection of a bandwidth compression system.

The Navy has a future requirement for a mini-RPV target surveillance/classification mission. The RPV will use an electro-optical sensor. The video link is desired to be transmitted over an A/J link.

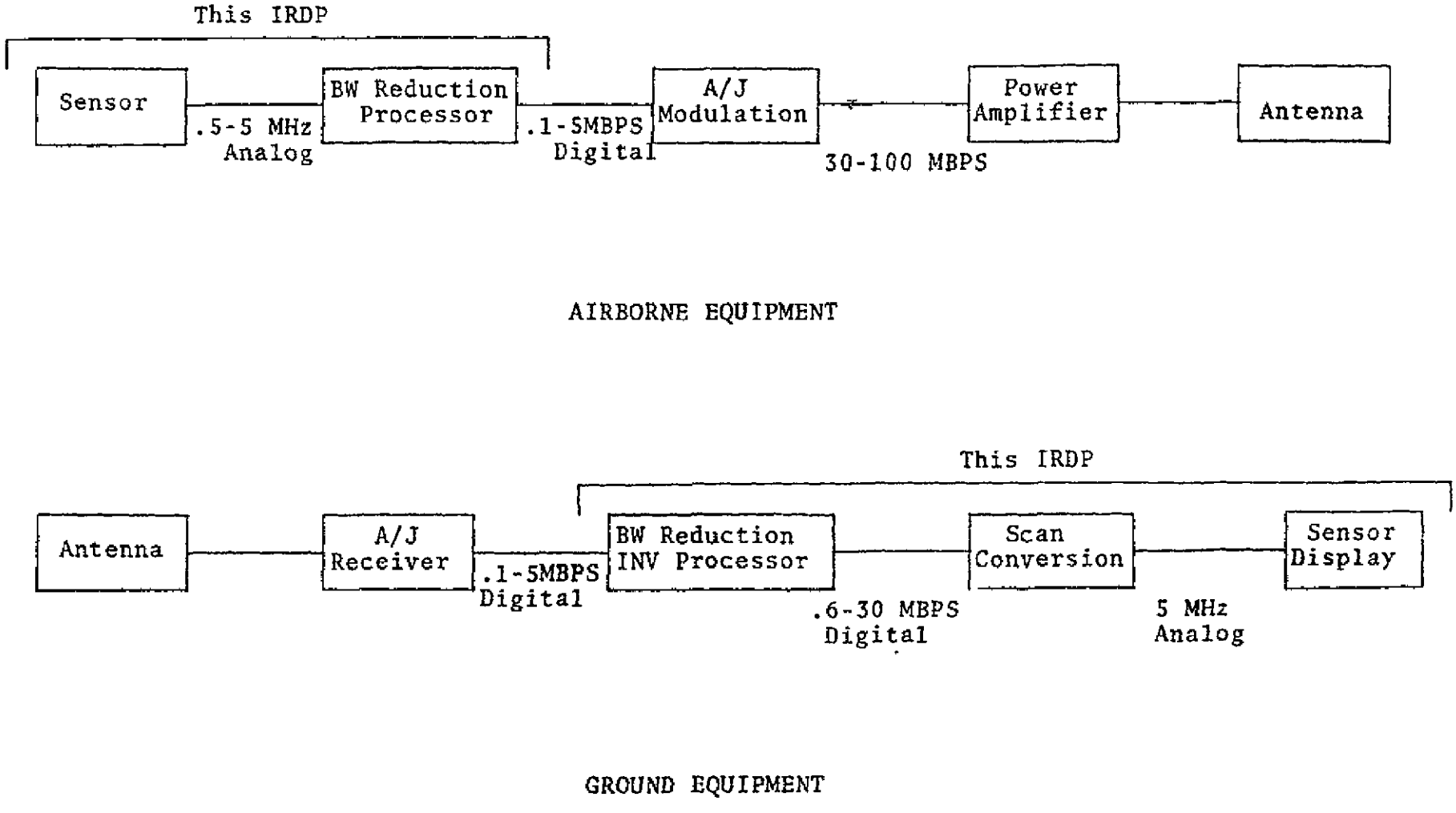

Figure 2-1. A/J Video Block Diagram

2.2 Method of Processing

The Army and DARPA have been funding the Naval Undersea Center (NUC) to design and build a bandwidth compression processor for at least one year. NUC selected a Cosine/DPCM transform utilizing analog CCD memories and transversal filters with analog multipliers. The quantizer is within the DPCM loop. The compaction/mean square error ratio for this type of transform processor is quite good. However, NUC is presently having error rate problems with their CCD/multipliers (in the region of 5% errors). They expect to get to 1% errors. They will release an RFQ for their processor in January 1976 and hope to have a final unit by September - October 1976. The primary reason that NUC selected an analog processor is that there was no acceptable A/D converter to operate with standard scan TV video rates ($\approx$ 3.5 MHz for 256 horizontal elements). But NUC samples 1/8 of the picture every field, effectively reducing the scan rate to 60/8 = 7.5 frames/sec. NUC was constrained to use a standard scan TV camera for their input signal.

We propose to examine the total mission problem and select the optimum sensor and bandwidth compression processor using a digital processor. We do not believe NUC will have an acceptable (especially including environmental objectives) unit by September - October 1976. Although the compaction/mean square error ratio of the Hadamard type transform is not as good as the Cosine/DPCM

type transform, we believe a digital bandwidth compression processor can be built with equivalent overall performance of the NUC system. With the advent of CCDs and bucket brigade devices, the analog memory processor may be feasible, but a digital processor would probably have better environmental performance, more flexibility and easier producibility. Also more dense digital CCD memories and higher speed processing are still being proposed by semiconductor product companies.

The proposed IRDP is to build an all digital processor for bandwidth reduction. The video data rate will be selected on the best combination of mission requirements and existing digital technology. If the NUC analog processor is successfully developed by the end of 1976, Motorola GED should investigate its use for future RPV systems.

2.3 Tools for Future Work

It is believed that the bandwidth compression technology will progress through analytical and hardware development stages over the next 10 years and that this technology is readily suited to the type of business/technological goals of Motorola GED. Therefore, any engineering analytical or hardware tools should be accomplished with the future in mind. Some items that bear on this are described below.

It is desirable to have a camera and refresh CRT display that would operate over a wide dynamic range of data rates. This would allow a microprocessor to be used for the bandwidth reduction processor (at very low TV data rates) so that other transforms could be evaluated as other business goals arise.

The resolution capability of the refresh memory and CRT display should be as high as feasible so that future sensor and processing could use the same refresh memory and CRT display. Probably a 1000 by 1000 element (pixel) refresh memory and CRT display will be adequate for any future display requirements.

Any engineering computer simulations should be well documented for future use.

Any set-ups for inputting real images to an engineering computer simulation should be adaptable to any sensor and any resolution.

3.0 IMAGE CODING APPROACH

Depending on particular system constraints, a Hadamard-based image coding scheme may be implemented in a variety of ways accommodating slow and fast scan TV and requiring low or high-memory storage. Below, we describe the transform options of such a system, note the principle of optimal quantization and give system block diagrams.

3.1 Transform Options

Two possible variations of an H-system come to mind; namely, H/DPCM and H/H.

3.1.1 Hadamard/DPCM

Let G be an N X N image matrix. Then, its H row-transformation is given by

$$T = GH \tag{3-1}$$

where

H = N X N matrix constituting the Hadamard transform operator

T = N X N matrix of the row or horizontally transformed image

Note that (3-1) may be viewed as a sequential row-by-row transformation. Buffering only two consecutive rows of transformed data we can employ a 1st order DPCM system as the vertical transformation. The resulting H/DPCM system is obviously applicable

to a real-time low-memory storage requirement.

3.1.2 Hadamard/Hadmard

A real-time large-memory storage system would result from the full two-dimensional transformation.

$$T = HGH \tag{3-2}$$

However, because the required storage of N^2 words (approximately 25 N^2 bits) would be excessive for an RPV application, we cannot take this option too seriously at this time. Note that when $N = 256$, the required storage is over 1 Mbit.

A real-time moderate-memory storage system that comes to mind is one involving a smaller-dimensioned vertical H-transformation; that is,

$$T' = H'GH \tag{3-3}$$

where

H = the $N \times N$ Hadamard matrix for horizontal transformation

H' = a smaller $n \times n$ Hadamard matrix for vertical transformation

Note that (3-3) is particularly suited to raster scanning and requires a buffer of nN words or 19 nN bits. When $N = 256$ and $n = 16$, the required storage is about 80 kbits.

A third alternative of an H/H transform is one involving transformation of small $n \times n$ blocks; namely,

$$T'' = H'GH' \tag{3-4}$$

Of course, such a system would correspond to a reduced frame rate of n/N of the normal rate. The advantage of this approach is that it requires a relatively small storage of n^2 words or $15n^2$ bits which amounts to 4 Kbits when n = 16. But it must be noted that this approach would be more susceptible to image motion distortion. If image motion distortion is a problem, the above approach could be modified. In fact, with sufficient memory to store all n X n blocks along the horizontal direction, (15nN = 64 kbits for n = 16 and N = 256) we could have a real time system.

3.2 Coding Schemes

The objective of a transformation is to operate on an image with a certain amount of pixel-to-pixel correlation and produce a transformed image with reduced transel-to-transel correlation. The consequence of such an operation is energy compaction, a concentration of the bulk of the image energy into a small number of transels. To actually achieve bandwidth compression, one has to exploit this energy compaction phenomenon by employing a suitable coding scheme.

One direct coding scheme is threshold coding. In this method, transels that exceed a preassigned threshold are quantized with a fixed number of levels and transmitted along with their locations via run-length encoding. All other pixels are ignored.

Another coding scheme is zonal coding. This coding method involves bit assignments of transel word-lengths over prespecified zones in proportion to the expected variance there as derived from a suitable statistical image model.

In both schemes quantization and reconstruction levels are selected to minimize the mean-square quantization error with respect to the probability density model employed for the transformed images, using Max's [2] optimal quantization algorithm. The net result of a coding scheme is to reduce the transformed image information into a bit-train with prespecified bit-rate

that insures a desired minimum mean-square quantization distortion.

3.3 System Block Diagram

Figure 3-1 shows the essential blocks of a video bandwidth compression system. The video information first undergoes the transformation from pixels to transels. Based on some quantization rule the transels are coded into an appropriate bit-stream with desired bit-rate and subsequently transmitted. Passing through a channel, the coded information is corrupted by white additive noise and an interfering jamming signal. At the receiver, the information is first decoded into distinct transels. If the noise statistics are known, it is possible to define the Weiner filter that would enhance the decoded transels. Finally, an inverse transformation results in the reconstructed video.

Figure 3-2 gives the basic block diagram of the one-dimensional Hadamard transformation, or, more specifically, a horizontal Hadamard transformation. As shown, input pixels enter the standby buffer at the sampling rate. When this buffer is filled, its contents are transferred in parallel to a working buffer. In the time it takes the standby buffer to get full again, the contents of the working buffer undergo a numerically efficient Fast Hadamard Transformation involving log N*

---

*N is the number of pixels in line to be transformed.

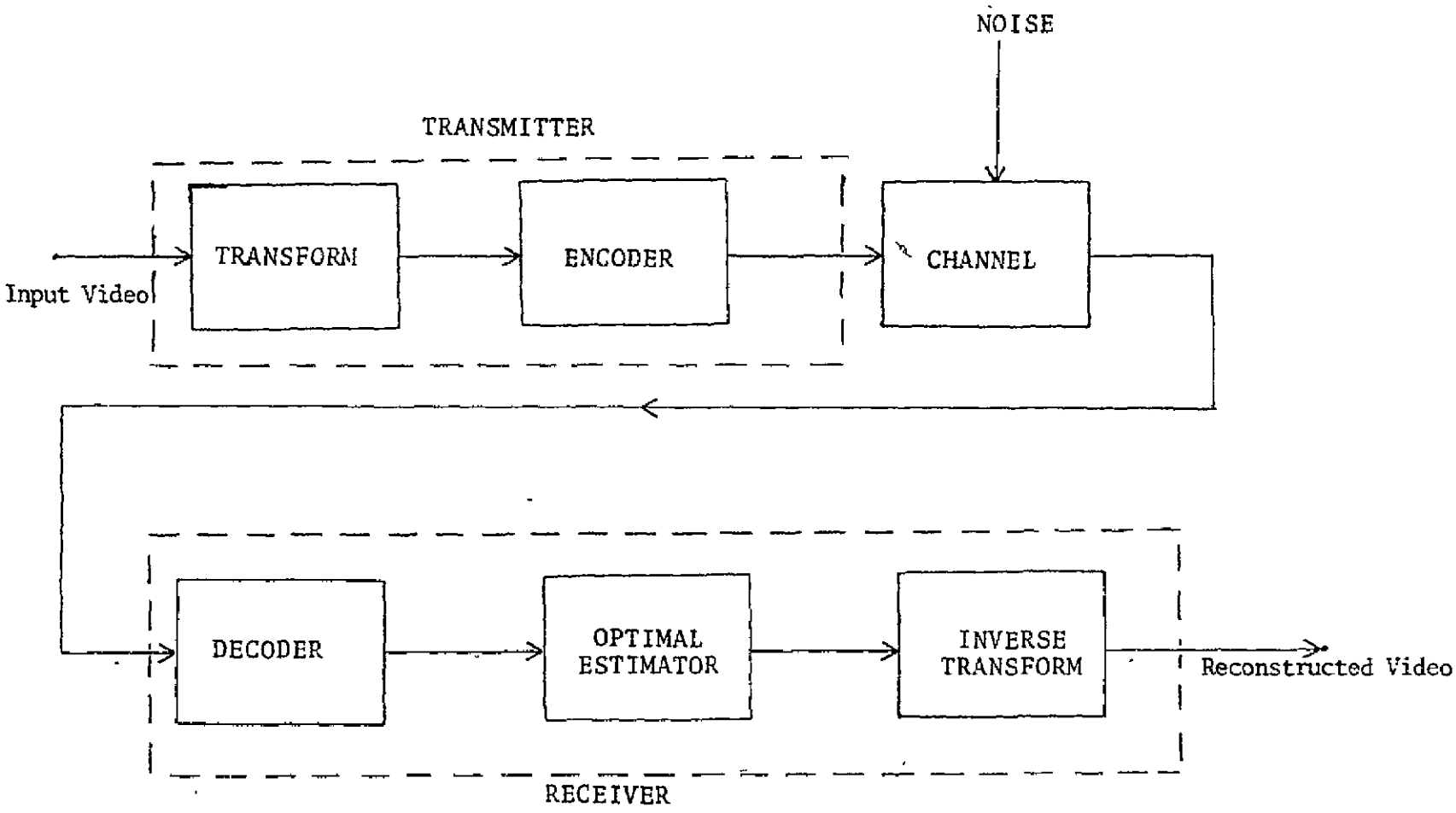

Figure 3-1. Essential Block Diagram of Video Bandwidth Compression System

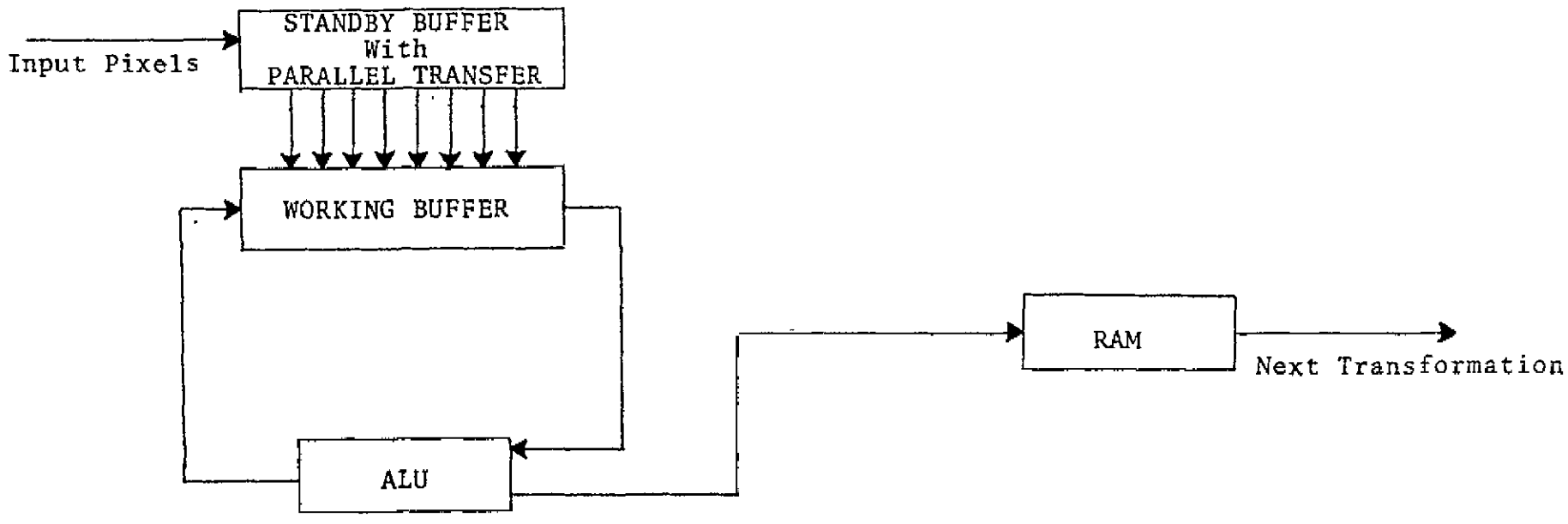

Figure 3-2. Basic Block Diagram for One-Dimensional Hadamard Transformation

recirculations via a program-controlled ALU. Strictly speaking, the last recirculation is not performed. Instead, the resulting transformed N-vector is transferred to a RAM, while the next N-pixel batch enters the working register. The data accumulated in the RAM, constituting the horizontal transformation, is available for further vertical transformation employing either another Hadamard transformation or a DPCM process.

It should be noted that the inverse Hadamard transform is identical to the forward transform. This is not true in the case of the DPCM [4] process as can be seen from the block diagram of the general n-th Order DPCM coder in Figure 3-3.

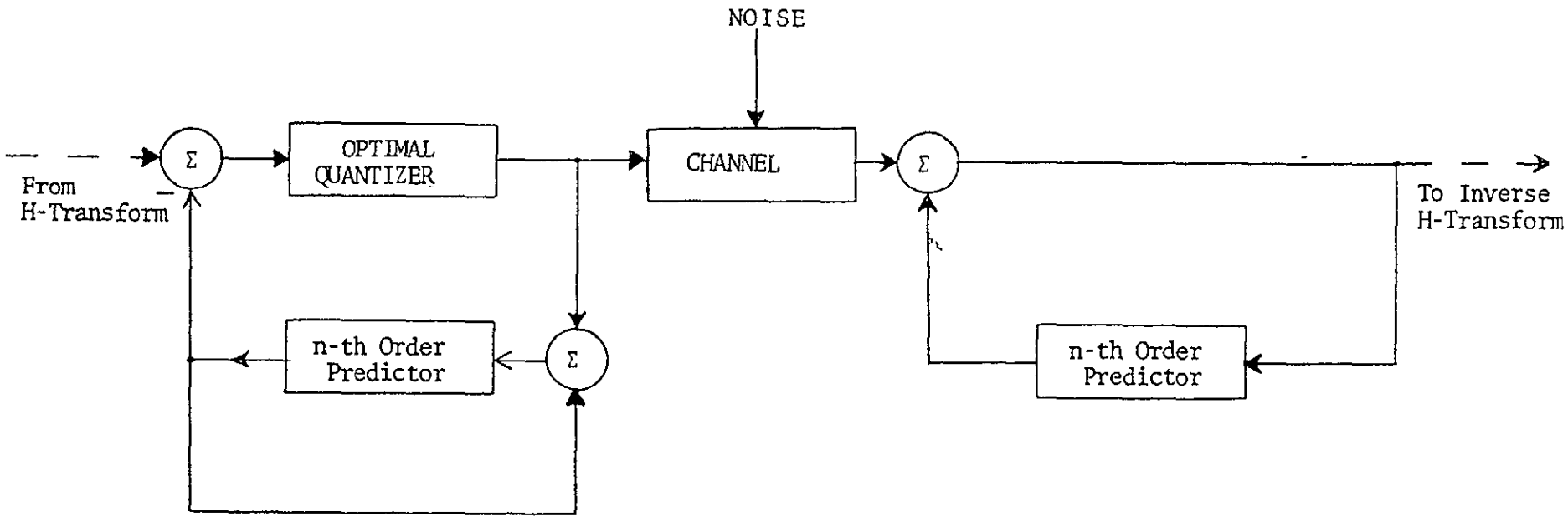

Figure 3-3. Block Diagram of n-th Order DPCM Coder

4.0 SYSTEM DEVELOPMENT PLAN

A meaningful plan for the development of a successful bandwidth compression system based on the Hadamard (H) transform should consist of a three-pronged effort; namely, analysis, computer simulation and hardware realization. Outlined below is a brief description of each category of effort.

4.1 Analysis

The purpose of analysis will be to provide an appropriate mathematical formulation of the bandwidth compression problem at hand. Some of the major outcomes from this effort will be the following:

(1) A precise definition of the fast H algorithm will be given for both the ordered and unordered versions of the transform. The H/DPCM and H/H transformations will be clearly described.

(2) A statistical model of a typical image will be assumed based on a first-order Markov process. This will allow us to define the pixel-to-pixel covariance. An expression for transel-to-transel covariance will then be derived for the H, H/DPCM and H/H transformations. Typical images will be analyzed to verify that the statistical first order Markov process is a reliable model.

(3) The probability density function of the typical transel amplitude will then be constructed based on information available in related literature. Because of the energy compaction induced by the above transformations, it is

expected that the transel amplitudes will exhibit a large dynamic range in variances and hence could not be characterized by the same density function.

(4) Given an information density constraint, (e.g., 1 bit/pixel), we will determine the bit allocations per transel location in such a way that the overall quantization distortion will be minimized. This will involve the use of optimal quantization.

(5) The precise nature of the optimal quantization process will be defined. One possible quantizer design would serve each transel according to its probability density. Another quantizer configuration could be designed for the transel density with the greatest variance. Using prewhitening, this quantizer could serve all transels. Unwhitening at the quantizer output will reinstate each transel to its appropriate dynamic range.

4.2 Computer Simulation

Especially for the system envisioned, a substantial computer simulation effort is imperative if we are to bridge the gap between analysis and realization. Briefly described below are some of the major aspects in this effort.

(1) The ordered and unordered version of the fast Hadamard transform will be incorporated into separate subroutines. Both subroutines will be checked by means of appropriate test functions.

(2) The H/H transform will then be programmed and tested using either or both versions of the H-subroutine. Simple image test examples will be used for this purpose.

(3) The DPCM algorithm excluding the quantization rule will be incorporated into a subroutine and tested.

(4) The H/DPCM transform will be programmed and tested.

(5) A variety of optimal or nearly-optimal quantization rules will be thoroughly exercised and evaluated. The aim will be to choose one coding scheme that will have the best combination of performance and hardware simplicity.

(6) H/H and H/DPCM programs will then be prepared employing suitable coding rules.

(7) A mean-square error (MSE) criterion will be incorporated into the programs.

(8) The transmission channel will be modeled as a binary channel with variable bit-error probability p. The MSE performance of each system will be tested for various p's.

(9) If it is feasible within the IRDP costs, some convenient means of displaying pictorial information could be devised if we are to visualize the performance of the

computer simulated system.

(10) If appropriate, image enhancement will be considered.

4.3 Hardware Realization

The design areas to be realized are the TV sensor, processor/inverse processor and the CRT display with refresh memory.

In addition to reviewing standard vidicon and silicon intensifier target vidicon TV cameras, the newer photodiode array and charge-coupled device (CCD) array cameras will be reviewed. Resolution, frame rate, light level range, size, weight, power and cost will be evaluated before a camera is purchased. A non-electromagnetic scanned type of sensor is desired so that the frame/data rate can be easily varied over a wide range (like 1-30 frames per second).

A/D devices and modules, memory devices, gates and arithmetic units of different logic families and semiconductor manufacturers will be reviewed regarding speed, cost, size, weight and power. This will assure that the processor architecture is designed in consonance with the state-of-the-art devices and we will know what future advances can be expected in digital semiconductor technology.

The CRT refresh memory approach will trade-off semiconductor memory devices versus fixed head disc memory devices.

After the research tasks are complete, a detail system design will be accomplished. The processor design, fab, integration and test will occur. Finally, system integration with inserted errors in the transformed image domain will be tested. It is also intended

to environmentally test the airborne bandwidth compression processor oven temperature.

The purchase of major items and the overall schedule is shown in Figure 4-1. The airborne processor design will use printed circuit boards. The schedule provides for redesign and fab of a second generation of these airborne boards. All ground based designs will use wired boards.

5.0 REMARKS

In choosing a Hadamard-based RPV video bandwidth compression system for a 1976 IRDP effort, we have tried to be realistic in view of the time involved. Although, as we have seen [1], the H-transform is inferior to others, its deficiency is offset by its hardware simplicity. It would be unwise of Motorola to attempt a CØS-based system and compete with several experts in its CCD implementation that has yet to prove feasible after three years of effort. On the other hand, the simplicity of the H-transform will allow more effort to be directed to the design of the remaining part of the system, a task that cannot be underestimated.

Having chosen the Hadamard-system at present, should not deter us from examining alternate approaches, keep up with advancements in technology applicable to the bandwidth compression problem and attend one or two image processing symposia a year.

Potential IRDP effort in 1977 that could reasonable extend 1976's proposed IRDP is:

1) Set-up a computerized technique to evaluate different transforms and coding for many different pictures.
2) Consider the utilization of LSI for the airborne bandwidth reduction processor.
3) Modification of the 1976 IRDP processor for explicit business goals of 1977 (such as higher speed, resolution, etc.).

PRECEDING PAGE BLANK NOT FILMED

Since we believe this technology could be of significant business potential, further effort in this area should be pursued continuously.

BIBLIOGRAPHY

[1] Daniel, S.M., "Survey of Image Coding Techniques", Motorola Final Report ESP. No. 510-270, June 30, 1975.

[2] Max, J., "Quantization for Minimum Distortion", IRE Trans. on Inf. Th., Vol. IT-6, March 1960, pp. 7-12.

[3] Abate, J.E., "Linear and Adaptive Delta Modulation", Proc. of the IEEE, Vol. 55, No. 3, March 1967, pp. 298-308.

[4] O'Neal Jr., J.B., "Predictive Quantizing Systems (Differential Pulse Code Modulation) for the Transmission of Television Signals", BSTS, Vol. 45, pp. 689-722, May-June 1966.

[5] Davenport, W.D., Jr., Root, W.L., "An Introduction to the Theory of Random Signals and Noise, pp. 96-98.

[6] Andrews, H.C., Pratt, W.K., "Foruier Transform Coding of Images", Hawaii International Conference on Systems Science, January 1968.

[7] Pratt, W.K., Chen, W-H, Welch, L.R., "Slant Transform Image Coding", IEEE Trans. on Com. Tech., Vol. COM-22, No. 8, August 1975.

[8] Pratt, W.K., Kane, J., Andrews, H.C., "Hadamard Transform Image Coding", Proc. of the IEEE, Vol. 57, No.1, January 1960.

[9] Haar, A., "Zur Theorie der Orthogonalen Funktionen-Systeme," Inaurural Dissertation, Math. Ann. 69, pp.331-371, 1910.

[11] Andrews, H.C., Patterson, C.L., "Outer Product Expansions and Their Uses in Digital Image Processing", Amer. Math. Assoc. Journal, Jan. 1975.

[13] Means, R.W., Spieser, J.M., Whitehouse, H.J., "Image Transmission Via Spread Spectrum Techniques", ARPA Quart. Tech. Rep. AD 780805, October-January 1974.

BIBLIOGRAPHY (Contd)

[14] Whitehouse, H.J., Means, R.W., "Bandwidth Reduction System Specification", Draft Copy of RFQ for CØS/DPCM CZT/CCD Implemented system obtained from NUC Dec. 1975.

[15] Bell, B., Greenwood, E., Daniel, S.M., "NUC Meeting", Trip Report Dec. 9, 1975.

[16] Pearson, J.J., "A CAQ Bandwidth Reduction System for RPV Video Transmission", Lockheed Palo Alto Res. Lab. Rep. LMSC-D457949, July 1975.

SURVEY OF IMAGE CODING TECHNIQUE

REPORT F-510-270

MOTOROLA, INC. - GED

S. M. Daniel
Systems Analysis Group
June 30, 1975

1.0 INTRODUCTION

When a TV picture conveys visually intelligible information, it necessarily contains a certain amount of intrinsic redundancy. Without this redundancy, manifested, for example, by substantial regions of constant or slowly varying image brightness, the picture would be unintelligible to the objective viewer.

Conventional TV transmits a picture on a carrier as analog modulation representing image brightness as sensed by an interlaced raster scanning process which, in effect, serializes the two-dimensional video information. As such, conventional TV transmission contains a large proportion of redundant information, thus wasting a substantial portion of the 4.5 MHz video bandwidth used. Ideally, one would want to remove all redundancy from the original picture, transmit the smallest set of essential features that characterize it, over a correspondingly reduced bandwidth, and, upon reception, reconstruct the picture by properly reinserting the redundancy. However, such an undertaking is neither warranted, nor economically feasible for conventional TV.

In contrast, a modern digital video transmission system employing 6 - 8 bit PCM and operating at conventional frame rates of 30/sec. would require exhorbitant bandwidth in excess of 50 MHz. It is in such special systems that bandwidth compression is a technical and/or economic imperative. A satellite digital TV link employing bandwidth compression would allow for a multiple channel operation, resulting in obvious economic benefit. A deep-space TV probe using a compressed bandwidth would provide better

quality imagery by virtue of SNR improvement. A compressed bandwidth RPV TV link would add to its AJ protection.

The subject of picture bandwidth compression [1] has captured the imagination of scores of investigators who, over the last 20 years, have introduced a wide variety of image coding techniques with varying sophistication and effectiveness as allowed by available technology at the time. Earlier coding schemes have involved easily implementable procedures including linear and adaptive delta modulation (LDM, ADM) [2], low-order DPCM [3] or some LDM-DPCM combination [4]. Such differential coding schemes, however, can become unstable in the presence of noise, resulting in undesirable streaking at reception.

With recent technological advances in the areas of SAW devices, CCD's [5] and digital logic*, it is now becoming possible to credibly consider realistic implementations of the more sophisticated transform coding techniques [6] which, unlike the differential coding schemes, exhibit some measure of noise immunity. Fundamentally, transform coding involves performing a generalized two-dimensional spectral analysis via a unitary matrix operator, mapping the space of a given number of sampled picture elements (pixels) onto the space of an equal number of transform elements (transels). For a given transform operator, image redundancy is reflected as a noticeable degree of transform domain energy compaction, in the sense that, say, 99% of the picture energy is confined within a small subset of transels.

---

* Motorola's MECL chip set including a 15 MHz 8-bit A/D - Private communication from J. Lavalle, GED.

Although not directly, it is this phenomenon of transform energy compaction that is capitalized for the purpose of realizing bandwidth compression. Note, for example, that by virtue of the energy conserving property of unitary operations, the essential transel subset will necessarily be characterized by transel magnitudes of a rather large dynamic range. As a consequence, transmission of the linearly quantized essential transel subset will occupy a substantial portion of the original PCM video bandwidth. However, based on statistical arguments, it is possible to derive a nonlinear quantization rule that assures minimum distortion [7] under the constraint of a maximum allowable number of quantizing levels. Employing such an optimal quantizer with, say, a maximum of 64 levels of quantization, it is possible to take advantage of the compaction provided by a given transformation and transmit the essential transel set over a compressed bandwidth that is more directly related to the degree of compaction.

Some of the better known transform operators include the Karhunen-Loève (KL), Fourier (F), Hadamard (H)*, Haar (A)** and the Slant (S) transforms. Of these, the KL is statistically optimal, providing maximum expected compaction. However, unlike the rest, it does not possess a fast computational algorithm and hence is numerically inefficient for most practical applications. The remaining transforms, listed in order of increasing numerical efficiency of their respective fast algorithms, are: F, S, H, A [6], [8].

---

*Sometimes referred to as Walsh transform.
**Alfred Haar, the famous German mathematician.

The present report constitutes a limited survey of the vast available literature on the subject of image coding. To the extent possible, an effort is made to touch briefly on a few of the most important coding schemes, giving, in each case, the underlying mathematical model. Keeping in mind that the main objective of this effort was to identify and recommend image coding schemes suitable to an RPV implementation, appropriate functional block diagrams of such schemes are included.

2.0 STATEMENT OF THE PROBLEM

A general bandwidth compression system may be viewed, fundamentally, in terms of its essential functional blocks, as shown in Fig. 1. The original redundant signal is first manipulated according to some rule for the purpose of extracting a set of identifying features displaying a minimum amount of correlation between themselves, thereby eliminating a corresponding amount of the redundancy. A select set of features are then classified according to some format which insures minimum average distortion in transmission through the noisy channel. Upon reception, a feature declassification precedes their synthesis into a fascimile of the original signal. Based on signal and noise statistics, the optimal estimator finally enhances the synthesized signal, producing the optimal estimate of the original signal with respect to some criterion.

In our more specific picture bandwidth compression problem, the original signal represents an M x N matrix of picture brightness samples commonly referred to as picture elements or pixels for short. In a PCM system, a pixel is a 6 - 8 bit binary word. The feature selection process is a rule for manipulating the highly redundant pixels into less redundant and more compact transform elements called transels. The feature classification process is a quantization rule (typically nonlinear) that assures minimum distortion in the subsequent transmission through the noisy channel, under the constraint of a fixed number of quantizing levels. Feature declassification consists of complementary quantization of the received transels. Feature synthesis constitutes the rule for constructing the fascimile of the original picture from the available transels. Employing a prori signal and noise statistics, a generalized Weiner filter produces an enhanced image.

TABLE OF CONTENTS

SECTION	TITLE	PAGE
1.0	INTRODUCTION	1
2.0	STATEMENT OF THE PROBLEM	5
3.0	IMAGE CODING TECHNIQUES	8
	3.1 Differential Coding	8
	3.1.1 DM	8
	3.1.2 DPCM	10
	3.2 Transform Coding	15
	3.2.1 Karkumen Loève Transform	17
	3.2.2 Fourier Transform	20
	3.2.3 Hadamard Transform	26
	3.2.4 Haar Transform	35
	3.2.5 Slant Transform	37
4.0	SYSTEM CONSIDERATIONS	52
	4.1 Optimal Quantization	52
	4.2 Optimal Estimation	56
5.0	CONCLUSIONS AND RECOMMENDATIONS	64

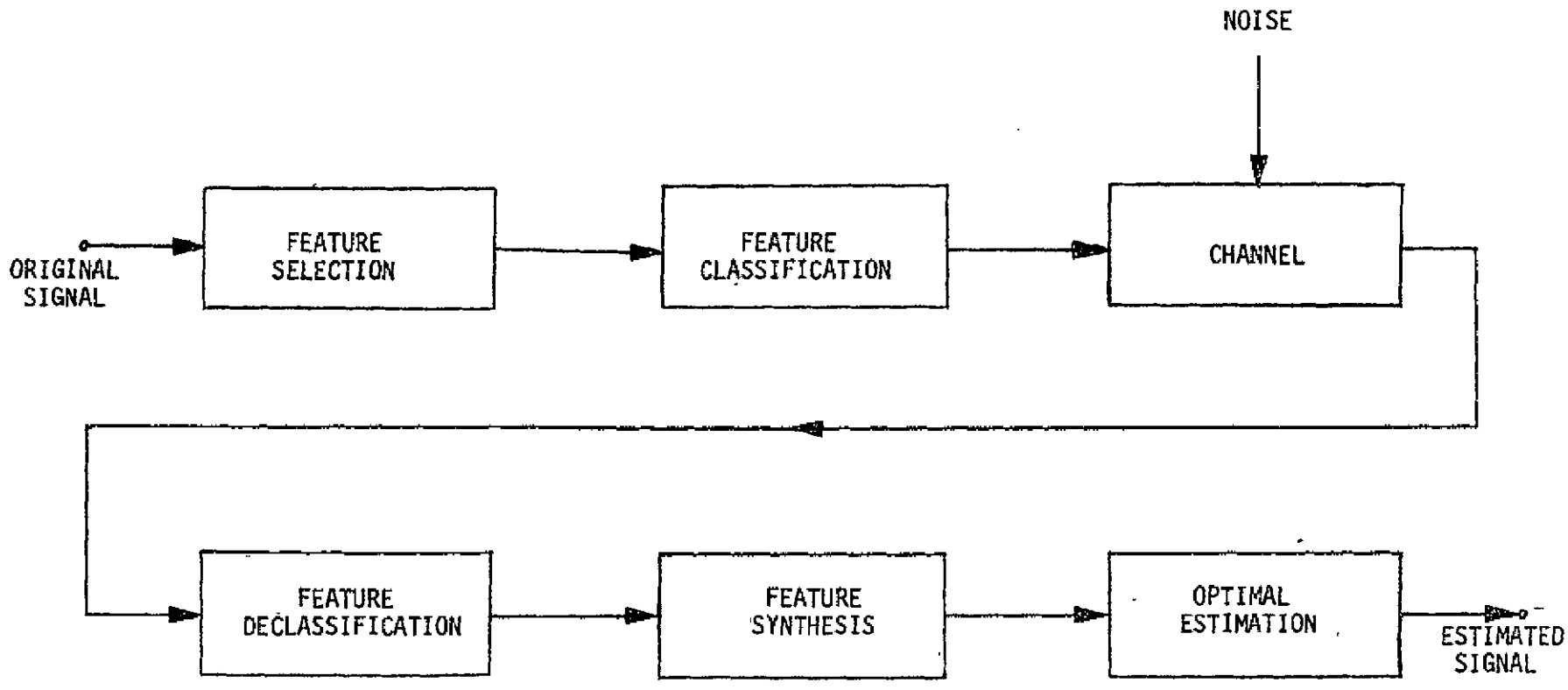

Fig. 2-1. Essential Aspects of a Bandwidth Compression System

In simple quantitative terms, the ultimate objective in a picture bandwidth compression system is to represent a given image with a minimum number of binary bits while insuring an acceptable average level of fidelity. In evaluating a given bandwidth compression system, it is common to denote its effectiveness in terms of the number of coding bits per pixel (B/P). In the next section we examine some of the currently more important image coding techniques capable of achieving B/P ratios ranging between 3 and .5 while maintaining an average distortion of less than 1% [4], [6], [9], [10], [11].

3.0 IMAGE CODING TECHNIQUES

Below we present brief descriptions of some of the better known image coding techniques. Following the discussion on two representative differential coding schemes, we examine the properties of a number of matrix transform operators. We conclude this section with a fairly explicit development of the latest most intriguing method for image coding.

3.1 Differential Coding

As its name implies, differential coding involves coding differential signals. We consider two such techniques: delta-modulation (DM), and differential pulse-code-modulation (DPCM).

3.1.1 DM

The simplest version of a DM system is shown in Fig. 3-1 where the accumulators are simple up/down counters, initially set to zero. An input pixel word compared with the accumulated count generates a sign bit which is transmitted and accumulated simultaneously. At the receive end these sign bits are accumulated in an up/down counter, thus constructing an estimate of the transmitted pixel.

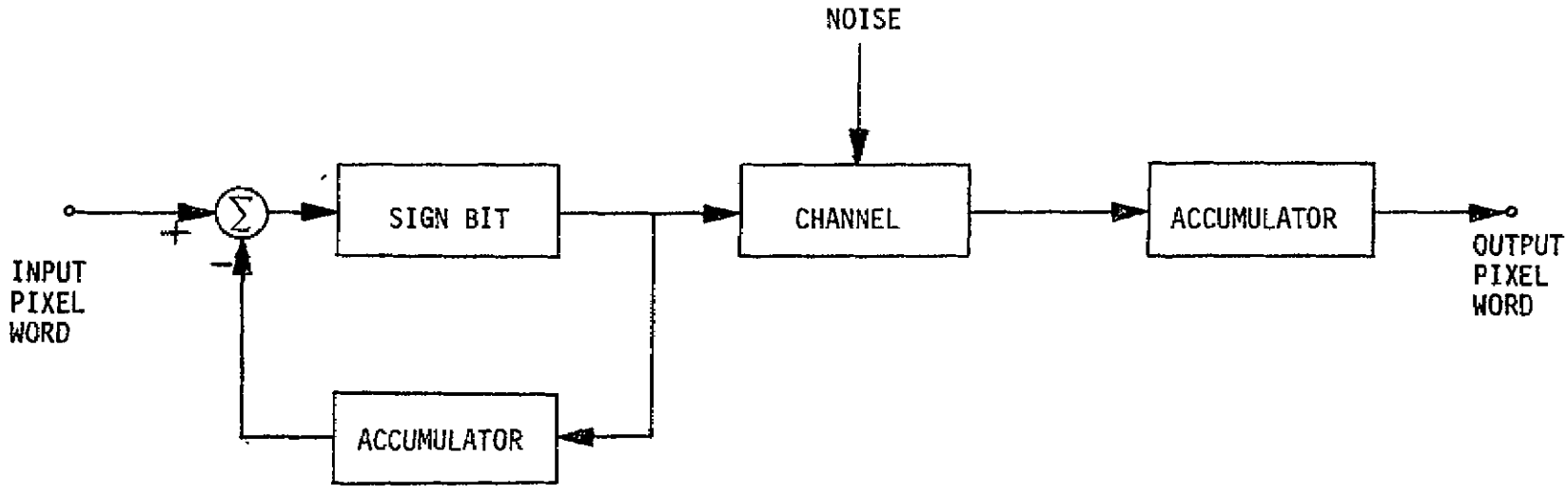

Fig. 3-1. Simple DM Image Coder

Although the information density of 1 B/P is certainly impressively low, by its very nature, the linear buildup DM (LDM) coder gives rise to excessive slope distortion and unacceptable edge smearing. This so called "slope-overload" difficulty may be allieviated somewhat by resorting to a higher sampling rate. Alternatively, an adaptive DM (ADM) using a set of adaptive step sizes gives even better results. In either case, however, the DM system would require an information density of about 3 B/P for a reasonably good transmission [4].

3.1.2 DPCM

The general n^{th} order DPCM coder is shown in Fig. 3-2. An nth order predictor provides a linear estimate of the current input pixel by means of a weighted sum of the n previous pixel words. The predicted pixel word is subtracted from the input pixel word, quantized and transmitted. This quantized difference is simultaneously added to the predicted pixel word and fed into the predictor memory, assuming the location of the most recent pixel after advancing the contents appropriately. As this process continues, each quantized difference signal arriving at the receiver adds synchronously with a locally predicted pixel word, thereby producing an output pixel word that is a reasonable estimate of the input pixel word.

Evidently, the two important functional blocks in a DPCM system are the predictor and the quantizer. Briefly, an nth-order linear minimum mean square predictor is one that estimates a signal sample by means of a weighted sum of the previous n samples; that is,

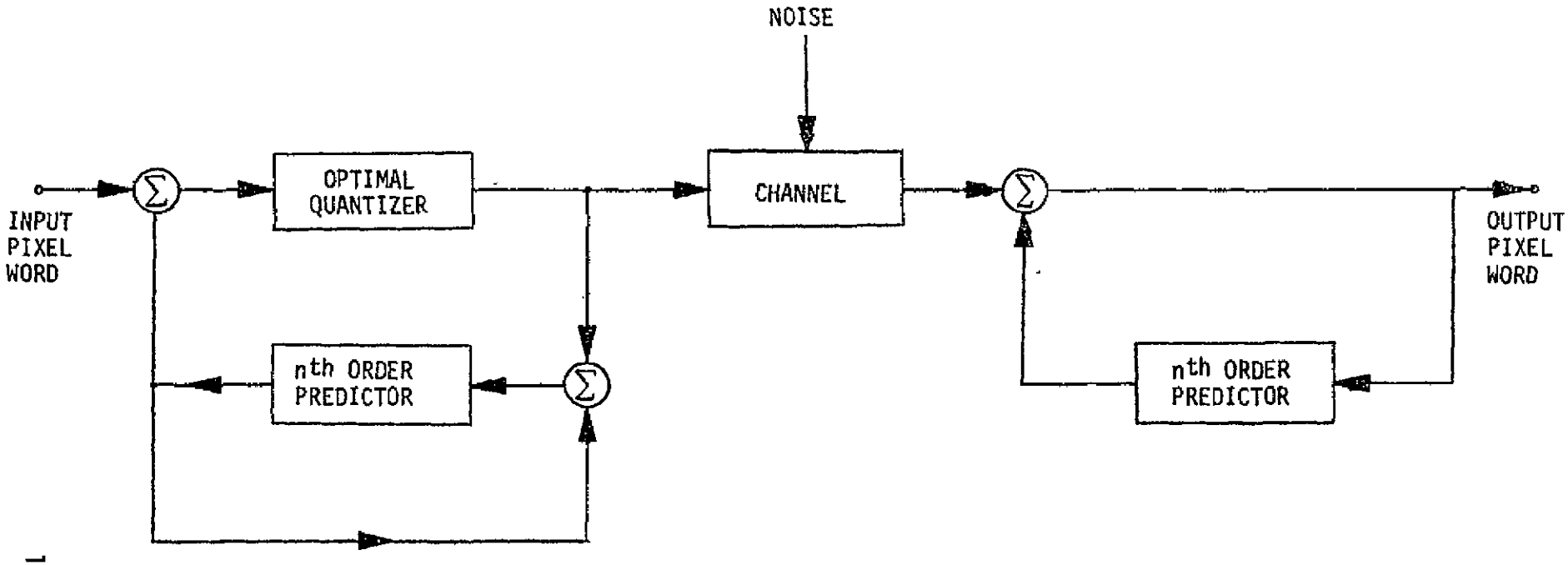

Fig. 3-2. Block Diagram of nth-Order DPCM Coder

$$s_i = \sum_{j=1}^{n} a_j \, s_{i-j} \tag{3-1}$$

where, the weighting coefficients $\{a_j\}$ satisfy the linear system

$$\sum_{j=1}^{n} R_{kj} \, a_j = R_{0k} \qquad ; \; 1 \leq k \leq n \tag{3-2}$$

and R_{kj} is the covariance of random variables s_k and s_j, namely,

$$R_{kj} = E\{s_k s_j\} \qquad ; \; 1 \leq k, j \leq n \tag{3-3}$$

The underlying signal s(t) is viewed as a zero mean stationary random process and, as such, its samples $\{s_k\}$ constitute a set of correlated random variables with some probability density. Note that the set of samples could represent pixels with the mean removed [3], [12].

The quantizer, restricted to a certain number of levels, can be optimized with respect to the probability density function of the difference signal [7] under some criterion for minimum distortion. Generally, this leads to a non-uniform quantization rule but could be constrained to be uniform. Given the difference signal probability density p(x), we define the distortion D as the expected value of $f(\varepsilon)$, where f is a reasonably chosen differentiable function and ε is the quantization error. Then

$$D = \sum_{i=1}^{N} \int_{x_i}^{x_{i+1}} f(x-y_i)\, p(x)\, dx \qquad (3\text{-}4)$$

where $\{x_k\}$ and $\{y_k\}$ are corresponding input and output levels that minimize D, with $x_1 = -\infty$ and $x_{N+1} = \infty$ and the convention that an input in (x_i, x_{i+1}) gives an output y_i. The necessary conditions for minimizing D with respect to $\{x_k\}$ and $\{y_k\}$ are found to be

$$\left.\begin{aligned} & f(x_j - y_{j-1}) = f(x_j - y_j) \quad ; \quad j = 2, \ldots, N \\ & \int_{x_j}^{x_{j+1}} f'(x-y_j)\, p(x)\, dx = 0 \quad ; \quad j = 1, \ldots, N \end{aligned}\right\} \qquad (3\text{-}5)$$

When $f(x) = x^2$, one obtains the more specific conditions for the minimum mean square optimal quantizer, namely,

$$\left.\begin{aligned} & y_j = 2x_j - y_{j-1} \quad ; \quad j = 2, \ldots, N \\ & \int_{x_j}^{x_{j+1}} (x-y_j)\, p(x)\, dx = 0 \quad ; \quad j = 1, \ldots, N \end{aligned}\right\} \qquad (3\text{-}6)$$

For typical exponentially-distributed differential signals, the optimal quantizer is non-uniform with greatest density of levels about zero, gradually decreasing in density away from zero, as indicated in Fig. 3-3 for an 8-level case. Intuitively, the finer levels near zero will tend to subdue undesired chatter in uniform or slowly varying regions, while the coarser levels away from zero accentuate rapidly changing regions and help emphasize edges.

Information densities for DPCM coders range from a typical 3 B/P to a low of 2 B/P when employing special level encoding [3], [4]. A system employing a combination of LDM and DPCM has been proposed [4] and shown to produce good imagery with approximately 1 B/P.

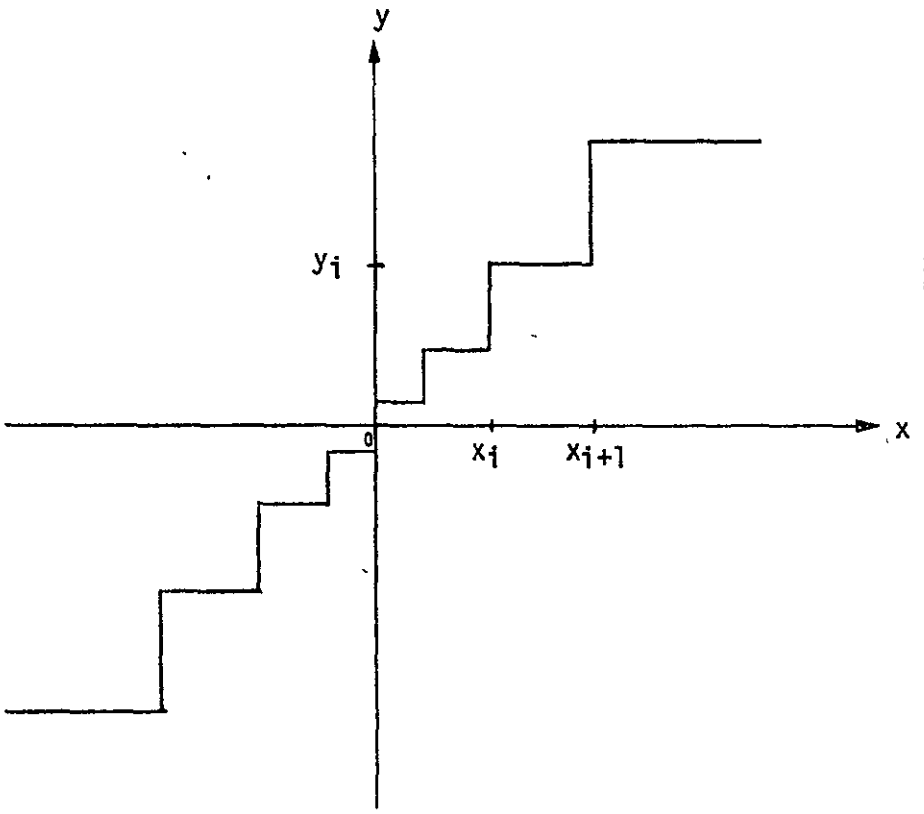

Fig. 3-3. Optimum 8-level Quantizer

3.2 Transform Coding

Consider a square array G of N^2 image samples and let $g(x,y)$ represent the pixel intensity at location (x,y). Then a two-dimensional transform of the image is a square array T of N^2 transform elements, where

$$t(u,v) = \sum_{y=0}^{N-1} \sum_{x=0}^{N-1} g(x,y)\, k(u,v,x,y) \qquad (3\text{-}7)$$

gives the intensity of the typical transel and $k(u,v,x,y)$ is the transform kernel. When the kernel is separable, it can be expressed as

$$k(u,v,x,y) = k_1(u,x)\, k_2(v,y) \qquad (3\text{-}8)$$

and when symmetric, it reduces to

$$k(u,v,x,y) = k_1(u,x)\, k_1(v,y) \qquad (3\text{-}9)$$

Letting $K = [k_1(i,j)]$ be the associated transform matrix, (3-7) becomes

$$T = KGK^T \qquad (3\text{-}10)$$

We now define the inverse transformation as a separable symmetric form which maps T back into G, namely,

$$G = LTL^T$$

where L is the inverse transform matrix. In view of (3-10), however,

$$G = LKGK^TL^T$$

requiring that $L = K^{-1}$. Consequently, the inverse transform becomes

$$G = K^{-1}\ TK^{-1T} \tag{3-11}$$

When K is a unitary matrix; that is, when the rows of K comprise a set of orthonormal vectors,

$$K^{-1} = K^{*T}$$

(3-11) specializes to

$$G = K^{*T}\ TK^{*} \tag{3-12}$$

Accordingly, separable-symmetric-unitary transformations serve to decompose an image G into a generalized spectrum T. The magnitude of a given transel t(u,v) represents the image energy in the associated spectral location; in other words, t(u,v) is the expansion coefficient corresponding to the two-dimensional orthogonal function $k_1(u,x)\ k_1'(v,y)$. For a given redundance in an image G, the objective of a transformation is to compact the largest portion of image energy into the smallest number of transels. As a consequence of energy compaction, one may represent the substantial image content with only the essential number of transels. The implication to bandwidth reduction is obvious.

Below, we examine a number of transform coding techniques which, with the exception of the Karhunen-Loève transform, belong to the class with two-dimensional separable symmetric kernels with unitary transform matrices.

3.2.1 Karhunen-Loève Transform

The Karhunen-Loève transform is not generally separable [6], [9] and hence not easily useful as a direct two-dimensional transformation. However, when the image G is viewed as an N^2-dimensional vector of concatenated row vectors, namely,

$$\underline{h} \equiv [g(1,1)\ldots g(1,N)\ldots g(N,1)\ldots,\ g(N,N)] \qquad (3\text{-}13)$$

we can make direct use of the one-dimensional Karhunen-Loève transform as specified in a well-established theorem [13]:

Theorem: (Karhunen-Loève)

Let x(t) be a non-periodic random process supported in a finite interval (a,b). Then x(t) has a unique orthonormal expansion over (a,b) with uncorrelated coefficients; i.e.,

$$x(t) = \sum_n \sigma_n x_n \phi_n(t); \quad a \leq t \leq b \qquad (3\text{-}14.1)$$

where

$$\int_a^b \phi_n(t)\ \phi_m^*(t)\ dt = \delta_{mn} = \begin{cases} 1\ , & m=n \\ 0\ , & m\neq n \end{cases} \qquad (3\text{-}14.2)$$

$$E\left\{x_n x_m^*\right\} = \delta_{mn} \qquad (3\text{-}14.3)$$

Note that $\left\{\sigma_k\right\}$ and $\left\{x_k\right\}$ are generally complex-valued, $\left\{\sigma_k x_k\right\}$ are the expansion coefficients which, in view of (3-14.3), are uncorrelated.

One can show that $\left\{\phi_k(t)\right\}$ and $\left\{|\sigma_k|^2\right\}$ are eigenfunctions and eigenvalues of the correlation function

$$R(t,s) = E\left\{x(t)\, x^*(s)\right\} \qquad ; a \leq t,\ s \leq b \qquad (3\text{-}15)$$

satisfying the integral equation

$$\int_a^b R(t,s)\, \phi_m(s)\, ds = |\sigma_m|^2\, \phi_m(t) \quad ; \quad a \leq t \leq b \qquad (3\text{-}16)$$

and that (3-14.3) is the happy consequence.

In our specific case, the random process is the discrete vector $\underline{h}$ given in (3-13). Consequently, (3-15) is a correlation matrix R whose elements are given by

$$R_{ij} = E\left\{h_i\, h_j\right\} \qquad (3\text{-}17)$$

and (3-16) is the eigevalue problem

$$R\, \underline{\phi}^m = \lambda_m \underline{\phi}^m \qquad (3\text{-}18)$$

where $\{\underline{\phi}^k\}$ and $\{\lambda_k\}$ are the corresponding eigenvectors and eigenvalues. Note that (3-18) implies that

$$\Phi\, R\, \Phi^T = \Lambda = \begin{bmatrix} \lambda_1 & & \bigcirc \\ & \ddots & \\ \bigcirc & & \lambda_{N^2} \end{bmatrix} \qquad (3\text{-}19)$$

where Φ is a unitary transform matrix whose rows correspond to eigenvectors arranged in descending order of eigenvalues. The expansion coefficients of $\underline{h}$ are then given in the one-dimensional transformation

$$\underline{\tau} = \Phi \underline{h} \tag{3-20}$$

The inverse transform matrix is obviously Φ^T. If only the first M of the N^2 rows of Φ are used in (3-20), the mean square error may be shown to be

$$\varepsilon^2 = \sum_{i=M+1}^{N^2} \lambda_i \tag{3-21}$$

Since $\{\lambda_k\}$ is a monotonically decreasing sequence, this error will be minimum for any M. Since the transels comprising $\underline{\tau}$ are statistically uncorrelated, the Karhunen-Loève transform achieves statistically optimal energy compaction.

Although the Karhunen-Loève transform constitutes the "natural transform", it is, unfortunately, numerically inefficient and so demanding of hardware complexity, that it is not practical with the present state of technology. In contrast to this transform, we consider below a few transformations which possess fast algorithms that allow for realistic implementations with available technology. In evaluating their effectiveness, the Karhunen-Loève transform serves as a standard of comparison.

3.2.2 Fourier Transform

The concept of two-dimensional discrete Fourier transform image coding was introduced as recently as 1968 [14] and shown to be practical because of its associated numerically efficient fast Fourier transform (FFT) algorithm [15]. For a given N x N image matrix G, the two-dimensional Fourier transformation is of the separable symmetric form

$$T = F\,G\,F \tag{3-22}$$

where, with $W \equiv e^{-j2\pi/N}$, the symmetric* transform matrix F is given by

$$F = \begin{bmatrix} W^{\circ} & W^{\circ} & \cdots & W^{\circ} \\ W^{\circ} & W^{1} & \cdots & W^{N-1} \\ \vdots & & & \\ W^{\circ} & W^{N-1} & \cdots & W^{(N-1)^2} \end{bmatrix} \tag{3-23}$$

The inverse transformation is obviously

$$G = F^{*}TF^{*} \tag{3-24}$$

---

*Note that $F = F^{T}$.

It should be clear from examining (3-22) that the two-dimensional Fourier transform of G consists of a sequence of two one-dimensional transforms, namely, the row transformation GF, followed by the column transformation F(GF). As such, the resulting two-dimensional transformed image T represents the spatial frequency content of G. For general scenes, T has been found to exhibit a high degree of energy compaction, approaching optimal compaction with large N.

Let us now consider briefly the numerical implications of a two-dimensional FFT microprocessor. Since the FFT transformation of an N-vector requires $N \log_2 N$ operation, the complete transformation of G requires $2N^2 \log_2 N$. For N = 256, the total number of operations needed is 2^{20}, which is approximately 10^6. Modern day microprocessor chips can carry out 10^6 operations in approximately 0.5 seconds*. The obvious implication here is that even with the fastest available logic today, we cannot exercise the 2D-FFT in a real-time TV situation. As a consequence, one is forced to consider partial-block transformations of TV pictures. For example, a 32 x 32 image block would require approximately 10^4 operations, which would take up only 5 ms of the 10 ms frame-time. Alternatively, one can consider transforming a 4 x 256 rectangular block which would also require $(4)(256)(2 + 8) = 10^4$ operations.

---

*Motorola/TRW EFL microprocessor is capable of multiplying two 8-bit words within 370 μs - Private communication from J. Gibson, GED.

Recent efforts toward accommodating real-time TV transmission have involved the use of an alternative formulation of the Fourier transform [5], namely, the Chirp-Z transform (CZT), in conjunction with DPCM. The basic motivation behind this work stems from the convolutional aspect of the CZT process, which can be carried out either by means of a surface acoustic wave (SAW) implementation, or a potentially more economical charge-coupled device (CCD) configuration.* We outline below the basic development of the CZT process.

Let $\{g_k\}$, $0 \leq k \leq N-1$, represent a sequence of image samples along a horizontal TV line. The discrete Fourier transform is then

$$G_m = \sum_{n=0}^{N-1} g_n W^{mn} \tag{3-25}$$

Noting that

$$W^{mn} = W^{\frac{m^2}{2}} W^{-\frac{(m-n)^2}{2}} W^{\frac{n^2}{2}} \tag{3-26}$$

(3-25) may be written as

$$G_m = P_m^* \sum_{n=0}^{N-1} (g_n P_n^*) P_{m-n} \tag{3-27}$$

where,

$$P_k = W^{-k^2}, \quad 0 \leq k \leq N-1 \tag{3-28}$$

---

*ARPA's Col. H. Federhen and NUC's H. Whitehouse, et.al, are presently advocating a CCD approach with the hope of producing a $50 CZT-DPCM 16:1 bandwidth compression system for RPV use.

are the so-called "chirp constants." Taking the symmetry

$$P_k = P_{-k} \tag{3-29}$$

into account, the functional block diagram of the CZT process follows immediately, as shown in Fig. 3-4. In fact, by (3-27), a term-by-term premultiplication of the gated video $\{g_k\}$ by the conjugate chirp constants $\{P_k^*\}$ is subsequently convolved with $\{P_k\}$ via a symmetric chirp filter and subsequently postmultiplied by $\{P_k^*\}$ delayed by N units of time, thus giving the transformed video $\{G_k\}$. The dual-line complex signal flow indicated throughout the block diagram may be simplified somewhat under certain conditions. For example, if the video input is viewed as an odd-symmetric signal $\{g_{-N+1} \cdots g_1 \ \frac{1}{2}g_0 \ g_1 \cdots g_{N-1}\}$, the transformed output $\{G_k\}$ is purely real, implying an additional 50% reduction in bandwidth. This particular version of the CZT is referred to as the odd discrete cosine transform (ODCT). An EDCT - CZT is also possible.

A real-time CZT-DPCM bandwidth compression system has been suggested [16]. In this system, each horizontal TV line is first transformed by a CZT and subsequently compared to the previously transformed line in a specially-designed DPCM process, transmitting only differential transformed signals. In effect, the CZT process acts to reduce horizontal redundancy, while the DPCM process acts in the vertical direction. The basic system block diagram is shown in Fig. 3-5. For real-time operation, the system must have access to two CZT processors, one feeding the DPCM process while the other is

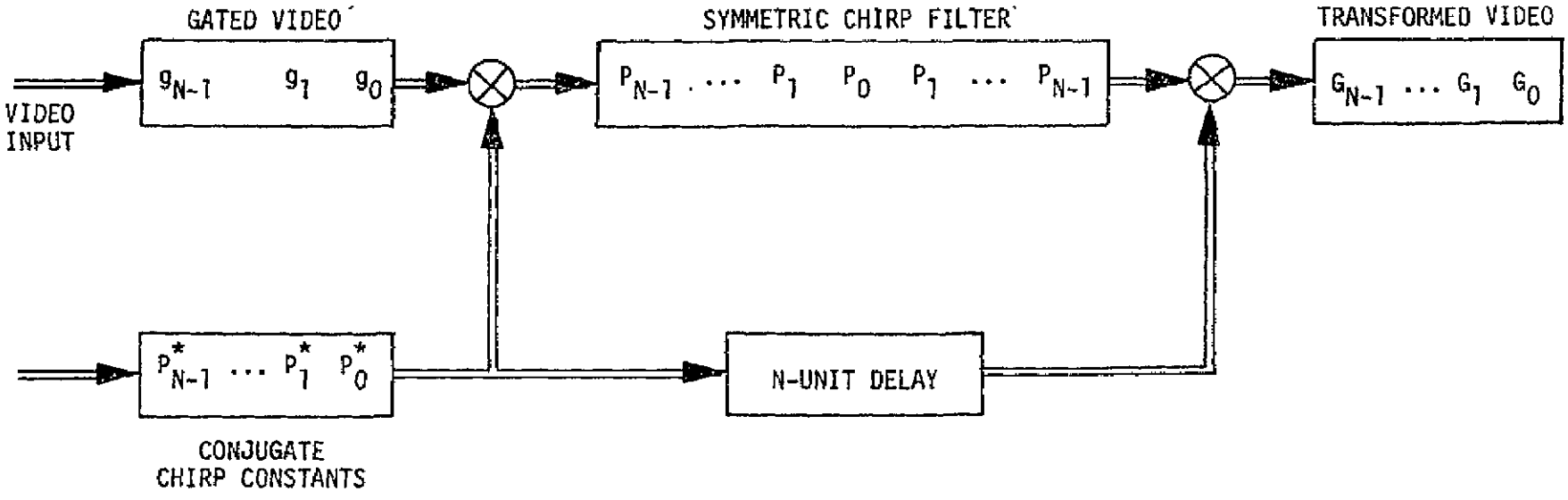

Figure 3-4. Functional Block Diagram of CZT Process

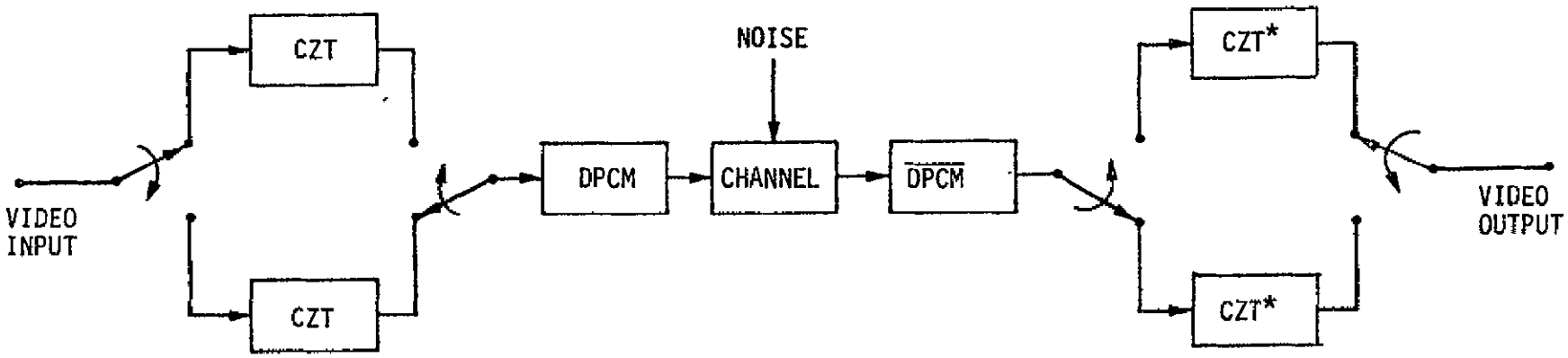

Figure 3-5. Essential Block Diagram of Real-Time CZT-DPCM System

in the process of becoming quiescent. Each transformed line is buffered in the DPCM block where, compared with previous line data, it is used to generate and transmit transformed differences. Upon reception, these differences are operated by a complementary DPCM block and fed appropriately into the two inverse CZT transformers giving rise to the reconstructed video output. It should be noted here that when the system is operated at half the frame rate (by cutting the vertical scanning rate to 50%) there is no need for the second CZT.

3.2.3 Hadamard Transform

The two-dimensional Hadamard transform of an N x N image matrix G is of the separable symmetric form

$$T = H G H \tag{3-30}$$

where H is a symmetric N x N Hadamard matrix whose rows (or columns) of $\pm$ 1's are mutually orthogonal N-vectors. A large Hadamard matrix is generally related to a smaller "core matrix," itself a Hadamard matrix, which constitutes its basic building block. Specifically, the 2 x 2 core matrix

$$H_1 = \begin{bmatrix} 1 & 1 \\ 1 & -1 \end{bmatrix} \tag{3-31}$$

generates a family of $2^n \times 2^n$ Hadamard matrices, for n = 1, 2, ..., by means of n successive Kronecker products. For example, given the $2^k \times 2^k$ H_k matrix, the H_{k+1} matrix is generated through the Kronecker product operation

$$H_{k+1} = H_1 \otimes H_k$$

$$= \begin{bmatrix} H_k & H_k \\ H_k & -H_k \end{bmatrix} \qquad (3\text{-}32)$$

which constitutes placing the rightmost matrix, H_k, into the framework of the core matrix as shown.

The Hadamard transform is appealing for several reasons. In view of (3-31) and 3-32), transformation (3-30) requires only additions. It possesses a fast computational algorithm which requires $2N^2 \log_2 N$ additions. It is capable of significant energy compaction, only somewhat inferior to the Fourier transform [6], [8], [9], [17].

Let us now examine the nature of the fast computational algorithm associated with the Hadamard matrix. Consider the 4 x 4 H_2 matrix

$$H_2 = \begin{bmatrix} 1 & 1 & 1 & 1 \\ 1 & -1 & 1 & -1 \\ 1 & 1 & -1 & -1 \\ 1 & -1 & -1 & 1 \end{bmatrix} \tag{3-33}$$

It has been shown [18] that H_2 may be expressed in the factored form

$$H_2 = \begin{bmatrix} 1 & 1 & 0 & 0 \\ 0 & 0 & 1 & 1 \\ 1 & -1 & 0 & 0 \\ 0 & 0 & 1 & -1 \end{bmatrix}^2 \tag{3-34}$$

which may be verified readily. Note that direct use of (3-33) in (3-30) with a 4 x 4 matrix G would require $2N^3 = 128$ additions; using (3-34), we only need $2N^2 \log_2 N = 64$ additions.

Observing (3-33) closely, we see that the orthogonal row (or column) vectors exhibit an oscillatory behavior that can be associated with generalized frequency. In fact, viewing the vectors as square waves, the number of sign changes or zero-crossings is referred to as sequency, which is indicated in Fig. 3-6.

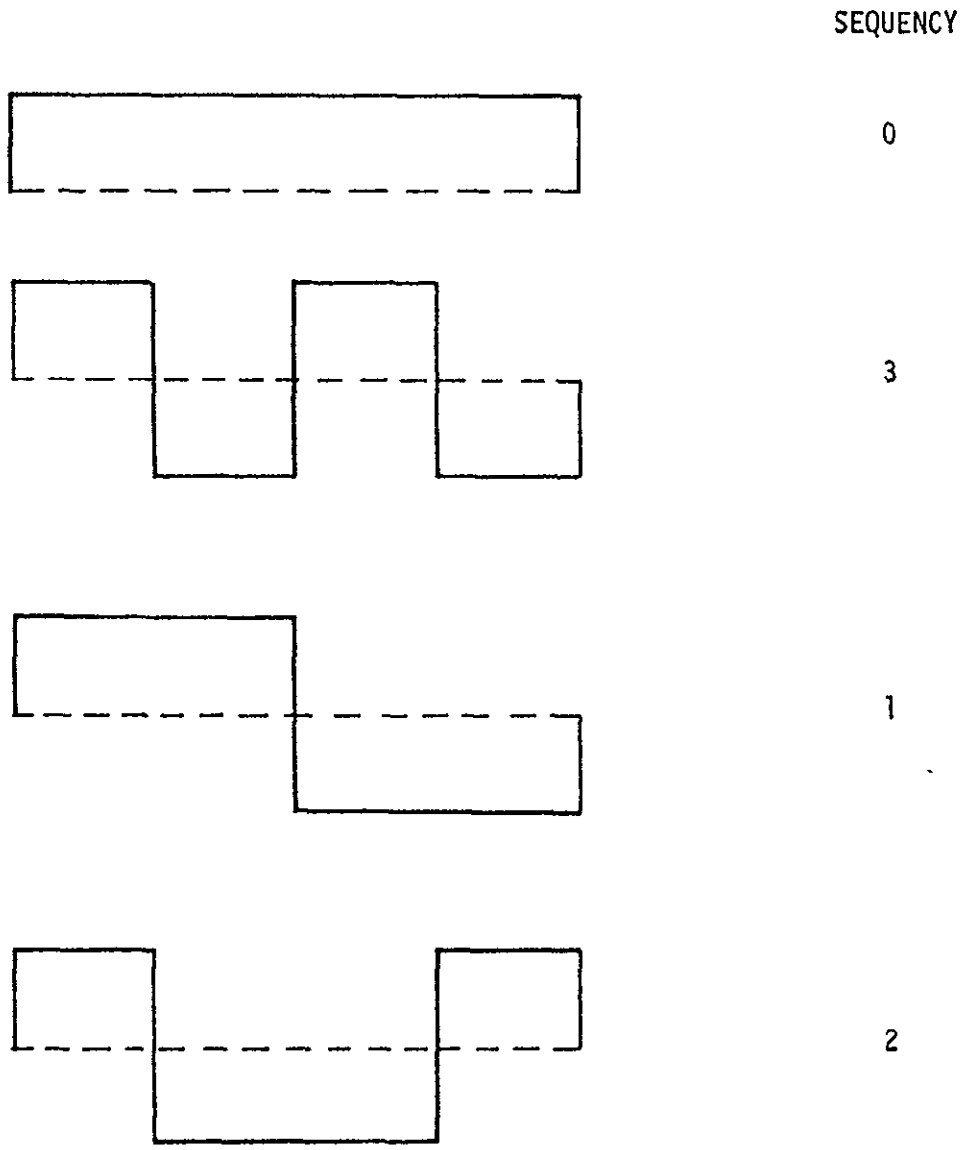

Figure 3-6. Square-Wave Representation of H_2 Row-Vectors and Their Sequency Assignment

As shown in Fig. 3-6, the H_2 row vectors are not ordered by sequency. Consequently, using form (3-32) in (3-30) will tend to disperse adjacent sequency transels, which, for large N, would make subsequent quantization assignment rather laborious [9]. For this reason, one is advised to use the sequency-ordered form of the Hadamard matrix. Specifically, the ordered form of H_2 is

$$H_2^0 \quad \begin{bmatrix} 1 & 1 & 1 & 1 \\ 1 & 1 & -1 & -1 \\ 1 & -1 & -1 & 1 \\ 1 & -1 & 1 & -1 \end{bmatrix} \tag{3-35}$$

which may be factored into its numerically efficient form as

$$H_2^0 = \begin{bmatrix} 1 & 1 & 0 & 0 \\ 1 & -1 & 0 & 0 \\ 0 & 0 & 1 & 1 \\ 0 & 0 & 1 & -1 \end{bmatrix} \begin{bmatrix} 1 & 1 & 0 & 0 \\ 0 & 0 & 1 & 1 \\ 1 & -1 & 0 & 0 \\ 0 & 0 & -1 & 1 \end{bmatrix} \tag{3-36}$$

which may be readily verified. It is not difficult to show that the two factored forms of H_3 are:

C-3

$$H_3 = \begin{bmatrix} 1 & 1 & 0 & 0 & 0 & 0 & 0 & 0 \\ 0 & 0 & 1 & 1 & 0 & 0 & 0 & 0 \\ 0 & 0 & 0 & 0 & 1 & 1 & 0 & 0 \\ 0 & 0 & 0 & 0 & 0 & 0 & 1 & 1 \\ 1 & -1 & 0 & 0 & 0 & 0 & 0 & 0 \\ 0 & 0 & 1 & -1 & 0 & 0 & 0 & 0 \\ 0 & 0 & 0 & 0 & 1 & -1 & 0 & 0 \\ 0 & 0 & 0 & 0 & 0 & 0 & 1 & -1 \end{bmatrix}_3 \qquad (3\text{-}37)$$

$$H_3^0 = \begin{bmatrix} 1 & 1 & & & & & & \\ 1 & -1 & & & & \bigcirc & & \\ & & 1 & 1 & & & & \\ & & 1 & -1 & & & & \\ & & & & 1 & 1 & & \\ & \bigcirc & & & 1 & -1 & & \\ & & & & & & 1 & 1 \\ & & & & & & 1 & -1 \end{bmatrix} \begin{bmatrix} 1 & 1 & & & & & & \\ & & 1 & 1 & & & \bigcirc & \\ 1 & -1 & & & & & & \\ & & -1 & 1 & & & & \\ & & & & 1 & 1 & & \\ & \bigcirc & & & & & 1 & 1 \\ & & & & 1 & -1 & & \\ & & & & & & -1 & 1 \end{bmatrix} \begin{bmatrix} 1 & 1 & & & & & & \\ & & 1 & 1 & & & \bigcirc & \\ & & & & 1 & 1 & & \\ & & & & & & 1 & 1 \\ 1 & -1 & & \bigcirc & & & & \\ & & -1 & 1 & & & & \\ & \bigcirc & & & 1 & -1 & & \\ & & & & & & -1 & 1 \end{bmatrix} \qquad (3\text{-}38)$$

Note that the factored form of H_3^0 possesses three matrices with very distinct substructures. In fact, letting the right-most 8 x 8 matrix be the identifying matrix of H_3^0 or "order-3" matrix, advancing to the right we see that each matrix is composed of diagonally disposed "order-2" and "order-1" blocks.

The numerical simplicity implied by the two possible factored forms, (3-37) and (3-38), may be clearly indicated in their respective digital implementations for the row transformation GH.

Fig. 3-7 gives the essential blocks of a digital mechanization of the one-demensional unordered fast Hadamard transformation using (3-37). An 8-pixel video input is fed into a working register. Pairwise accumulations with appropriate signs are routed through paths 1 and 5 into the updating register, followed by appropriate single shift commands from the strobing logic. When filled, the updating register is dumped into the working register. The process is repeated two more times, at which point the 8-transel transformed video is routed out. While accessing the transformed video, another row of image G is fed into the working register which undergoes a similar three-circulation process prior to access. When all rows of G are exhausted, the row transformation GH is completed.

In contrast to the unordered transformation, the ordered fast Hadamard transformation GH using (3-38) is slightly more involved as can be seen in Fig. 3-8. The additional complexity comes about from the need to exercise each of the three updates with the three distinct matrices in (3-38). The first update involves routing paths 1 and 5 with single-shift strobing for all four counts of the update. The second update involves routing paths 1 and 3 with single-shift strobing for two-counts. Following a two-shift command, the second half of the second update is completed. The third update involves paths 1 and 2 with two-shift strobing.

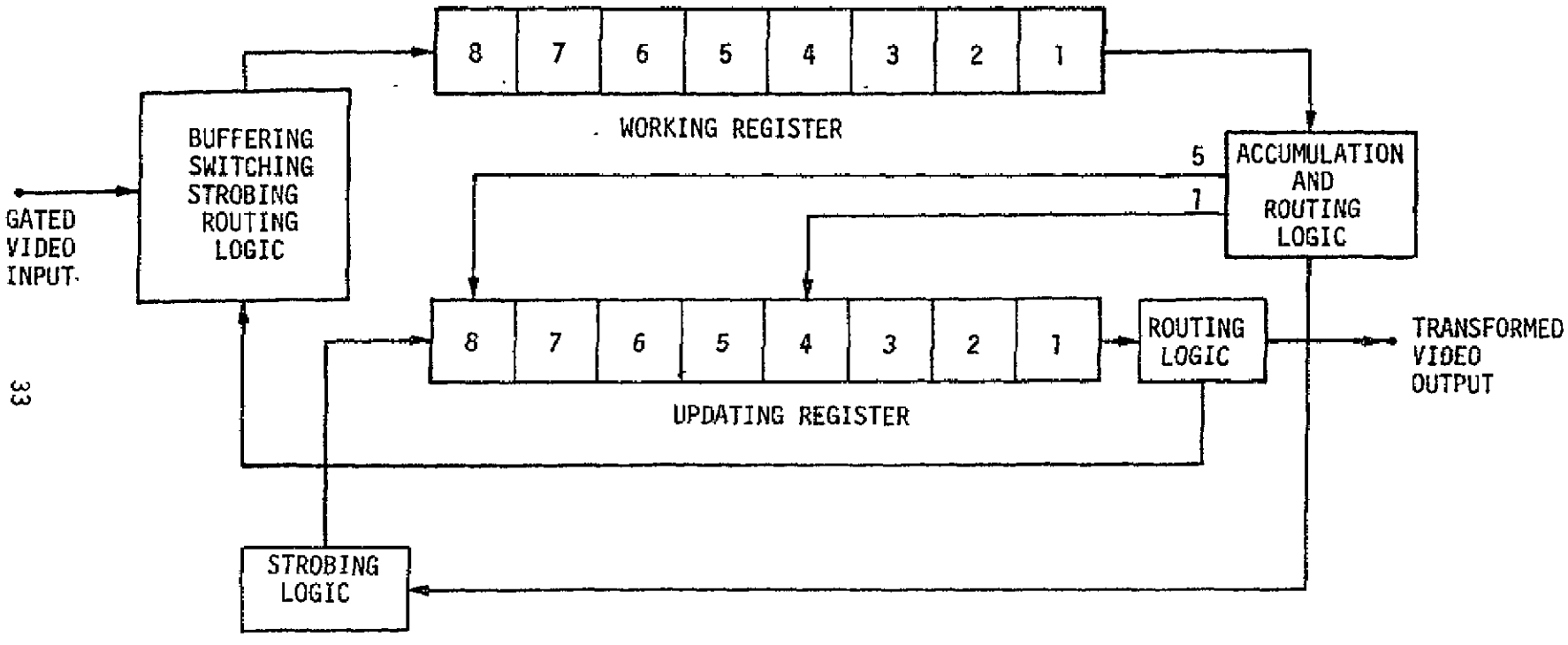

Fig. 3-7. Digital Mechanization of One-Dimensional Unordered Fast Hadamard Transformation

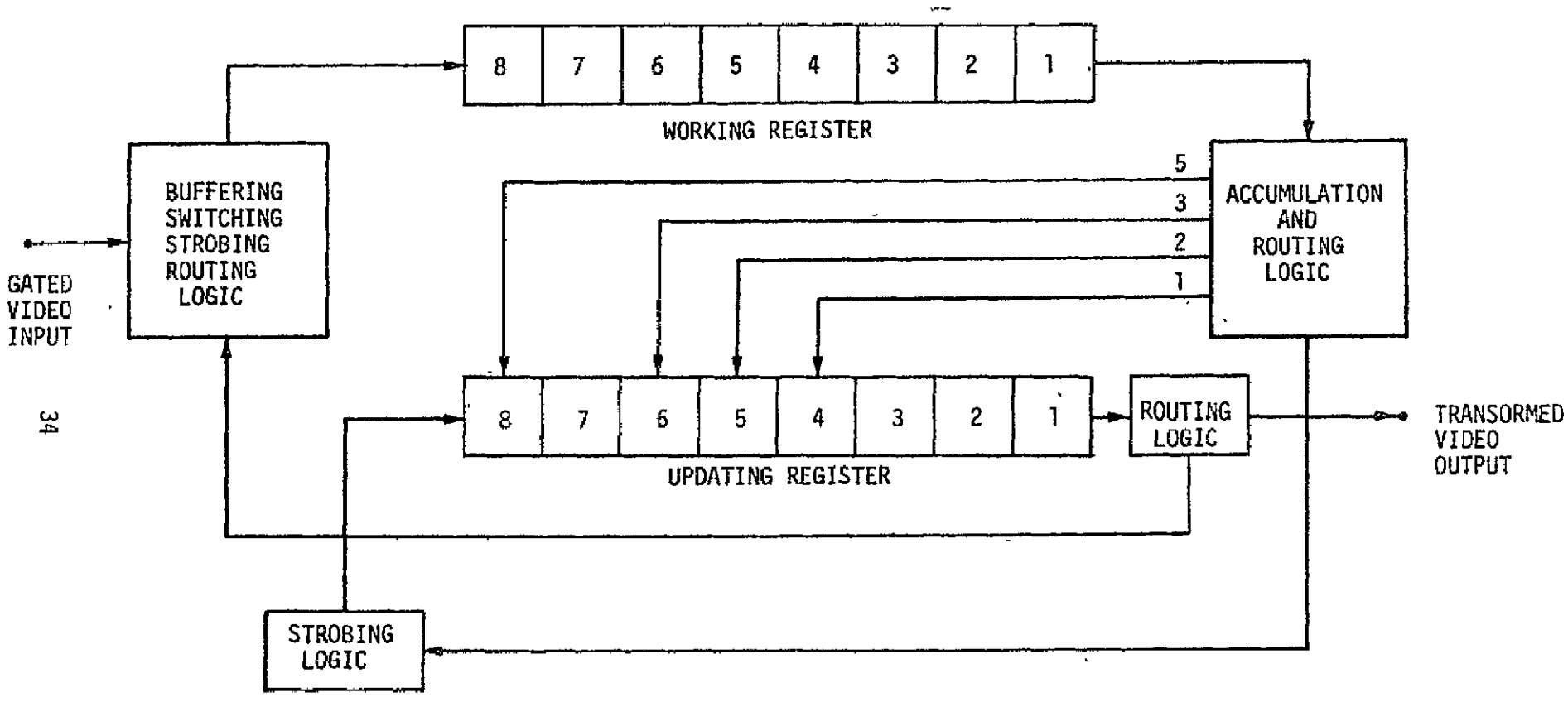

Fig. 3-8. Digital Mechanization of One-Dimensional Ordered Fast Hadamard Transformation

The two-dimensional Hadamard transformation (3-30) may be accomplished by first buffering the row-transformed image GH and, subsequently, carrying out the column transform H(GH) using a second one-dimensional system. If buffering is objectionable, one could revert to the less complex Hadamard-DPCM option. A real-time Hadamard-DPCM bandwidth compression system could be accomplished with presently and soon-available fast, low-power, digital logic. Such a system would be capable of information densities approaching 1 B/P.

3.2.4 Haar Transform

The two-dimensional Haar transform of an N X N image matrix G is of the separable symmetric form

$$T = A\,G\,A^T \tag{3-39}$$

where A is the N x N Haar matrix having a structure as indicated below for the case where N = 8 [11].

$$A = \begin{bmatrix} 1 & 1 & 1 & 1 & 1 & 1 & 1 & 1 \\ 1 & 1 & 1 & 1 & -1 & -1 & -1 & -1 \\ \sqrt{2} & \sqrt{2} & -\sqrt{2} & -\sqrt{2} & 0 & 0 & 0 & 0 \\ 0 & 0 & 0 & 0 & \sqrt{2} & \sqrt{2} & -\sqrt{2} & -\sqrt{2} \\ 2 & -2 & 0 & 0 & 0 & 0 & 0 & 0 \\ 0 & 0 & 2 & -2 & 0 & 0 & 0 & 0 \\ 0 & 0 & 0 & 0 & 2 & -2 & 0 & 0 \\ 0 & 0 & 0 & 0 & 0 & 0 & 2 & -2 \end{bmatrix} \begin{matrix} \left.\begin{matrix} \\ \\ \end{matrix}\right\} 1 \\ \left.\begin{matrix} \\ \\ \end{matrix}\right\} 1 \\ \left.\begin{matrix} \\ \\ \end{matrix}\right\} \frac{N}{4} \\ \left.\begin{matrix} \\ \\ \\ \\ \end{matrix}\right\} \frac{N}{2} \end{matrix} \tag{3-40}$$

Note that the number of each type of row (number of nonzero entries) is given to the far right. From this, one can easily extrapolate the general Haar matrix for $N = 2^n$.

In terms of energy compaction, the Haar transformation (3-39) is only slightly inferior to the Hadamard transform (3-30); numerically, however, it is said to be much more efficient when used with its associated fast algorithm which makes use of the factored form of the Haar matrix. For the case $N = 8$ the factored form is

$$A_8 = \begin{bmatrix} 1 & 1 & & & & & & \\ 1 & -1 & & & & & \bigcirc & \\ & & \sqrt{2} & & & & & \\ & & & \sqrt{2} & & & & \\ & & & & \sqrt{2} & & & \\ & & & & & \sqrt{2} & & \\ & \bigcirc & & & & & \sqrt{2} & \\ & & & & & & & \sqrt{2} \end{bmatrix} \begin{bmatrix} 1 & 1 & & & & & & \\ & & 1 & 1 & & & \bigcirc & \\ 1 & -1 & & & & & & \\ & & 1 & -1 & & & & \\ & & & & \sqrt{2} & & & \\ & & & & & \sqrt{2} & & \\ & \bigcirc & & & & & \sqrt{2} & \\ & & & & & & & \sqrt{2} \end{bmatrix} \begin{bmatrix} 1 & 1 & & & & & & \\ & & 1 & 1 & & & \bigcirc & \\ & & & & 1 & 1 & & \\ & & & & & & 1 & 1 \\ 1 & -1 & & & & & & \\ & & 1 & -1 & & & \bigcirc & \\ & & & & 1 & -1 & & \\ \bigcirc & & & & & & 1 & -1 \end{bmatrix} \qquad (3\text{-}41)$$

Upon close examination, we see that the transformation of a single vector by (3-41) requires 14 additions and 2 multiplications; the 4 single bit shifts are computationally negligible. In general, one would need $2(N-1)$ additions and $N/4$ multiplications by $\sqrt{2}$, where N is some power of 2. In contrast, the Hadamard transformation of an N-vector requires $N\log_2 N$ additions. Consequently, using a lookup table involving multiplications by $\sqrt{2}$, the Haar transformation may be made computationally very efficient. Without such an aid, all multiplications will have to be carried out directly, which would make the Haar transformation computationally less efficient than the Hadamard transformation.

The orthogonal row vectors comprising the Haar matrix may be viewed as square waveforms as shown in Fig. 3-9 for case N = 8. Evidently, the most notable feature characterizing these basis waveforms is their limited interval of support which decreases to a two-pixel extent for N/2 of the functions. Although the Haar transformation does exhibit a substantial energy compaction comparable to that of the Hadamard transformation, its very structure can give rise to substantial transel dispersion which may hamper the subsequent quantization assignment. It is not difficult to see that unlike the Hadamard transformation, the Haar transformation basis functions cannot be given a "frequency" interpretation. As a consequence, no systematic overall ordering exists for the purpose of minimizing dispersion and alieviating the difficulty in the quantization process. Finally, because of its limited-support structure, it is expected that the Haar transformation will be susceptible to more distortion than the Hadamard transformation during transmission over a noisy channel [10].

3.2.5 Slant Transform

The latest entry in the class of transform coding techniques is the Slant transform [10], first introduced in 1971 [20]. For an N x N image matrix G, the Slant transformation is of the separable symmetric form

$$T = S\,G\,S^T \qquad (3\text{-}42)$$

where S is the associated N x N Slant matrix whose rows are the mutually orthogonal Slant basis vectors. This transformation has been developed with the aim of accommodating not only constant, but linear brightness variations that characterize typical images, other than text, etc. As such, the Slant

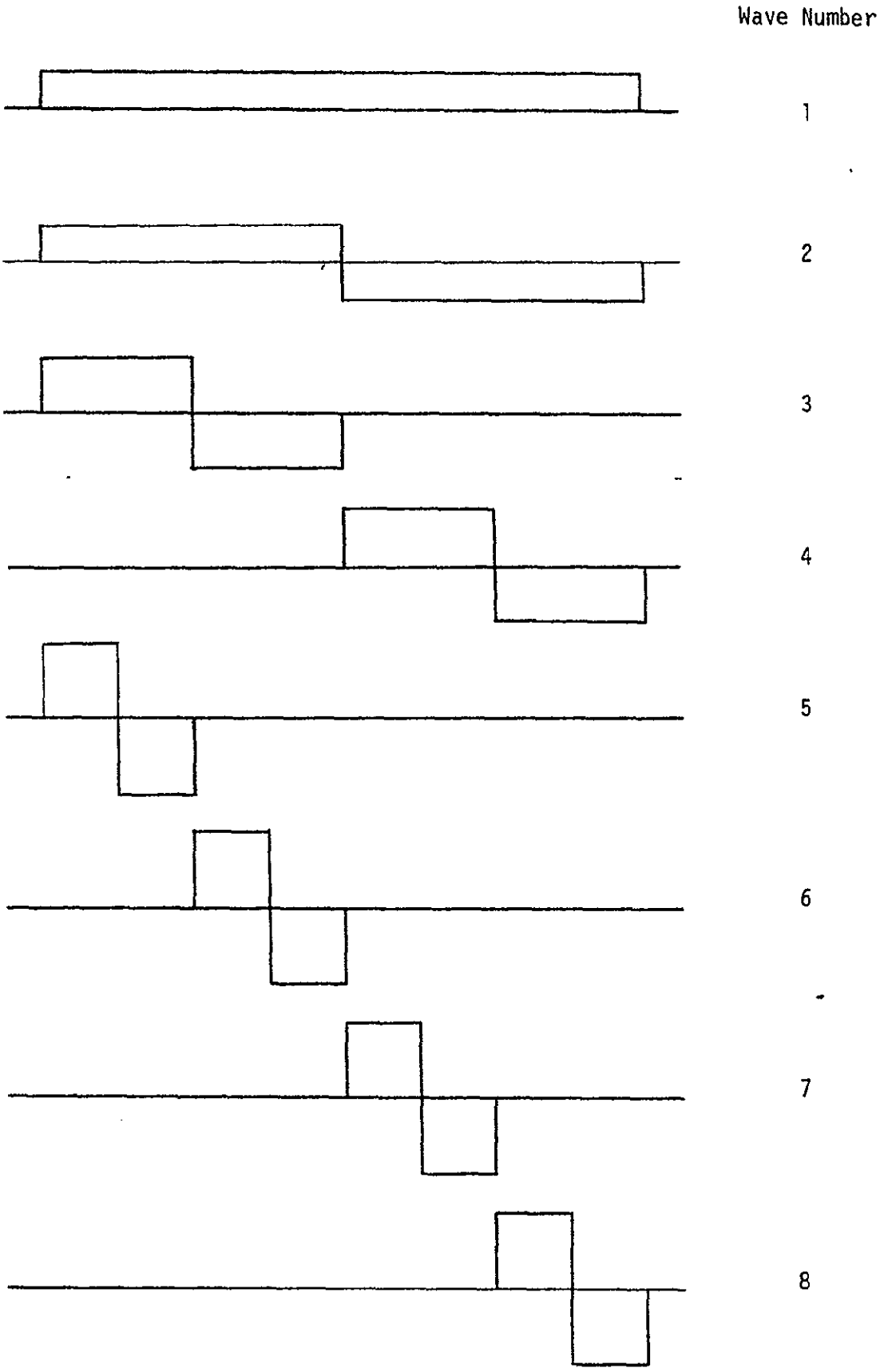

Fig. 3-9. Haar Transform Basis Waveforms for N = 8.

matrix has been designed to include orthogonal rows which exhibit saw-tooth properties. For the general case when N is some power of 2, it has been shown that the Slant matrix may be expressed as an iterative product of rather sparse matrices which when manipulated lead to a fast computational algorithm.

The general base-2 Slant matrix evolves from the simple order-2 matrix

$$S_2 = \frac{1}{\sqrt{2}} \begin{bmatrix} 1 & 1 \\ 1 & -1 \end{bmatrix} \tag{3-43}$$

containing one constant and one slant basis vector. The order-4 Slant matrix evolves from (3-43) through the iterative operation

$$S_4 = \frac{1}{\sqrt{2}} \left[\begin{array}{cc|cc} 1 & 0 & 1 & 0 \\ a_4 & b_4 & -a_4 & b_4 \\ \hline 0 & 1 & 0 & -1 \\ -b_4 & a_4 & b_4 & a_4 \end{array}\right] \left[\begin{array}{c|c} S_2 & \\ \hline & S_2 \end{array}\right] \tag{3-44}$$

which expands to

$$S_4 = \frac{1}{2} \begin{bmatrix} 1 & 1 & 1 & 1 \\ a_4 + b_4 & a_4 - b_4 & -a_4 + b_4 & -a_4 - b_4 \\ 1 & -1 & -1 & 1 \\ a_4 - b_4 & -a_4 - b_4 & a_4 + b_4 & -a_4 + b_4 \end{bmatrix} \tag{3-45}$$

Here a_4 and b_4 are scaling constants to be determined. Requiring the second row in (3-45) to be linear with negative slope gives the condition

$$a_4 = 2b_4 \tag{3-46.1}$$

The orthonormality condition $S_4 S_4^T = I$, on the other hand, gives the condition

$$\frac{1}{4}(4a_4^2 + 4b_4^2) = 1 \tag{3-46.2}$$

As a consequence of (3-46.1) and 3-46.2), $b_4 = 1/\sqrt{5}$ and $a_4 = 2\sqrt{5}$, whence (3-45) becomes

$$S_4 = \frac{1}{2}\begin{bmatrix} 1 & 1 & 1 & 1 \\ 3/\sqrt{5} & 1/\sqrt{5} & -1/\sqrt{5} & -3/\sqrt{5} \\ 1 & -1 & -1 & 1 \\ 1/\sqrt{5} & -3/\sqrt{5} & 3/\sqrt{5} & -1/\sqrt{5} \end{bmatrix} \tag{3-47}$$

Upon examination, we note that S_4 is composed of sequency-ordered row vectors whose staircase waveforms are shown in Fig. 3-10.

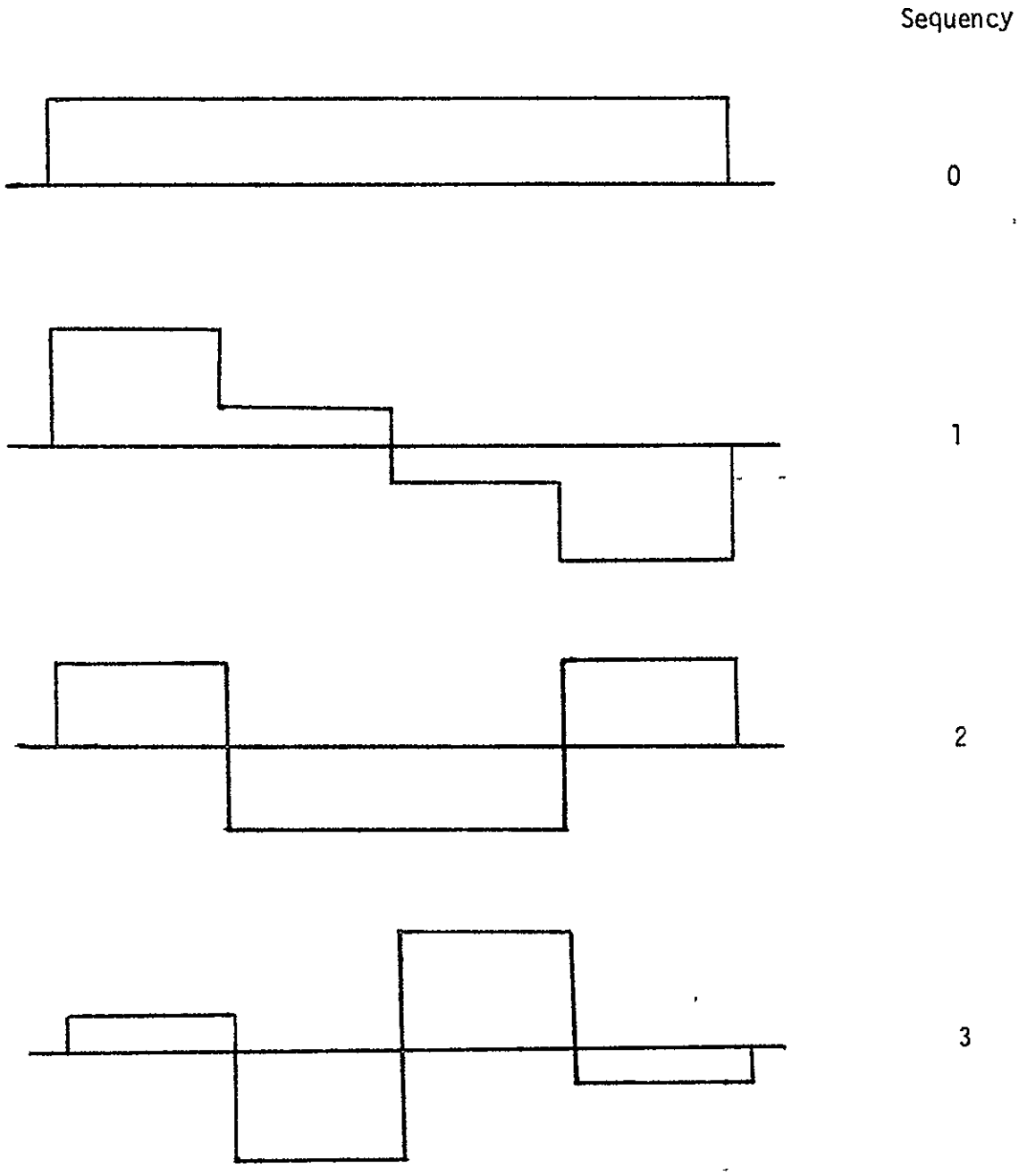

Fig. 3-10. Slant Transform Basis Waveforms for N = 4.

Eq. (3-44) has been generalized to give the Slant matrix of order N in terms of the Slant matrix of order N/2 by the recursive relationship

$$S_N = \frac{1}{2}\left[\begin{array}{cc|c|cc|c} 1 & 0 & & 1 & 0 & \\ a_N & b_N & O & -a_N & b_N & O \\ \hline & & & & & \\ O & & I_{(N/2)-2} & O & & I_{(N/2)-2} \\ \hline 0 & 1 & & 0 & -1 & \\ -b_N & a_N & O & b_N & a_N & O \\ \hline & & & & & \\ O & & I_{(N/2)-2} & & & -I_{(N/2)-2} \end{array}\right] \left[\begin{array}{c|c} S_{N/2} & O \\ \hline O & S_{N/2} \end{array}\right] \tag{3-48}$$

where it can be shown that the constants may be computed recursively from

$$\left.\begin{aligned} a_2 &= 1 \\ b_N &= \sqrt{1 + 4\left(a_{N/2}\right)^2} \\ a_N &= 2b_N\, a_{N/2} \end{aligned}\right\} \tag{3-49}$$

or, by

$$\begin{bmatrix} a_N \\ b_N \end{bmatrix} = \frac{1}{2\sqrt{N^2-1}} \begin{bmatrix} \sqrt{3}\, N \\ N^2-4 \end{bmatrix} \tag{3-50}$$

$$
S_N = \frac{1}{2}
\left[\begin{array}{cc|c|cc|c}
1 & 0 & & 0^* & 0 & \\
0 & b_N & \bigcirc & a_N & 0 & \bigcirc \\
\hline
\multicolumn{2}{c|}{\bigcirc} & I_{(N/2)-2} & \multicolumn{2}{c|}{\bigcirc} & \bigcirc \\
\hline
0 & 0 & & 0 & 1 & \\
0 & a_N & \bigcirc & -b_N & 0 & \bigcirc \\
\hline
\multicolumn{2}{c|}{\bigcirc} & \bigcirc & \multicolumn{2}{c|}{\bigcirc} & I_{(N/2)-2}
\end{array}\right]
\left[\begin{array}{c|c}
I_{N/2} & I_{N/2} \\
\hline
I_{N/2} & -I_{N/2}
\end{array}\right]
\left[\begin{array}{c|c}
S_{N/2} & \bigcirc \\
\hline
\bigcirc & S_{N/2}
\end{array}\right]
\tag{3-51}
$$

*Typographical error in [10].

The fast computational algorithm is based on a factorization of (3-48) given in (3-51)* and a further more efficient factorization of S_4 [10], namely,

$$S_4 = \frac{1}{2} \begin{bmatrix} 1 & 1 & 0 & 0 \\ 0 & 0 & a_4 & b_4 \\ 1 & -1 & 0 & 0 \\ 0 & 0 & b_4 & a_4 \end{bmatrix} \begin{bmatrix} 1 & 0 & 0 & 1 \\ 0 & 1 & 1 & 0 \\ 1 & 0 & 0 & -1 \\ 0 & 1 & -1 & 0 \end{bmatrix} \qquad (3\text{-}52)$$

Operating on a column data vector, (3-52) requires 8 additions and 4 multiplications. Denoting additions by A_4 and multiplications by M_4, $A_4 = 8$ and $M_4 = 4$. The subscript denotes the order of the Slant matrix. The number of operations for S_N as given in (3-51) are $A_N = 2\ A_{N/2} + N + 2$ and $M_N = 2M_{N/2} + 4$, or $A_N = N \log_2 N + (N/2) - 2$ and $M_N = 2N - 4$. Although (3-51) is not sequency-ordered, a rearrangement of rows and columns exists that leads to an ordered form.

Employing the fast computational algorithm, the Slant transformation (3-42) of an N x N image matrix G requires $N^2(2 \log_2 N + 1) - 2N$ additions and $4N(N-2)$ multiplications. For N = 256, this would amount to approximately 1×10^6 additions and 0.25×10^6 multiplications. With available microprocessor chips this entire process would take approximately 0.25 seconds of real time which would not be objectionable for slow-scan TV.

The performance of the Slant transform has been evaluated statistically and shown to exhibit energy compaction superior to the Haar, Hadamard and even the Fourier transform for block sizes less than 64 X 64. Fig. 3-11

The 0 entry has been reported as 1 in [10]. This appears to be a typographical error.

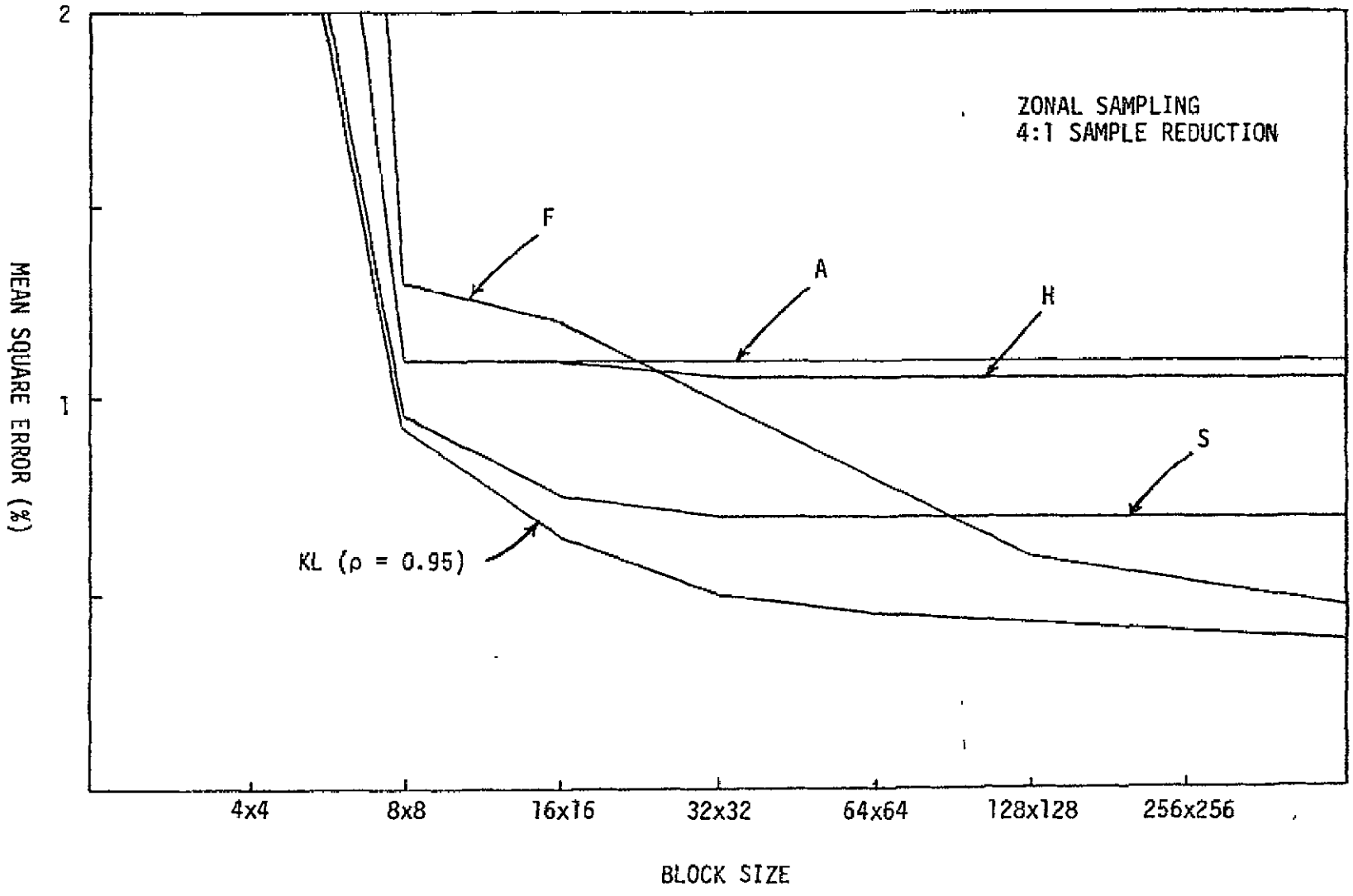

Fig. 3-11. Mean Square Error Performance Comparison of Image Transforms Using Zonal Sampling as a Function of Block Size

4.0 SYSTEM CONSIDERATIONS

In the previous section we have presented the elements of a few of the better known image coding techniques, emphasizing their respective underlying mathematical models, identifying possible mechanizations and alluding to their energy compaction capabilities. In the discussion concerning differential encoding we noted that although the difference signal samples exhibit a smaller amount of correlation when compared to the original samples, one cannot realize a reduced data rate without the use of optimal quantization based on a probability density model of the difference signal process. No such system consideration was made in discussing transform coding techniques. The first subsection that follows indicates statistical considerations involved in arriving at suitable quantization strategies for transform image coding. Employing signal and noise statistics, the second section presents the fundamental concept of optimal estimation useful in image enhancement.

4.1 Optimal Quantization

An N x N image matrix G may be considered as a sample of a stochastic process with mean

$$E\{[G(x,y)]\} = [\overline{G(u,v)}] \tag{4-1}$$

and covariance

$$E\{[G(x_1,y_1) - \overline{G(x_1,y_1)}]\,[G(x_2,y_2) - \overline{G(x_2,y_2)}]\} = [C_G(x_1,y_1,x_2,y_2)] \tag{4-2}$$

Pre PRECEDING PAGE BLANK NOT FILMED

A generally used covariance model is one corresponding to a first order Markov process [8], [9], [10], [23], in which the typical entry is given by

$$C_G\ (x_1,y_1,x_2,y_2) = \sigma_R^2\ \sigma_C^2\ \rho_R^{|x_1-x_2|}\ \rho_C^{|y_1-y_2|} \tag{4-3}$$

where σ_R^2 and σ_C^2 are the row and column variances, and ρ_R and ρ_C are the adjacent pixel correlation factors.

A general transformed image

$$T = KGK^T \tag{4-4}$$

is also a sample of a stochastic process with mean

$$\begin{aligned} E\{[T(u,v)]\} &= [\overline{T(u,v)}] \\ &= K[\overline{G(x,y)}]K^T \end{aligned} \tag{4-5}$$

and covariance

$$[C_T(u_1,v_1,u_2,v_2)] =$$

$$= \sum_{x_1} \sum_{x_2} \sum_{y_1} \sum_{y_2} K(u_1,x_1)K(u_2,x_2)\ C_G(x_1,y_1,x_2,y_2)K(v_1,y_1)K(v_2,y_2) \tag{4-6}$$

Noting that the transform operation (4-4) is a weighted sum over all pixels, we can specify a reasonable probability density model for the transformed image based on arguments connected with the central limit theorem [24], eventhough the probability density of the original image is not clearly specified. Since transel T(0,0) is a nonnegative sum of pixel values it can be modeled by a Rayleigh density

$$p_{T(0,0)}(x) = \frac{x}{\alpha^2} e^{-x^2/2\alpha^2} \quad ; \quad x \geq 0 \tag{4-7}$$

All other transels may be modeled by a zero mean Gaussian density

$$p_{T(u,v)}(x) = \frac{1}{2\pi\sigma^2(u,v)} e^{-x^2/2\sigma^2(u,v)} \quad ; \; u,v \neq 0 \tag{4-8}$$

where $\sigma^2(u,v) = E\{T^2(u,v)\} = C(u,u,v,v)$, the variance or expected energy in transel T(u,v).

As pointed out in the previous section, the objective of a transformation is to operate on an original image with a given pixel-to-pixel correlation and produce a transformed image with reduced transel-to-transel correlation. The consequence of such an operation is energy compaction, a clustering of the bulk of the image energy into a small number of transels. To achieve bandwidth compression, one has to exploit this phenomenon of energy conpaction.

One direct way of achieving bandwidth compression is through the use of threshold sampling. In this approach, all transel values whose magni-

tudes exceed a specific preassigned threshold level are quantized into a binary word of a given length and transmitted; the remaining transels are ignored. Of course, in addition to transmitting the transel magnitude, one has to identify its location which must also be transmitted. Using run-length encoding techniques one may minimize the bandwidth waste associated with transmitting transel locations [8]. The threshold employed is typically chosen to be one that will insure a certain level of fidelity in the reconstructed image using an energy or minimum mean square error criterion.

Alternatively, one may employ zonal sampling. This approach involves partitioning a transformed image into zones of different average variances. Transels in each zone are coded by means of binary words whose bit-length is proportional to the average variance there as suggested by rate distortion theory [10], [11]. In fact, the bit assignment at transel location (u,v) is given by

$$N_B(u,v) = \ln \sigma^2(u,v) - \ln D \tag{4-9}$$

where $\sigma^2(u,v)$ is the transel variance and D is the average quantizing distortion. Using (4-9) one may construct a bit assignment map for a given block size. Since $\sigma^2(u,v)$ is transform-dependent, the bit assignment distribution will vary from transform to transform. Such a bit assignment distribution has been reported in [8] for the Slant transform of a 16 x 16 block size. It is included here in Figure 4-1. This particular choice of assignment requires an information rate of 1.5 B/P giving rise to only 0.05% mean square quantization error. Quantization decision levels are selected

8	8	8	7	7	7	5	5	4	4	4	4	4	4	4	4
8	8	7	5	5	5	3	3	3	3	3	3	2	2	2	2
8	7	6	4	4	4	3	3	2	2	2	2	2	2	2	2
7	5	4	3	2	2	2	2								
7	5	4	2	2	2	2	2								
7	5	4	2	2	2	2	2								
5	3	3	2	2	2										
5	3	3	2	2	2										
4	3	2													
4	3	2													
4	3	2													
4	3	2													
4	2	2													
4	2	2													
4	2	2													
4	2	2													

Fig. 4-1. Bit Assignment Map for Slant Transform Zonal Coding of 16 x 16 Pixel Block

in such a way as to minimize mean square quantization distortion according to the Max quantization algorithm [7] discussed in Section 3.1.2, using the probability density model developed in this section. When compared with an 8-bit PCM alternative Figure 4-1 indicates a bandwidth reduction of 5:1.

4.2 Optimal Estimation

Where a transformed image is transmitted through a noisy channel, it arrives at the receiver corrupted according to the nature of the noise involved. Direct reconstruction of the image by inverse transformation will result in a distorted version of the original, reflecting the effects of the noise. For the case when the noise is white and additive, it is possible

to enhance the reconstructed image by Weiner filtering techniques, provided signal and noise statistics are specified. Below, we present the basic notions of optimal signal estimation as it applies to the case of an M-sample signal vector. The extension to the M x M image matrix is subsequently indicated.

Let $\underline{s}$ be a zero-mean M-sample signal vector whose unitary transformation A $\underline{s}$ is to be transmitted through a channel with additive white zero-mean noise. Figure 4-2 shows the block diagram of a generalized one-dimensional* Weiner filtering system where the additive noise has been referred back to the source as a zero-mean M-sample vector $\underline{n}$. The unitary transform of $\underline{s} + \underline{n}$ may be denoted by

$$A(\underline{s} + \underline{n}) = \underline{S} + \underline{N} \tag{4-10}$$

At the receiver, a symmetric matrix W operates on $\underline{S} + \underline{N}$ prior to the final inversion which yields the signal estimate

$$\hat{\underline{S}} = A^{-1}\, WA(\underline{s} + \underline{n}) \tag{4-11}$$

The Weiner matrix W is chosen to minimize the mean square error

$$\varepsilon = \|\underline{s} - \hat{\underline{s}}\|^2$$

$$= \mathrm{Tr}\,[E\{(\underline{s} - \hat{\underline{s}})(\underline{s} - \hat{\underline{s}})^T\}] \tag{4-12}$$

*One-dimensional, here, refers to the one-dimensional unitary transformation.

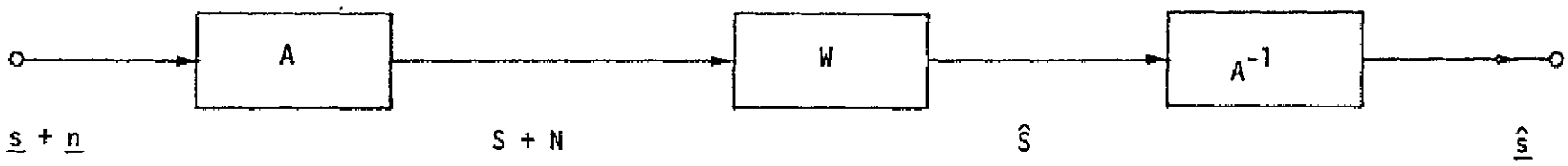

Fig. 4-2. Generalized One-Dimensional Weiner Filtering System

between the actual signal $\underline{s}$ and the estimated signal $\underline{\hat{s}}$. This is done using signal and noise statistics. In fact, to minimize ε with respect to W we only need to specify the covariances of the signal and the noise. Viewing the signal vector $\underline{s}$ as a sample of a random process with covariance

$$C_s = [E\{\underline{s}\ \underline{s}^T\}] \tag{4-13}$$

and denoting the noise covariance by C_n, (4-12) may be rewritten as

$$e = Tr[E\{(\underline{s} - A^{-1}WA(\underline{s} + \underline{n}))(\underline{s} - A^{-1}WA(\underline{s} + \underline{n}))^T\}]$$

$$= Tr[C_s - (A^{-1}WA)C_s - C_s(A^{-1}WA)^T + (A^{-1}WA)(C_s + C_n)(A^{-1}WA)^T]$$

$$= Tr[C_s - 2(A^{-1}WA)C_s + (A^{-1}WA)^2(C_s + C_n)] \tag{4-14}$$

assuming that the signal and noise vectors are independent. Minimizing (4-14) with respect to $(A^{-1}WA)$, we get the optimal Weiner matrix

$$W^o = A\ C_s(C_s + C_n)^{-1}\ A^{-1} \tag{4-15}$$

resulting in a minimum mean square error

$$\varepsilon_{min} = Tr\ [C_s C_n (C_s + C_n)^{-1}] \tag{4-16}$$

which, interestingly enough, does not depend on the unitary transformation. Note, however, that the optimal Weiner filter matrix W^o is dependent on the

unitary transformation A as shown in (4-15), apparently a two-dimensional transformation of matrix $C_s(C_s + C_n)^{-1}$.

When signal $\underline{s}$ is a sample of a first-order Markov process, it has a covariance matrix

$$C_s = \sigma_s^2 \begin{bmatrix} 1 & \rho & . & . & . & \rho^{M-1} \\ \rho & 1 & . & . & . & \rho^{M-2} \\ . & . & . & . & . & . \\ . & . & . & . & . & . \\ . & . & . & . & . & . \\ \rho^{M-1} & \rho^{M-2} & . & . & . & 1 \end{bmatrix} \tag{4-17}$$

where ρ is the pixel-to-pixel correlation factor. The covariance of the white noise vector $\underline{n}$ is given by

$$C_n = \sigma_n^2 \, I \tag{4-18}$$

a diagonal M x M matrix, where σ_n^2 is the noise variance. To construct W^0, we first diagonalize the signal plus noise covariance using the matrix K_s of signal covariance eigenvectors; specifically,

$$K_s(C_s + C_n) \, K_s^{-1} = \mathrm{diag}[\sigma_n^2 + \lambda_s(i)] \; ; \; i = 1, 2, \ldots, N \tag{4-19}$$

where $\lambda_s(i)$ are the eigenvalues of C_s. Then

$$(C_s + C_n)^{-1} = K_s^{-1} \operatorname{diag}\left(\frac{1}{\sigma_n^2 + \lambda_s(i)}\right) K_s \tag{4-20}$$

and

$$W^0 = AC_s\, K_s^{-1} \operatorname{diag}\left(\frac{1}{\sigma_n^2 + \lambda_s(i)}\right) K_s A^{-1}$$

$$= A\, K_s^{-1} \operatorname{diag}\left(\frac{\lambda_s(i)}{\sigma_n^2 + \lambda_s(i)}\right) K_s A^{-1} \tag{4-21}$$

It is worth noting at this point that if A is the Karhunen-Loève matrix, K_s, W^0 is simply the diagonal matrix

$$W_{KL}^0 = \operatorname{diag}\left(\frac{\lambda_s(i)}{\sigma_n^2 + \lambda_s(i)}\right) \tag{4-22}$$

which, when implemented, serves to provide varying emphasis over spectral component elements of $\underline{S} + \underline{N}$. When A is a Fourier transform matrix, W^0 has off-diagonal components which diminish rapidly with distance from the diagonal. This, of course implies that the spectral components $\underline{S} + \underline{N}$ are mixed and emphasized in accordance with the degree of dispersion in the filter matrix W^0. In general the dispersion in W^0 seems to be a measure of residual correlation among the spectral components after a particular transformation.

In practice, when employing one of the computationally efficient transformations, it would be self-defeating to implement the full-fledged Weiner matrix. On the other hand, one could greatly reduce the computational burden it poses by resorting to suboptimal Weiner filtering, which would involve using a narrow main band of W^o that would require relatively few operations.

The extension of the Weiner filtering concept to two-dimensional signals follows readily. Let

$[s(i,j)]$ = original signal matrix

$[n(i,j)]$ = additive white noise matrix

A separable symmetric transformation of the signal plus noise matrix produces the corrupted transformed signal matrix

$$[S(k,l) + N(k,l)] = A[s(i,j) + n(i,j)]A^T \tag{4-23}$$

Note that the computations performed here are done sequentially on rows and columns. Restricting the Weiner filtering process to similar sequential operations, the optimal estimate of the signal matrix becomes

$$[\hat{S}(i,j)] = A^{-1}\, W[S(k,l) + N(k,l)]\, WA^{-1T} \tag{4-24}$$

which is a sequential application of one-dimensional Weiner filtering to rows and columns of the transformed signal plus noise matrix. Successful use of (4-24) in enhancing images corrupted by white additive noise has been reported in [23].

As a final note, it must be pointed out that Weiner filtering is not limited to unitary transformations. In [25] it is shown that viewing the DPCM process as a lower-trangular matrix operator, one can derive the Weiner filter matrix in a similar way as shown above.

5.0 CONCLUSIONS AND RECOMMENDATIONS

The present work is the result of a twelve week effort to survey the modern science of image coding. Because of the time constraint and the numerous interruptions imposed by other committments, this study has been necessarily selective. Provoked by the latest trends in the subject, we have largely ignored the vast available literature [1], [26], [27] that preceded the present-day philosophy. Thus, after investigating the basic notions of differential encoding, we concentrated in the more modern transform coding techniques which hold the key to present and future bandwidth compression systems.

Following the introduction, Section 2.0 defines the bandwidth compression system as a pattern recognition problem. Starting with the basic premise that a typical image is highly redundant, the hypothetical bandwidth compression system generates a set of uncorrelated features that characterize the image, classifies them according to improtance and transmits an essential subset that guarrantees a certain level of fidelity upon reconstruction. Precluding the transmission of unnecessary redundant information, the ideal system serves to conserve bandwidth.

Section 3.0 presents the basic principles that describe some of the better known image coding techniques. While discussing differential coding in Section 3.1, we find it necessary to delve into such notions as optimal linear prediction and optimal quantization, especially useful in DPCM systems and essential to achieving bandwidth reduction. Section 3.2 introduces the general concept of a two-dimensional linear transformation of an image matrix and concludes with the definition of a very special transformation

of the separable and symmetric form. The following subsections describe five well-known tranform coding techniques, putting particular emphasis on their underlying mathematical models and energy compaction capability. It is shown in Section 3.2.1 that the Karhunen-Loève (KL) transform derived from probabilistic considerations is statistically optimal. As described, the KL transform is not of a separable form. Used as a one-dimensional transformation, it operates on sampled raster data, which, in itself, is not objectionable in practice. What is objectionable, however, is that, unlike the other four transformation procedures, it does not possess a fast computational algorithm. At the present time the KL transform is viewed as a basis for evaluating the performance of other techniques and is not considered as a serious contender for practical application.

Section 3.2.2 describes the two-dimensional Fourier (F) transform. It is noted that using its fast computational algorithm, an N x N image matrix G may be transformed with $2N^2 \log_2 N$ operations. For N = 256, it would take a modern microprocessor 0.5 seconds to perform the transformation. With the necessary buffering this fast Fourier transform (FFT) implementation can find application in a slow-scan TV situation. An interesting alternative to the FFT approach is the analog implementation of the CZT formulation of the Fourier transform. As pointed out, ARPA and NUC are advocating a CZT-DPCM bandwidth compression system implemented either in a SAW or a CCD configuration. Although they claim a 16:1 bandwidth reduction, they have not yet idenitified the level of fidelity this ratio corresponds to.

Section 3.2.3 develops the essentials of the two-dimensional Hadamard (H) transformation. Involving only ±1's, this transformation re-

quires $2N^2\log_2 N$ additions when exercized by means of its fast algorithm. Digital implementations of the one-dimensional transformation of both sequency-ordered and unordered forms are given. The apparent simplicity in the hardware involved makes this transformation attractive in practice. With appropriate buffering a two-dimensional implementation follows easily. If buffering is objectionable an H-DPCM system could be considered.

The Haar (A) transform examined in Section 3.2.4 is shown to have an extremely fast algorithm when equipped with a lookup table of multiplications by $\sqrt{2}$, requiring only 2(N-1) additions. Its digital implementation is otherwise very similar to that of the H transformation as indicated by its factored form (3-41) for N = 8. It is pointed out that the limited-support structure among the basis vectors in the A matrix accounts for a larger amount of residual correlation in the transformed image and smaller noise immunity in transmission when compared with the H transform.

In Section 3.2.5 we consider the latest numerically efficient transform, the Slant (S) transform. This transform has been especially developed to possess basis vectors with saw-tooth properties in order to efficiently match linearly varying image brightness. The associated fast algorithm requires $A_N = 2N^2\log_2 N + N^2-2N$ additions and $M_N = 4N(N-2)$ multiplications to produce a transformed N x N image. It has been shown (Fig. 3-11) that for $N \leq 64$, the Slant transform is superior to the F transform, comparing rather well with the KL transform.

ORIGINAL PAGE IS
OF POOR QUALITY

In general, it is not possible to chose from among the image coding methods discussed without taking into account the particular nature of the situation where it is to be applied. For example, the requirement of real-time TV transmission alone eliminates from consideration most of the approaches described, namely, the KL, FFT, S techniques, leaving DM, DPCM, H, A and CZT as likely choices. With an additional constraint of small buffer usage, one is forced into using such combinations as DPCM-DPCM, H-DPCM, A-

DPCM, CZT-DPCM, etc. In an RPV application, a transmission-time constraint will most likely be dictated by the mission to be carried out; the low-buffer constraint will be imposed by the physical space available as well as by the cost it might incur. If a slow-scan mode is in order, one may be well-advised to employ two-dimensional transform coding of square image blocks just small enough to permit a computation within one frame time. Two-dimensional H, A, S, FFT are preferred over their respective DPCM hybrids, on the basis of their superior noise immunity, eventhough this may require a certain amount of buffering. As mentioned before, a DPCM process can become unstable in the presence of noise, giving rise to image streaking, etc.

Ranked according to noise immunity and energy compaction capabilities, the above two-dimensional transforms are FFT, S, H, A. From the point of view of simplicity of implementation, they are ranked in reverse order. Of these, the one logical and expedient choice for Motorola's RPV aims would be H, since it shares a good combination of noise immunity, energy compaction and ease of implementation. This is not to say that Motorola cannot afford to consider other approaches. In fact, using a minicomputer with a slow-scan TV setup, Motorola can gain valuable first-hand experience with all the techniques mentioned, if not others, which could eventually serve to substantiate the reasons for a final choice suitable to the application in mind.

Since the early stages of this investigation it became increasingly obvious that the process of transforming the image, by itself, did not constitute bandwidth compression. We have seen that the basic aim of a transformation is redundancy removal manifested by the phenomenon of energy compaction, that is, the concentration of the bulk of the uniformly distributed energy over the pixels into a relatively smaller set of transels. To achieve band-

width compression, one needs to exploit this situation. Section 4.1 describes sampling and optimal quantization strategies that could be used for the purpose. While a sampling procedure selects the transels to be transmitted, optimal quantization provides for minimum distortion.

In Section 4.2 we formulated the concept of optimal estimation as it relates to enhancing the received transformed image corrupted by white additive noise. A generalized Weiner filter kernel of separable and symmetric form, whose structure is a function of image transform used, is derived from statistical considerations. The diagonal character of the associated Weiner matrix W for the KL transform deteriorates into an increasingly dispersed structure for less effective transforms, namely, FFT, S, H and A transforms. It is noted that employing a small main diagonal band of W one could achieve reasonable suboptimal enhancement with only modest computational burden. Arguments are presented indicating that the Weiner matrix corresponding to the A transform exhibits substantially more dispersion than that of the H transform. This further supports the case for choosing the H transform over the A transform.

Judging from information at hand, I recommend that Motorola pursue a development of a bandwidth compression system based on the H transform. I do believe that with consistent and dedicated effort, Motorola could develop a demonstration model of such a system by late next year. It is my hope, however, that a successful completion of this work would not spell the end to serious considerations of alternatives. For example, valuable experience with other approaches may be gained via a minicomputer. Advances in the semiconductor technologies (CCD, IIL, ECL, EFL, Schottky, etc.) should be followed closely and constantly in case they might have an impact on future choices. In

addition, research with liquid crystal [28] and plasma displays [29], [30], [31] might be applicable to our problem.

Finally, it must be said in no uncertain terms, that in such a highly mathematical subject as image coding, one cannot afford to proceed without a reasonable understanding of the underlying theory. Clearly, without some grasp of the theoretical notions of optimal prediction, optimal quantization, optimal estimation and rate-distortion theory, one might well resort to the dubious domain of experimental science....

BIBLIOGRAPHY

[1] Huang, T. S., Tretiak, O. J., Picture Bandwidth Compression, Gordon and Breach, N.Y., 1972.

[2] Abate, J. E., "Linear and Adaptive Delta Modulation," Proc. of the IEEE, Vol. 55, No. 3, Mar. 1967, pp. 298-308.

[3] Habibi, A., "Comparison of nth-Order DPCM Encoder with Linear Transformations and Block Quantization Techniques," IEEE Trans. on Com. Tech., Vol. COM-19, No. 6, Dec. 1972.

[4] Pratt, W. K., et. al., USCEE Report 425, Mar. - Aug. 1972.

[5] Means, R. W., Speiser, J. M., Whitehouse, H. J., "Image Transmission Via Spread Spectrum Techniques," ARPA Quarterly Technical Report AD 780805, Oct. - Jan. 1974.

[6] Andrews, H. C., et. al., Computer Techniques in Image Processing, Academic Press, N.Y., 1970.

[7] Max, J. "Quantization for Minimum Distortion," IRE Trans. on Inf. Th., Vol. IT-6, Mar. 1960, pp. 7-12.

[8] Pratt, W.K., Chen, W-H, Welch, L.R., "Slant-Transform Image Coding," IEEE Trans. on Com. Tech., Vol. COM-22, No. 8, Aug. 1975.

[9] Habibi, A., Wintz, P. A., "Image Coding by Linear Transformation and Block Quantization," IEEE Trans. on Com. Tech., Vol. COM-19, No. 1, Feb. 1971.

[10] Pearl, J., Andrews, H. C., Pratt, W. K., "Performance Measure for Transform Image Coding," IEEE Trans. on Com., June 1972.

[11] Davisson, L. D., "Rate-Distortion Theory and Application," Proc. of the IEEE, Vol. 60, No. 7, July 1972.

[12] O'Neal Jr., J. B., "Predictive Quantizing Systems (Differential Pulse Code Modulation) for the transmission of Television Signals," BSTJ, Vol. 45, pp. 689-722, May - June 1966.

[13] Davenport, W. D., Jr., Root, W. L., An Introduction to the Theory of Random Signals and Noise, McGraw-Hill, New York, 1958.

[14] Andrews, H. C., Pratt, W. K., "Fourier Transform Coding of Images," Hawaii International Conference on Systems Science, Jan. 1968.

[15] Cooley, J. W., Tukey, J. W., "An Algorithm for the Machine Calculation of Complex Fourier Series", Math of Comp., Vol. 19, pp 297 - 301, 1956.

[16] Habibi, A., Pratt, W. K., Robinson, G., Means, R., Whitehouse, H., Speiser, "Real-Time Image Redundancy Reduction Using Transform Coding Techniques," included in [5].

[17] Pratt, W. K., Kane, J., Andrews, H. C., "Hadamard Transform Image Coding," Proc. of the IEEE, Vol. 57, No. 1., Jan. 1960.

[18] Good, I. J., "The Interaction Algorithum and Practical Fourier Analysis," J. Roy. Statist. Soc. (London) B20, 361 (1958).

[19] Haar, A., "Zur Theorie der Orthogonalen Funktionen-Systeme," Inaugural Dissertation, Math. Ann. 69, pp. 331-371 (1910).

[20] Emomoto, H., Shibata, K., "Orthogonal Transform Coding System for Television Signals", IEEE Trans. Electromag. Compat., Vol. EMC-13, pp. 11-17, Aug. 1971.

[22] Andrews, H. C., Patterson, C. L., "Outer Product Expansions and their Uses in Digital Image Processing", Amer. Math. Assoc. Journal, Jan. 1975.

[23] Pratt, W. K., "Generalized Wiener Filtering Computation Techniques", IEEE Trans. on Comp., Vol. C-21, No. 7, July 1972.

[24] Papoulis, A., Probability, Random Variables and Stochastic Processes, McGraw-Hill, N.Y. 1965.

[25] Habibi, A., "Applications of Lower-Triangular Transformations in Coding and Restoration of Two-Dimensional Sources", NTC 1973, Atlanta, Ga., Vol. 1, 12D.

[26] "Redundancy Reduction", Special Issue of Proc. of the IEEE, Mar. 1967.

[27] "Bibliography on Digital Image Processing and Related Topics", USCEE Rep. 410, AD 745790, Feb. 1972.

[28] Inokuchi, S. et. al., "Optical Pattern Processing Utilitizing Nematic Liquid Crystals", Appl. Opt. Vol. 11, No. 10, pp. 2223-2227, Oct. 1972.

[29] Judice, C. N., Jarvis, J. F., Ninke, W. F., "Using Ordered Dither to Display Continuous Tone Pictures on an AC Plasma Panel", Univ. of Ill. presentation obtained from J. Studier, Urbana, Ill., June 1975.

[30] Limb, J. O., "Design of Dither Waveforms for Quantized Visual Signals", BSTJ, Vol. 48, pp. 2555-2582, 1969.

[31] Bayer, B. E., "An Optimum Method for Two-Level Rendition of Continuous-Tone Pictures", ICC 1973, pp. (26-11)-(26-15).